

CR-172035

Contract No: NAS9-17195

DRL No: T-1884

Line Item No: 1

DRD No: TM-4787

A STUDY OF TWO-PHASE FLOW IN A REDUCED GRAVITY ENVIRONMENT

FINAL REPORT

OCTOBER 16, 1987

(NASA-CR-172035) A STUDY OF TWO-PHASE FLOW
IN A REDUCED GRAVITY ENVIRONMENT Final
Report (Sundstrand Corp.) 173 p CSCL 22A

N88-12617

Unclas
G3/29 0110580

SUNDSTRAND ENERGY SYSTEMS
A UNIT OF SUNDSTRAND CORPORATION
ROCKFORD, ILLINOIS

CONTRACT NO: NAS9-17195

DRL NO: T-1884

LINE ITEM NO: 1

DRD NO: TM-478T

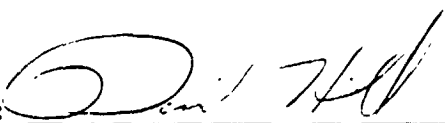
A STUDY OF TWO-PHASE FLOW IN A REDUCED GRAVITY ENVIRONMENT

FINAL REPORT

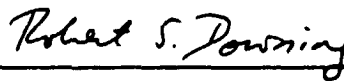
OCTOBER 16, 1987

SUNDSTRAND ENERGY SYSTEMS
A UNIT OF SUNDSTRAND CORPORATION
ROCKFORD, ILLINOIS

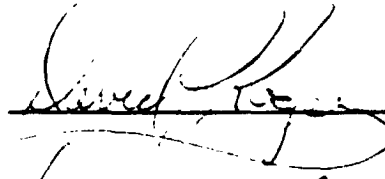
PREPARED BY:



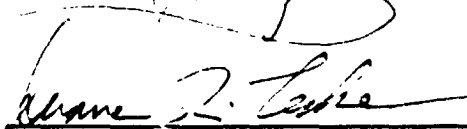
PREPARED BY:



APPROVED BY:



APPROVED BY:



APPROVED BY:



Abstract

A test loop was designed and fabricated for observing and measuring pressure drops of two-phase flow in reduced gravity. The portable flow test loop was then tested aboard the NASA-JSC KC135 reduced gravity aircraft. The test loop employed the Sundstrand Two-Phase Thermal Management System (TPTMS) concept which was specially fitted with a clear two-phase return line and condenser cover for flow observation. A two-phase (liquid/vapor) mixture was produced by pumping nearly saturated liquid through an evaporator and adding heat via electric heaters. The quality of the two-phase flow was varied by changing the evaporator heat load.

The test loop was operated on the ground before and after the KC135 flight tests to create a one-gravity data base. The ground testing included all the test points run during the reduced gravity testing. Two days of reduced gravity testing aboard the NASA-JSC KC135 were performed. During the flight tests, reduced-gravity, one-gravity and nearly two-gravity accelerations were experienced. Data was taken during the entire flight which provided flow regime and pressure drop data for the three operating conditions. The test results show that two-phase flow pressure drops and flow regimes can be accurately predicted in zero-gravity.

TABLE OF CONTENTS

<u>Section</u>	<u>Page Number</u>
Table of Figures	v
Nomenclature/Definitions	ix
1.0 Summary	1
2.0 Test Results	2
2.1 Reduced Gravity Test Results	2
2.1.1 Overview	2
2.1.2 Two-Phase Adiabatic Test Section	7
2.1.2.1 Two-Phase Flow Regime	7
2.1.2.2 Pressure Drops	27
2.1.3 Condenser Test Section	36
2.1.3.1 Liquid Carry-over	42
2.1.3.2 Simulation of Condenser Test Results	46
2.1.4 System Operation	50
2.1.4.1 Sundstrand TPTMS Responses to a Reduced-Gravity Flight Profile	50
2.1.4.2 System Transient Tests	57
2.2 Ground Test Results	63
2.2.1 Overview	63
2.2.2 Two-Phase Adiabatic Test Section	69
2.2.2.1 Two-Phase Flow Regime	69
2.2.2.2 Pressure Drops	76
3 0 Test Conclusions	85
3.1 Two-Phase Adiabatic Test Section	85
3.2 Condenser	86
4.0 Recommendations For Further Investigation	87
5.0 Program Description	89
5.1 Introduction (Background)	89

TABLE OF CONTENTS (continued)

<u>Section</u>		<u>Page</u> <u>Number</u>
5.2	Scope/Objective	91
5.3	Test Stand Description	92
5.4	Design Considerations	103
5.5	Test Plan Overview	105
5.5.1	Ground Testing	105
5.5.2	Reduced Gravity Test Overview	106
5.5.2.1	Filming During Flight	107
5.5.2.2	Reduced Gravity Tests	109
6.0	References	110
7.0	Appendices	112
A.	R. Niggemann Flight Test Narration Transcription	113
B.	E. Keshock Flight Test Narration Transcription	119
C.	Chisholm B and C - Type Method For Pressure Drop Prediction Through Bends	145
D.	Pressure Drop Predictive Method Flow Charts	149
E.	Film Log	159

TABLE OF FIGURES

<u>Figure Number</u>	<u>Description</u>	<u>Page Number</u>
2.0-1	TPTMS Test Loop Schematic	3
2.0-2	Adiabatic Test Section	4
2.1.1-1	Data Acquisition Channels	5
2.1.1-2	Reduced-Gravity Flight Profile Summary	6
2.1.1-3	Reduced-Gravity Flight Test Aboard NASA-JSC KC135	8
2.1.1-4	Reduced-Gravity Flight Test Aboard NASA-JSC KC135	9
2.1.1-5	Reduced-Gravity Flight Test Aboard NASA-JSC KC135	10
2.1.2.1-1	Reduced-Gravity Flow Regime Observations	11
2.1.2.1-2a	Flow Regimes in Reduced Gravity	13
2.1.2.1-2b	Reduced-Gravity Frothy Annular Flow	14
2.1.2.1-3	One-Gravity Flow Patterns in Vertical Up Flow	15
2.1.2.1-4	Reduced-Gravity Taitel and Dukler Flow Regime Map	19
2.1.2.1-5	Reduced-Gravity HTRI Flow Regime Map	21
2.1.2.1-6	Reduced-Gravity Baker Flow Regime Map	23
2.1.2.1-7	Reduced-Gravity Modified Dukler Flow Regime Map	25
2.1.2.2-1	Straight Section Pressure Drop vs. Quality; Reduced-Gravity; HTRI	28

TABLE OF FIGURES (continued)

<u>Figure Number</u>		<u>Page Number</u>
2.1.2.2-2	Curved Section Pressure Drop vs. Quality; Reduced Gravity; HTRI	29
2.1.2.2-3	Straight Section Pressure Drop vs. Quality; Reduced Gravity; Wet Walled Modified HTRI	31
2.1.2.2-4	Curved Section Pressure Drop vs. Quality; Reduced Gravity; Wet Walled Modified HTRI	32
2.1.2.2-5	Reduced Gravity Straight Section Pressure Drop Data and Predictions	34
2.1.2.2-6	Reduced Gravity Test Data Predictions Summary	35
2.1.2.2-7	Reduced Gravity Straight Section HTRI Predicted Pressure Drop vs. Test Data Pressure Drop Scatter Plot	37
2.1.2.2-8	Reduced Gravity Straight Section Friedel Predicted Pressure Drop vs. Test Data Pressure Drop Scatter Plot	38
2.1.2.2-9	Reduced-Gravity Straight Section Wet Walled Modified HTRI Predicted Pressure Drop vs. Test Data Pressure Drop Scatter Plot	39
2.1.3-1	Condenser Test Setup	40
2.1.3.1-1	Condenser Flow Variation	43
2.1.3.1-2	Estimate of Liquid Carry-over	44
2.1.3.2-1	Simulation of Condenser Reduced Gravity Test	47
2.1.3.2-2	Condenser Temperature Distribution	49
2.1.4.1-1	Accumulator Position vs. Time	52
2.1.4.1-2a	SFE Liquid Flow Rate vs. Time	53
2.1.4.1-2b	SFE Liquid Flow Rate vs. Time	54
2.1.4.1-3	Evaporator Pump Outlet Pressure vs. Time	55

TABLE OF FIGURES (continued)

<u>Figure Number</u>		<u>Page Number</u>
2.1.4.1-4	Cavitating Venturi Inlet Pressure vs. Time	56
2.1.4.1-5	SFE Coil Surface Temperature vs. Time	58
2.1.4.2-1	Condenser Water Flow Rate vs. Time, Coolant Shutdown	59
2.1.4.2-2	Evaporator Pump Outlet Pressure vs. Time, Coolant Shutdown	60
2.1.4.2-3	Condenser Liquid Exit Temperature vs. Time, Coolant Shutdown	61
2.1.4.2-4	SFE Liquid Flow Rate vs. Time, Coolant Shutdown	62
2.1.4.2-5	RFMD RPM vs. Time, RFMD Shutdown	64
2.1.4.2-6	SFE Liquid Flow Rate vs. Time, RFMD Shutdown	65
2.1.4.2-7	Evaporator Pump Outlet Pressure vs. Time, RFMD Shutdown	66
2.2.1-1	Ground Testing at NASA-JSC	67
2.2.1-2	Ground Testing at NASA-JSC	68
2.2.2.1-1	Ground Test Flow Regimes	70
2.2.2.1-2	Ground Test Taitel and Dukler Flow Regime Map	71
2.2.2.1-3	Ground Test HTRI Flow Regime Maps	72
2.2.2.1-4	Ground Test Mandhane Flow Regime Map	73
2.2.2.1-5	Ground Test Revised Baker Flow Regime Map	74
2.2.2.2-1	Straight Section Pressure Drop vs. Quality; Ground Test; HTRI	77
2.2.2.2-2	Straight Section Pressure Drop vs. Quality; Ground Test; Transition Modified HTRI	78
2.2.2.2-3	One Gravity Straight Section Pressure Drop Data and Predictions	79
2.2.2.2-4	One Gravity Straight Section HTRI Predicted Pressure Drop vs. Test Data Pressure Drop Scatter Plot	80

TABLE OF FIGURES (continued)

<u>Figure Number</u>		<u>Page Number</u>
2.2.2.2-5	One Gravity Straight Section Transition Modified HTRI Predicted Pressure Drop vs. Test Data Pressure Drop	81
2.2.2.2-6	One Gravity Straight Section Taitel and Dukler Predicted Pressure Drop vs. Test Data Pressure Drop Scatter Plot	82
2.2.2.2-7	Test Section Delta Pressure vs. Quality	84
5.3-1	Test Loop Instrumentation Accuracies	91
5.3-2	Heat Rejection Cart	97
5.3.2a	Heat Rejection Cart Schematic	98
5.3-3	Electrical/Control Console	99
5.5.1-1	SFE Heat Loads	106
5.5.2-1	KC135 Aircraft Trajectory	108

NOMENCLATURE/DEFINITIONS

Abbreviations:

BPRV	Back Pressure Regulating Valve
CV	Cavitating Venturi
EGW	Ethylene Glycol/Water
HTRI	Heat Transfer Research Institute *
GPM	Gallons Per Minute
RFMD	Rotary Fluid Management Device
R114	Refrigerant 114
SFE	Swirl Flow Evaporator
TPTMS	Two-Phase Thermal Management System

- * Heat Transfer Research, Inc.
1000 South Fremont Avenue
Alhambra, California 91802-3900

NOMENCLATURE/DEFINITIONS - continued

Equation Variables:

C	=	Correlational Parameter Developed From Data
C_b	=	Ratio of Bubble Velocity to Supercritical Velocity
C_g	=	HTRI Flow Regime Parameter
D_i	=	Inner Diameter
Fr	=	Froude Number
G_T	=	Total Mass Flux
G_c	=	Gravity Constant (one-gravity)
L	=	Length
P	=	Pressure
(dP/dx)	=	Pressure Gradient Assuming Single-Phase Alone Flow
R_{fn}	=	Liquid Volume Fraction
Re	=	Reynolds Number
U	=	Velocity
We	=	Weber Number
X	=	Martinelli Parameter
X'	=	Mandhane Map Parameter
Y	=	Quality
Y'	=	Mandhane Map Parameter
β	=	Void Fraction
ϕ^2	=	Two-Phase Frictional Pressure Drop Multiplier
ρ	=	Density
μ	=	Viscosity
σ	=	Surface Tension
λ	=	Correction Factor
ψ	=	Correction Factor

NOMENCLATURE/DEFINITIONS - continued

Subscripts:

a	=	Air
g	=	Gas
h	=	Homogeneous
l	=	Liquid
l _o	=	Total Liquid Flow
l _s	=	Liquid Superficial
m	=	Homogeneous
tr	=	Transition
v	=	Vapor
v _s	=	Vapor Superficial
v _o	=	Total Vapor Flow
T	=	Total
w	=	Water

1.0 Summary

A test loop was designed, fabricated and tested which allowed two-phase flow observation and pressure drop measurement in reduced gravity. The test loop employed the Sundstrand Two-Phase Thermal Management System (TPTMS) concept which was instrumented for flow, pressure and temperature measurement. Two-phase flow was generated by pumping nearly saturated liquid into a Swirl Flow Evaporator (SFE) (Reference 1) and adding heat via electric heaters. The SFE exit quality was varied by changing the evaporator heat load.

The test loop was specially fitted with a clear two-phase return line and condenser cover for flow observation. The clear two-phase return line and condenser were instrumented for precise pressure drop measurements. The test loop was run on the ground to generate one gravity data, and aboard the NASA-JSC KC135 reduced gravity aircraft to generate reduced-gravity data. The TPTMS test loop operated as expected during the flight and provided both two-phase flow management and thermal control in reduced-gravity. The two-phase flow regimes and vapor condensation were documented on film (Reference 2) and by observation through the clear sections. The ground and reduced-gravity flight data were compared, showing the differences in two-phase flow in one gravity versus reduced-gravity conditions. The test results showed that two-phase flow pressure drops and flow regimes can be accurately predicted in reduced-gravity using existing two-phase flow predictive techniques. The data collected from these tests has greatly increased the present reduced-gravity two-phase flow data base. The data was correlated to enhance present predictive techniques so that pressure drops and line sizes for future two-phase flow applications in zero-gravity can be more accurately predicted.

2.0 Test Results

Results are presented for both reduced gravity flight tests and ground tests which were performed before and after the flight tests. Flight and ground test results are presented for the two-phase test section and condenser test section as well as overall system performance. A schematic of the test loop is shown in Figure 2.0-1. The two-phase clear test section is shown in Figure 2.0-2. See Section 5.3 for a detailed description of the test stand.

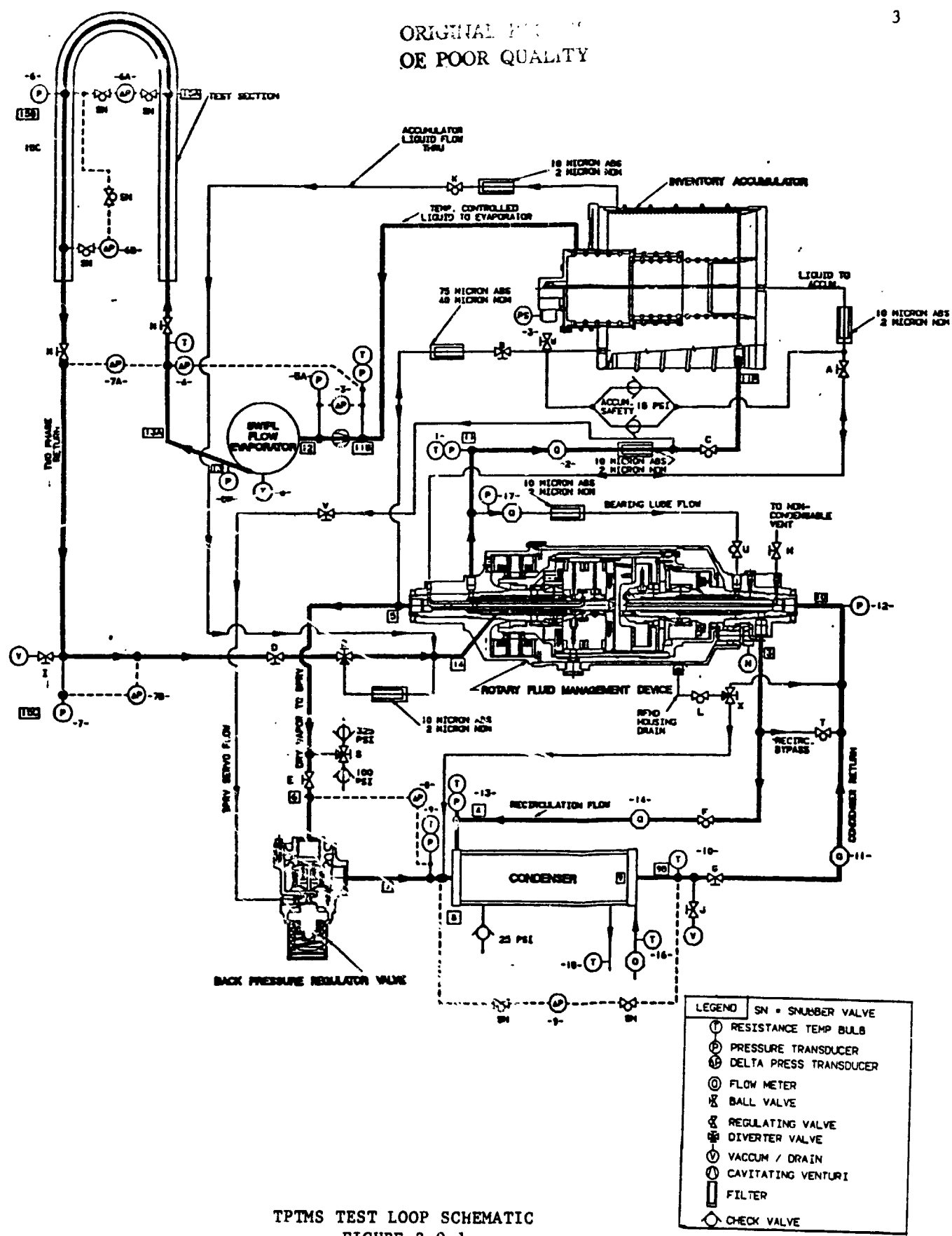
2.1 Reduced Gravity Test Results

2.1.1 Overview

During the flight test, digital data was taken at 2.5 second intervals for the data acquisition channels listed in Figure 2.1.1-1. For the purpose of data reduction, the digital data was averaged after a screening process was used to eliminate gravity levels above 0.1-gravity for the flight test. This screening process left an average of 7 to 9 data points for each flight parabola. A numerical average of the 7 to 9 digital data points of each parabola was used to generate a single data point for correlation of the test results.

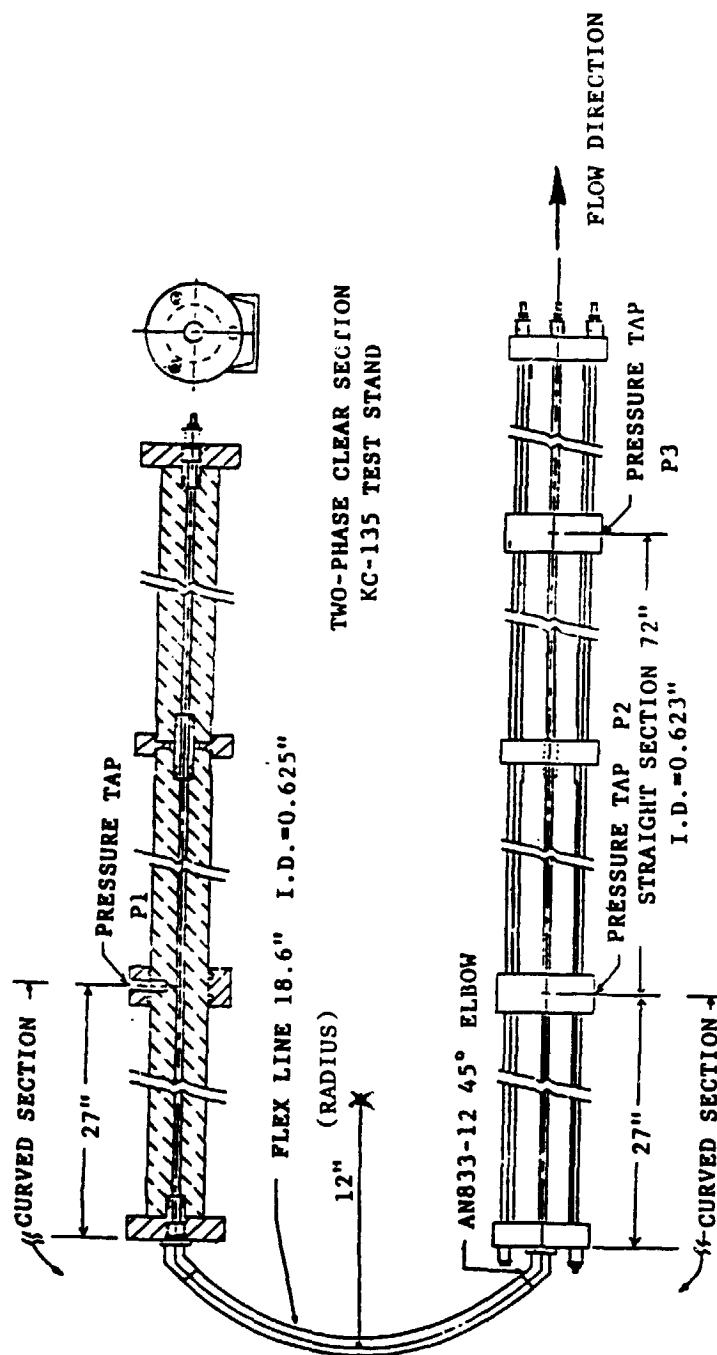
A total of fifty-four parabolae were flown during two days of testing. On the first day, nine SFE heat loads were selected per NASA requirements and each heat load was fixed for three consecutive parabolae (Figure 2.1.1-2) for a total of twenty-seven parabolae. Each heat load provided the required two-phase quality in the test section. The flight profile for the second day (Figure 2.1.1-2) was similar with the addition of three system reduced gravity operation tests. During each parabola, the flow was assumed to be constant at the average value measured during the

ORIGINAL FIGURE
OF POOR QUALITY



TPTMS TEST LOOP SCHEMATIC
FIGURE 2.0-1

$\Delta P_{\text{curved}} = P_1 - P_2 = DP6A$
 $\Delta P_{\text{straight}} = P_2 - P_3 = DP6B$



ADIABATIC TEST SECTION

FIGURE 2.0-2



DATA ACQUISITION CHANNELS
FIGURE 2.1.1-1

<u>CHAN</u>	<u>LOC</u>	<u>CHANNEL NAME</u>	<u>UNITS</u>	<u>COMMENTS</u>
0	T5	TPSFE 01	DEG F	SFE COIL SURFACE TEMP
1	T5	TPSFE 02	DEG F	
2	T5	TPSFE 03	DEG F	
3	T5	TPSFE 04	DEG F	
4	T5	TPSFE 05	DEG F	
5	T5	TPSFE 06	DEG F	
6	T5	TPSFE 07	DEG F	
7	T5	TPSFE 08	DEG F	
8	T5	TPSFE 09	DEG F	
9	T5	TPSFE 10	DEG F	
14		ACCEL X AXIS	G	FORWARD/REAR
15		ACCEL Y AXIS	G	SIDE/SIDE
16		ACCEL Z AXIS	G	UP/DOWN
17		ACCUMUL POSIT	MV	
18	N	RFMD ROT RATE	RPM	RFMD SPEED
20		REF PRESS ATMO.	PSIA	
21	P1	RFMD OUT PRESS	PSIA	EVAP PUMP OUTLET PRESS
22	P3	CAV VEN IN PRESS	PSIA	
23	P5A	EVAP IN PRESS	PSIA	
24	P5B	EVAP MIDPOINT P	PSIA	SFE OUTLET PRESS
25	P6	TEST SECT. PRESS	PSIA	TEST SECTION MIDPOINT PRESS
26	P7	CLEAR SECT P	PSIA	TEST SECTION EXIT PRESSURE
27	P9	COND VAP PRESS	PSIA	
28	P12	CONDNSD LIQ P	PSIA	COND LIQ OUT PRESSURE
29	P13	RECIRC LIQ PR	PSIA	
	P17		PSIA	BEARING PRESSURE SAFETY
30	△P3	CAV VEN DELTA P	PSID	
31	△P4	EVAPOR DELTA P	PSID	SFE + CAV. VENT. DELTA PRESS
32	△P6A	CURVED T SECT DP	PSID	
33	△P6B	ST. T SECT DP	PSID	STRAIGHT TEST SECT. DELTA PRESS
34	△P7A	CLEAR SECT DP	PSID	
35	△P7B	2PH RETURN DP	PSID	
36	△P8	BK 2R DEV R DP	PSID	BPRV DELTA PRESSURE
37	△P9	COND DELTA P	PSID	
40	T1	RFMD OUT TEMP	DEG F	EVAP PUMP LIQUID OUT TEMP
41	T9	COND IN TEMP	DEG F	COND VAPOR IN
42	T4	EVAP OUTLET TEMP	DEG F	
43	T3	CAVIT VENTURI IN	DEG F	
44	T10	COND OUT TEMP	DEG F	
45	T13	RECIRCUL TEMP	DEG F	
46	T15	HEX OUT TEMP	DEG F	COND WATER OUT TEMP
47	T16	HEX IN TEMP	DEG F	COND WATER IN TEMP
48	Q2	EVAP FLOW RATE	GPM	
49	Q11	COND FLOW RATE	GPM	
50	Q14	RECIRC FLOW RATE	GPM	
51	Q16	H ₂ O FLOW RATE	GPM	COOLING CART WATER FLOW RATE
	Q17		GPM	BEARING FLOW SAFETY
52		HEATER NO. 1 PWR	WATTS	OUTER SFE HEATERS
53		HEATER NO. 2 PWR	WATTS	INNER SFE HEATERS

TPTMS REDUCED GRAVITY FLIGHT PROFILE SUMMARY

FIGURE 2.1.1-2

Parabola Number	Heat Load (Watts)	Swirl Flow Evaporator Exit Quality	Comments
Thursday, April 16, 1987:			
1 - 3	240	.05	
4 - 6	480	.1 *	
7 - 9	720	.15	
10 - 12	950	.2	
13 - 15	1330	.3	
16 - 18	1900	.4	
19 - 21	2800	.6	
22 - 24	3800	.8	
25 - 27	240	.05	
Friday, April 17, 1987:			
1 - 3	3800	.8	
4 - 6	2800	.6	
7 - 9	2400	.5	
10 - 12	1330	.3	Condenser recirculation on
13 - 15	950	.2	
16 - 18	720	.15	
19 - 21	480	.1	
22 - 24	1900	.4	Loss of heat rejection test
25	1900 to 0	.4 to 0	Reduced-gravity RFMD shutdown
26	0 to 1900	0 to .4	Reduced-gravity RFMD startup
27	1900	.4	

* No digital data available

parabola. The flow rate varied for two reasons during the course of the experiment. During the flight maneuvers, changing hydrostatic loadings resulted in a short-term transient in the evaporator mass flow. This small variation in mass flow is further discussed in Section 2.1.4.1. Also, the mass flow changed slightly with the heat load, as the cavitating venturi was not fully choked. The cavitating venturi was sized before the test loop design was completed. At the time of the test a decision was made not to resize the cavitating venturi and to control the flow by the throttle valve upstream of the system evaporator. The throttle valve was set at a position to give approximately 80 percent quality at the full heat load at design power of the swirl flow evaporator heater. As the power was reduced, thereby reducing the effective quality through the adiabatic test section, the mass flow increased slightly with the changing quality due to the decreased pressure drops in the two-phase sections. The test results, however, fell within the predicted range of mass flows and results could be compared with pretest predictions.

Photographs of the test setup during the flight tests are shown in Figures 2.1.1-3 to 2.1.1-5.

2.1.2 Two-Phase Adiabatic Test Section

2.1.2.1 Two-Phase Flow Regimes

Observations were made of the two-phase flow test section during real time by Dr. E. Keshock, and a transcript of his observations is included in Appendix B. High speed cinematography was also used to inspect the flow regimes. A list of the films is given in Appendix E. Figure 2.1.2.1-1 summarizes the observations made of two-phase flow regimes during this test sequence at different qualities. These flow regime observations have been summarized to match those given by Dukler (Reference 3). Dukler's regimes may be

ORIGINAL PAGE IS
OF POOR QUALITY



Figure 2.1.1-3 Reduced Gravity Flight Test Aboard
NASA-JSC KC-135

ORIGINAL PAGE IS
OF POOR QUALITY

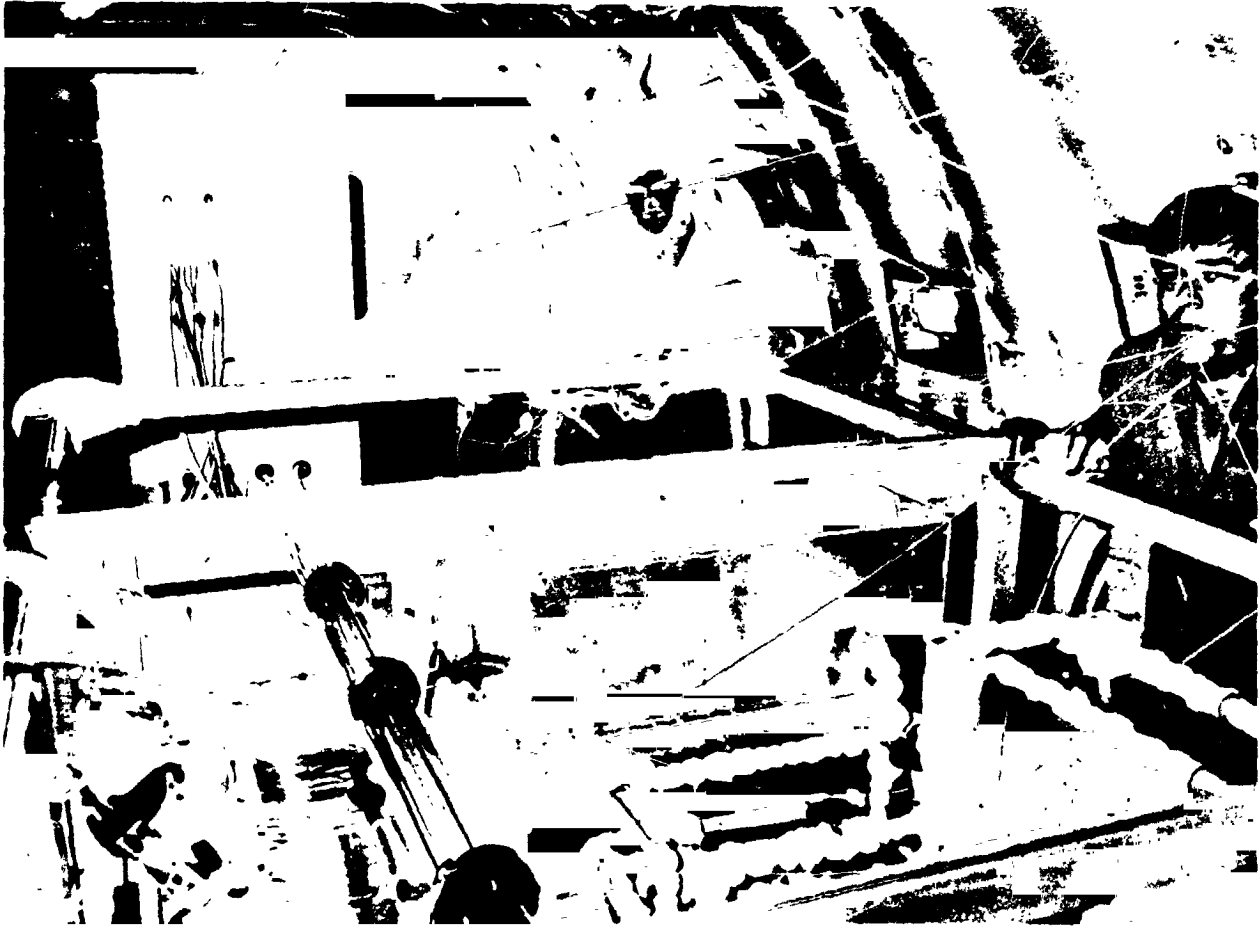


**Figure 2.1.1-4 Reduced Gravity Flight Test Aboard
NASA-JSC KC-135**

ORIGINAL PAGE IS
OF POOR QUALITY



**Figure 2.1.1-5 Reduced Gravity Flight Test Aboard
NASA-JSC KC-135**

REDUCED GRAVITY FLOW REGIME OBSERVATIONSFIGURE 2.1.2.1-1

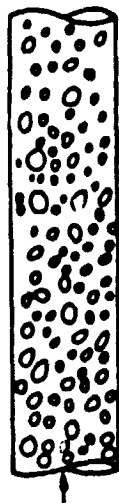
<u>Quality</u>	<u>Observed Flow Pattern Description</u>	<u>Flow Regime</u>
0.05	Long Taylor bubbles followed by liquid slugs	Slug
0.1	Short Taylor bubbles followed by liquid segments	Slug
0.15	Annular flow separated by liquid segments	Slug/Annular
0.2	Fully developed continuous annular flow with occasional droplet mist bridging	Annular
0.3	Fully developed annular flow with thinner film with occasional droplet mist bridging	Annular
0.4	More pronounced annular flow	Annular
0.5	Annular/mist	Annular
0.6	Annular/mist	Annular
0.8	Annular/mist (thinner annular film)	Annular

summarized as bubble, slug, and annular and are shown in Figure 2.1.2.1-2a. A fourth flow regime, mist flow should also occur for high qualities at large mass fluxes.

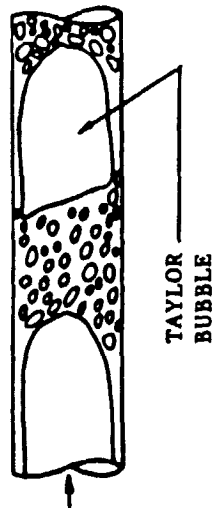
Bubble flow is designated when the gas bubbles observed are less than or equal to the tube diameter size. The liquid flow is continuous in this flow regime. Slug flow occurs when bubbles exist which are greater in length than the tube diameter separated by regions where liquid completely fills the flow area, even though this liquid may carry dispersed bubbles. Annular flow occurs when the liquid never bridges across the tube, but flows in an annular film along the tube perimeter. The fourth flow regime, mist flow, should also be considered. For high mass fluxes at qualities near unity, mist flow should occur in reduced gravity as it does in normal gravity. In mist flow, small liquid droplets are dispersed in the vapor flow. A transition type flow pattern, mist-annular has been identified for the condition of both mist and annular phase distributors.

Using this nomenclature, only two of the four flow regimes were observed in the reduced gravity testing. For qualities below 10 percent continuous liquid slugs were interspersed with bubbles of high vapor void fraction. These bubbles took the form of classical "Taylor bubbles" which are bullet nosed and boat-tailed and generally exist in a one-gravity upflow environment, as shown in Figure 2.1.2.1-2a and -3. Above about 15 percent quality, an annular film was observed to exist and liquid never completely bridged across the tube. In the transition region, between 10 and 15 percent quality, the liquid surface seemed to have an increased roughness and occasional areas of droplet mist were seen to exist. This flow pattern is very similar to a churn type flow that has been shown to exist in other applications in one-gravity vertical upflow (Figure 2.1.2.1-3) except flow reversal never was observed to occur. At the highest qualities tested, mist-annular flow was observed.

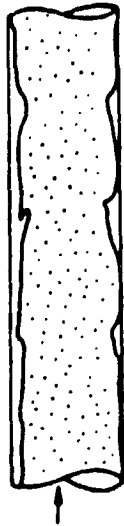
BUBBLE



SLUG



ANNULAR/ANNULAR MIST



- CONTINUOUS LIQUID PHASE
- DISPERSED BUBBLES SMALLER THAN THE TUBE DIAMETER

- INTERMITTENT CONTINUOUS LIQUID SEGMENTS WITH BUBBLE LENGTH LONGER THAN THE TUBE DIAMETER

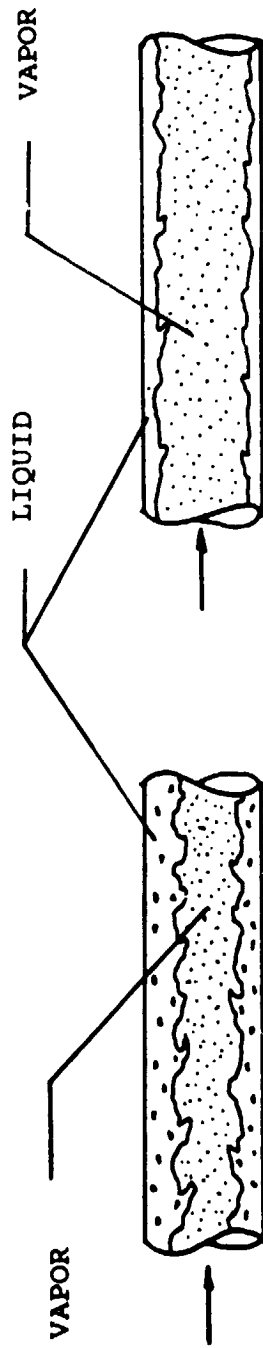
- LIQUID FLOW IN CONTINUOUS ANNULAR FILM ON TUBE WALL WITH VAPOR CORE

MIST



- SMALL DISPERSED LIQUID DROPLETS

FLOW REGIMES IN REDUCED GRAVITY
FIGURE 2.1.2.1-2a



REDUCED-GRAVITY FROTHY ANNULAR FLOW

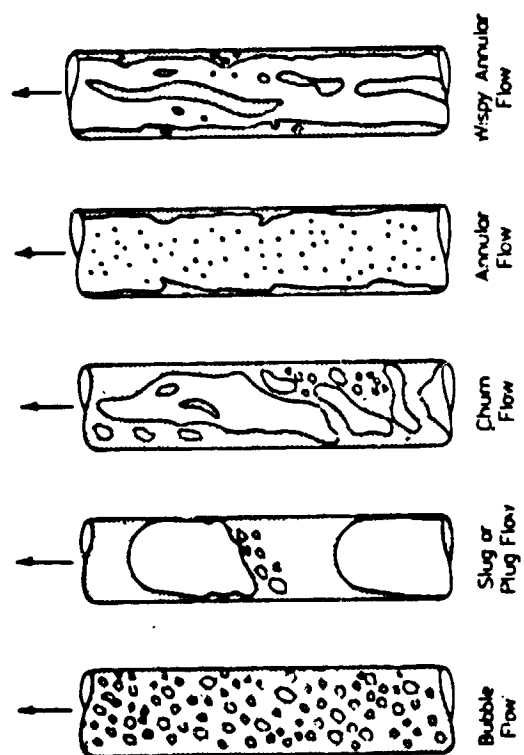
- LIQUID FLOW IN CONTINUOUS THICK ANNULAR FILM ON TUBE WALL WITH VAPOR CORE
- LIQUID VELOCITY IS GREATER THAN IN ONE-GRAVITY ANNULAR FLOW
- VOID FRACTION IS LESS THAN IN ONE-GRAVITY ANNULAR FLOW
- SMALL DISPERSED BUBBLES IN THICK ANNULAR FILM

ONE-GRAVITY ANNULAR FLOW

- LIQUID FLOW IN CONTINUOUS THIN ANNULAR FILM ON TUBE WALL WITH VAPOR CORE

REDUCED-GRAVITY FROTHY ANNULAR FLOW

FIGURE 2.1.2.1-2b



ONE-GRAVITY

FLOW PATTERNS IN VERTICAL UPFLOW

FIGURE 2.1.2.1-3

Preliminary investigations of the film footage at higher qualities indicate that a fifth flow regime may exist in reduced-gravity. Observations show considerable thickening of the annular liquid film compared to ground testing (approximately two-to-one), with what appears to be a significant vapor phase content. Figure 2.1.2-2b, shows a graphical interpretation, contrasting the flow patterns of reduced gravity with that of normal gravity. The "enriched" liquid film tumbles with considerable turbulence and occasional 'roll-waves', entraining the vapor phase bubbles in a frothy mixture at the liquid film surface.

The increased film thickness, surface roughness and reduced vapor core flow area that occurs as a result of this vapor entrainment may explain the somewhat higher pressure drops than anticipated at the high qualities as will be discussed in Section 2.1.2.2. Analytical pursuit of this "frothy annular" flow regime was not undertaken since it was not within the scope of the contract. However, it may be worthy of future efforts, both analytical and experimental.

The major reason for performing the KC135 series of tests was to generate sufficient reduced-gravity data that accurate predictions can be made of pressure drops in a two-phase system for future space applications such as space station. Previous data generation indicates that pressure drop tends to increase in reduced-gravity, presumably due to changes in two-phase flow regime. Thus an accurate prediction of the reduced-gravity flow regimes in zero-gravity is important. An element of the data reduction was to take the observed data and correlate it with anticipated flow regimes by plotting it on various flow regime maps and ultimately use this for future predictions with the working fluids and different geometries, qualities and mass fluxes.

Four different maps for horizontal two-phase flow patterns were selected. The Taitel and Dukler (Reference 4) and the Heat Transfer Research Institute (HTRI) (Reference 15) have some dependence on the gravity field since a "g" term is utilized in the plotting parameters. The Baker map (Reference 11) and the modified Dukler (Reference 3) have no gravity-dependence. The Baker map is a standard one-gravity horizontal flow predictor while the modified Dukler map was derived for zero-gravity. The data from the KC135 tests have been plotted on the maps with each data point identified for the observed flow type and operating quality.

The Taitel and Dukler map, Figure 2.1.2.1-4, utilizes the modified Froude number plotted versus the Martinelli perimeter. The modified Froude number is a measure of the interfacial shear forces as compared to the gravity forces in the fluid and is defined by:

$$Fr = G_t y / \sqrt{(\rho_L - \rho_V) \rho_V g D_i}$$

Where:

G_t = is the total mass flux

y = quality

D_i = tube diameter.

ρ_L = Liquid Density

ρ_V = Vapor Density

g = Gravity

The Martinelli parameter, X , is the ratio of the liquid pressure drop flowing alone in the tube to the gas pressure drop flowing alone in the tube. The Martinelli parameter is given by:

$$X = \frac{(dP/dx)_L}{(dP/dx)_V}$$

Where:

$(dP/dx)_l$ = Pressure gradient assuming the liquid is flowing alone

$(dP/dx)_v$ = Pressure gradient assuming the vapor is flowing alone

An important transition on this flow regime map is the transition between annular type flow and slug flow. It was shown by Taitel and Dukler (Reference 4) to occur where the value of the Martinelli parameter is 1.6. This transition is expected to be a gradual one since it is not possible to distinguish between a highly aerated slug and an annular flow with large roll waves.

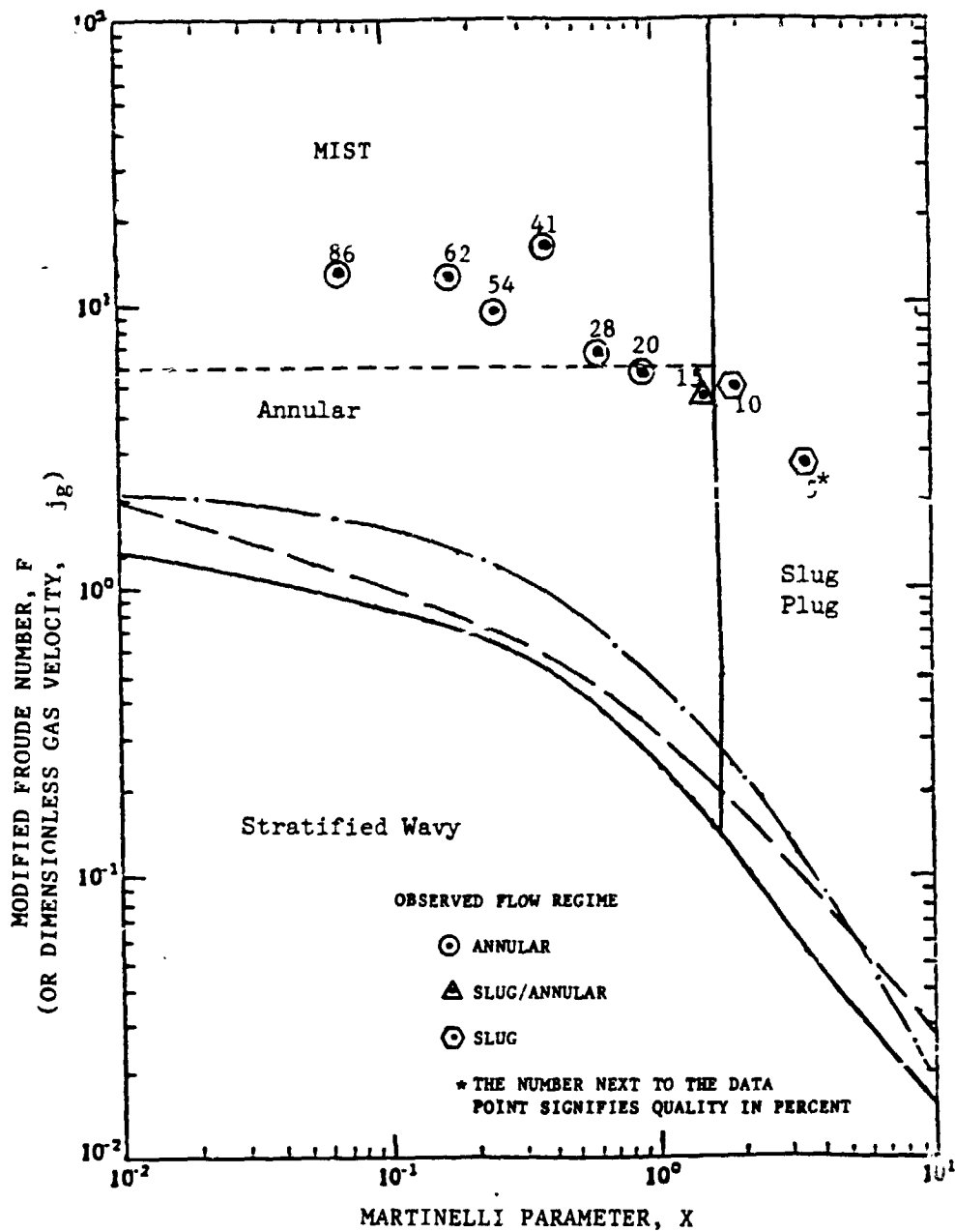
Using visually observed flow regimes for reduced gravity testing, the boundary between slug and annular flow correlates well with the Taitel and Dukler transitional Martinelli parameter of 1.6 as can be seen by referencing to Figure 2.1.2.1-4. The quality at which this transition was expected to occur can be found by substituting the liquid and vapor densities and viscosities into the definition of the Martinelli parameter. With rearrangement,

$$y \text{ (slug/annular transition)} = \frac{1}{\{ [1.6 (\rho_l/\rho_v)^{0.5} (\mu_v/\mu_l)^{0.1}]^{1.1} + 1 \}}$$

Where: μ_v = Vapor Viscosity
 μ = Liquid Viscosity

using the average conditions of the reduced gravity data, this reduces to transition quality value $y = 0.1125$. This value of quality corresponds well with the actual value observed for the flow pattern transition.

FIGURE 2.1.2.1-4



Flow Map Proposed by Taitel and Dukler

- Taitel & Dukler (Reference 4)
- . - . Sardesi et al. Transition for Condensation Between Annular and Stratified Flow Regimes (Reference 12)
- Modified Taitel & Dukler
($f_l = 3f_g$, Proposed by Kawaji et al (Reference 13))
- Tandom et al (Reference 14)

The transition between annular and mist flow on the Froude vs. Martinelli flow regime map should occur when the amount of liquid carried as a droplet mist exceeds the amount of liquid flowing in the liquid film along the pipe wall. For the range of data observed in the KC135 flight tests, annular flow persisted even to the highest qualities tested with a fairly uniform liquid film around the entire tube perimeter but also with significant mist flow in the vapor core. Thus the Taitel and Dukler flow regime map seems to provide a good fit of observed flow regimes with predictions in reduced-gravity.

Figure 2.1.2.1-5 shows the Heat Transfer Research Institute (HTRI) flow regime map with the reduced gravity data plotted on the map. HTRI flow regime maps are plots of a parameter, C_g , versus the homogeneous liquid volume fraction R_{gh} . HTRI, a member proprietary group, has formulated a dimensionless parameter C_g which is similar to the Froude number. It represents the relative importance of the gravity force as compared to the vapor shear forces.

The homogeneous liquid volume fraction is defined by:

$$R_{gh} = 1 - \beta_h$$

where: β_h = Homogeneous void fraction

The homogeneous liquid volume fraction is computed assuming the two phases to be flowing at the same velocity.

For the HTRI map, the important transition is at the homogeneous liquid volume fraction value of 0.1. Below this point the interspersed type bubble flows give way to an annular type flow designated as a froth on the flow regime map. The basis for this flow regime transition criteria is that the bubble population density can only reach approximately 0.9 void fraction without the bubbles coalescing and forming a continuous vapor core flowing down the center of the tube.

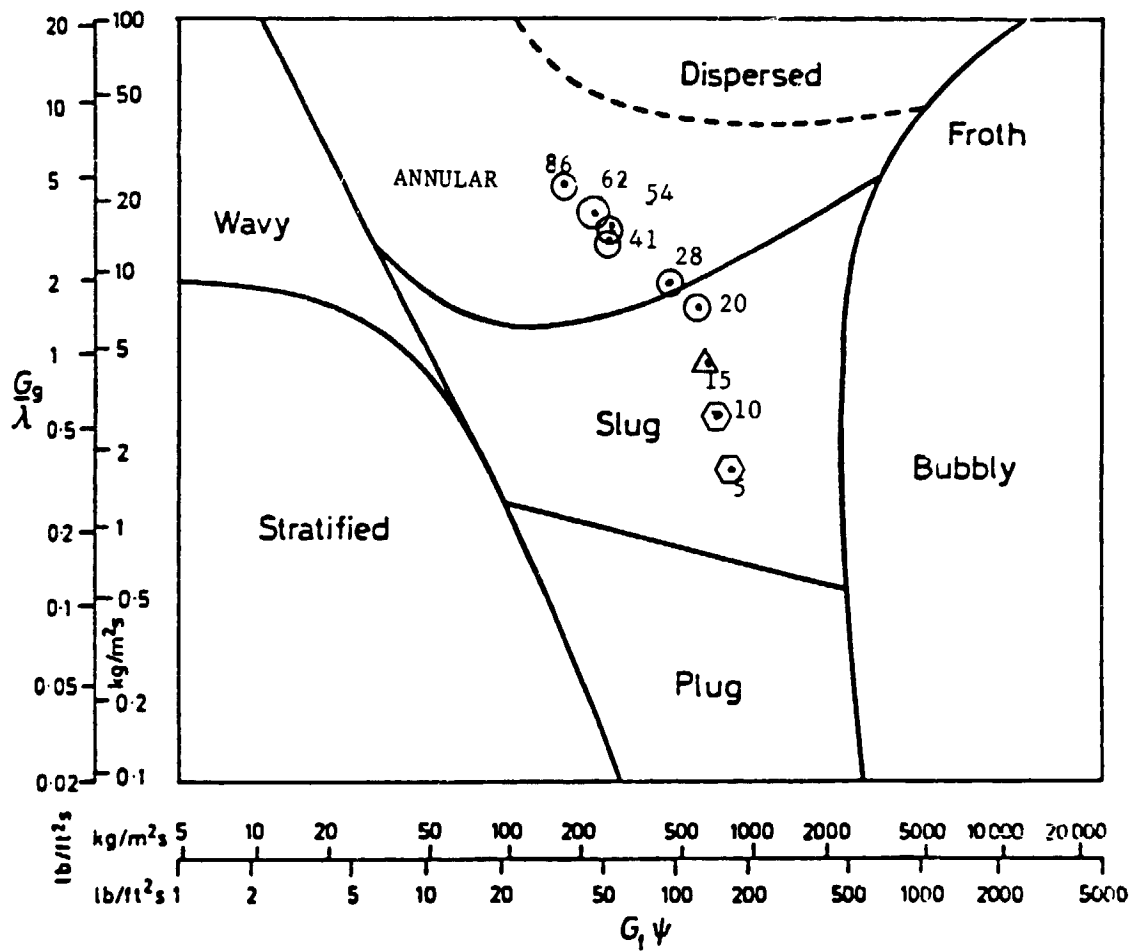
When the data is plotted on the HTRI flow regime map, the anticipated flow regimes would be mist/froth flow changing to bubble flow at a quality of 20 to 25 percent. The observed flow regimes were actually annular, passing through a transition zone to slug flow as quality is reduced. It can be seen that a modification of the location of the transition line on the ordinate, in terms of C_g would provide an excellent fit to the data. When these transition boundaries were altered, the HTRI pressure drop algorithm, which is flow regime dependent, correlated well with the test data. This modification is probably valid since the HTRI map was generated from data for horizontal condensation rather than adiabatic flow.

The third map that was investigated is the Baker type map (Figure 2.1.2.1-6) as presented by Bell in 1970, (Reference 11). This empirically derived horizontal flow map relates the vapor and liquid mass fluxes which have been corrected for property effects. The two-phase test data was primarily generated using air and water mixtures, but some data was generated using oil and gas mixtures. To account for the differences in properties using the map for other than air and water at one atmosphere, correction factors and were developed. These parameters are defined by:

$$\lambda = \left(\frac{\rho_g \rho_l}{\rho_a \rho_w} \right)^{0.5}$$

$$\psi = \frac{\sigma_w}{\sigma} \left(\frac{\mu_l}{\mu_w} \left(\frac{\rho_w}{\rho_l} \right)^2 \right)^{1/3}$$

Where ρ , σ and μ represent the density, surface tension and viscosity, the subscripts g and l represent the gas and liquid



Flow pattern map for horizontal flow (Baker)

OBSERVED FLOW REGIME

⊙ ANNULAR

△ SLUG/ANNULAR

⊙ SLUG

* THE NUMBER NEXT TO THE DATA POINT SIGNIFIES QUALITY IN PERCENT

REDUCED-GRAVITY
BAKER FLOW REGIME MAP

FIGURE 2.1.2.1-6

phases, and the subscripts a and w represent the values for air and water at atmospheric conditions. Clearly λ and ψ are unity for air-water flows at one atmosphere. For the R114 at the average test conditions these property correction factors are quite large, with $\lambda=7.3$ and $\psi=3.1$.

This map is based on a one-gravity empirical correlation and has no explicit gravity dependence. However, it can be seen that a relatively good fit of reduced-gravity data was obtained with a transition from annular to slug occurring at qualities somewhat lower than expected. It will be shown in Section 2.2 that a very poor fit was obtained for one-gravity testing, where this map should be appropriate.

Finally, the KC135 flight data was plotted on the modified Dukler flow regime map, shown in Figure 2.1.2.1-7. This map was specifically derived for reduced-gravity two-phase flows, and has been developed from air-water data from drop tower and Lear jet experiments (Reference 5). The transition boundaries are partially derived from phenomenological reasoning rather than purely empirical data. The flow transition between bubble and slug flow is based on the coalescence of smaller bubbles into slugs. For homogenous flow of the vapor bubbles within the liquid, the bubble/slug transition would occur at a quality of 2.5%, lower than that tested.

The transition from slug to an annular flow pattern is based on the physical models of each type of flow. When the void fraction of the slug flow model matches the apparent void fraction of the annular flow model, the transition is assumed to take place.

The void fraction for annular flow can be determined knowing the phase velocities and using correlations for the interfacial and

REDUCED—G KC-135 R-114 Data on Modified Dukler Map

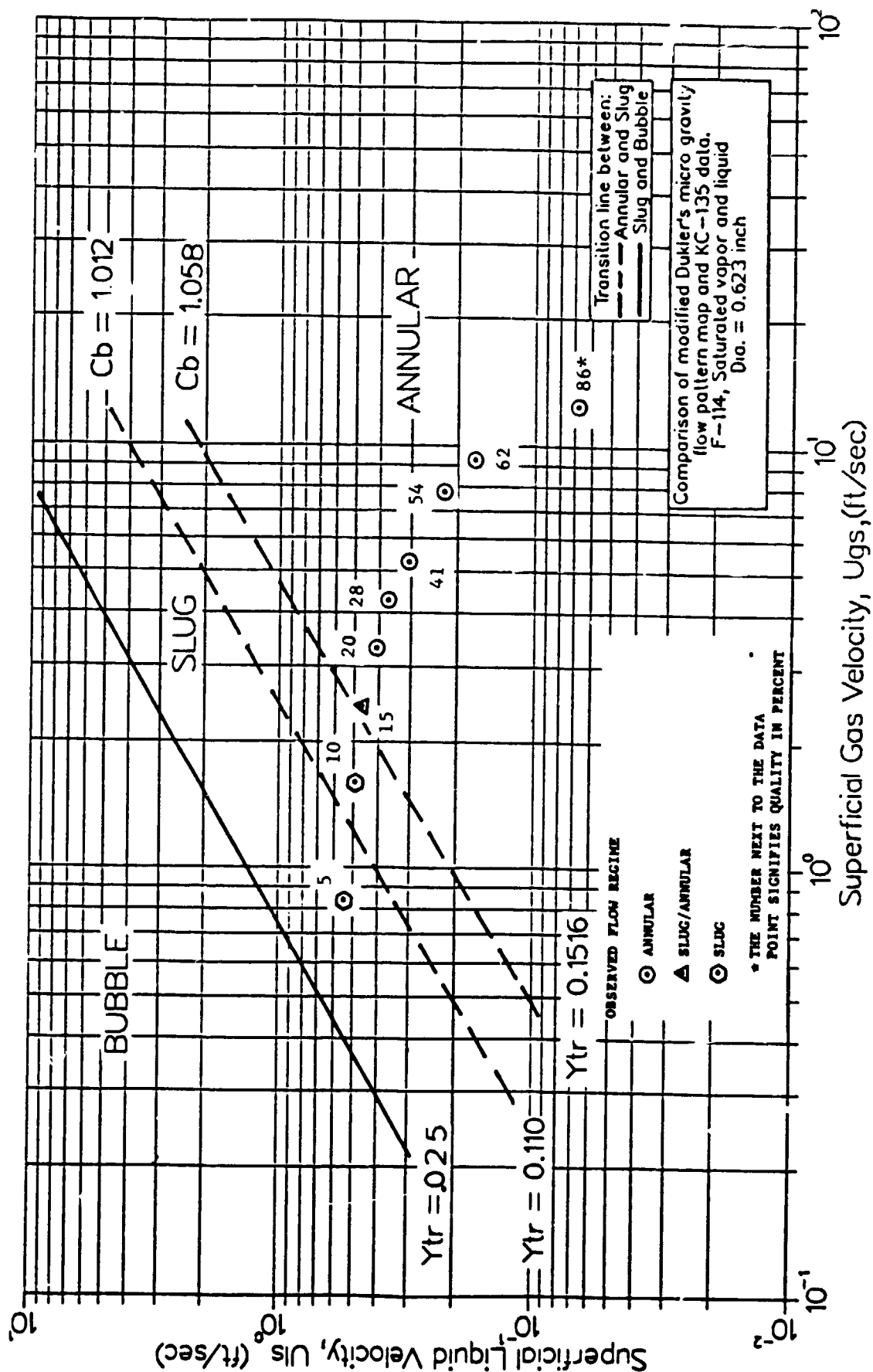


Figure 2.1.2.1-7

wall friction factors. For this analysis, the interfacial shear stress suggested by Wallis (Reference 6) was utilized.

Flow visualization studies can be used for determining the void fraction in slug flow. The reduced gravity film footage was inspected and it was observed that the velocity of the bubbles is the same as the liquid slugs. The bubble velocities can also be measured from the films and related to the total overall superficial velocities, calculated from the test data. This relationship can then be used to determine the void fraction of the slug flow, and thereby the transition boundary to annular flow. The empirical constant used for this analysis, C_b , is defined by:

$$C_b = U_b / (U_{vs} + U_{ls})$$

Dukler has determined that the bubble velocity is 20 percent greater than the superficial mixture velocity for his air-water testing ($C_b = 1.2$). Using the R114 properties and this value for C_b , no transition boundary exists as the void fraction from the slug model is always higher than the annular value. A study was made to measure the ratio of the bubble velocity to the overall superficial velocity of the phases. Preliminary measurements for the Taylor bubble velocities from the films indicate that C_b ranges from 0.94 to 1.13 with an average value of about 1.012. Using a value of $C_b = 1.012$, the transition quality between annular and slug would be 8.2%, which is less than the observed transition quality. Transition lines are plotted in Figure 2.1.2.1-7 for various values of C_b . It can be seen that the use of a value of $C_b = 1.058$ most closely matches the observed transition from slug to annular flow. From observations of the flow and the fact that the liquid slugs appear relatively clean of smaller bubbles, it can be presumed that for our testing the bubble velocities were much closer to the overall superficial velocity. Thus more homogeneous flow is presumed to exist as compared to air-water testing. This

makes physical sense in that the density ratio of the R114 system is roughly thirty times less than the air-water system tested in the NASA-LeRC drop tower and Lear jet experiments (Reference 5).

In conclusion, two flow regimes were observed in the reduced-gravity testing, slug flow and annular flow. Bubble flow would be expected at lower qualities than those tested and the transition from mist-annular to mist would occur at higher qualities than those tested. The boundary between slug and annular flow was best predicted by the flow map of Dukler and Taitel (Reference 4), and the reduced-gravity map of Dukler, with the modified value of $C_D = 1.058$. It should be noted that these predictive methods are essentially identical.

2.1.2.2 Pressure Drops

Averaged test data of measured pressure drop versus quality for a variety of mass flows is shown in Figure 2.1.2.2-1 for the straight test section and Figure 2.1.2.2-2 for the curved test section during reduced gravity testing. The data points from flight test date April 16 are shown as circles and those of flight April 17 shown as squares.

Prior to the flight tests, HTRI techniques were used to predict pressure drops at varying mass flows, which are represented by dashed lines in Figures 2.1.2.2-1 and 2. Each test data point is connected to the predicted pressure drop (indicated by a triangle) for those actual test conditions by a line whose length represents both the error in the predictive method and error in the experimentally determined pressure drop. The pressure drops were somewhat higher on the second day of testing as compared to the first day of testing. The agreement between predicted pressure drops and those experimentally measured is, in general, excellent. The best agreement occurs in the middle quality ranges from

STRAIGHT SECTION PRESSURE DROP VS QUALITY

REDUCED GRAVITY

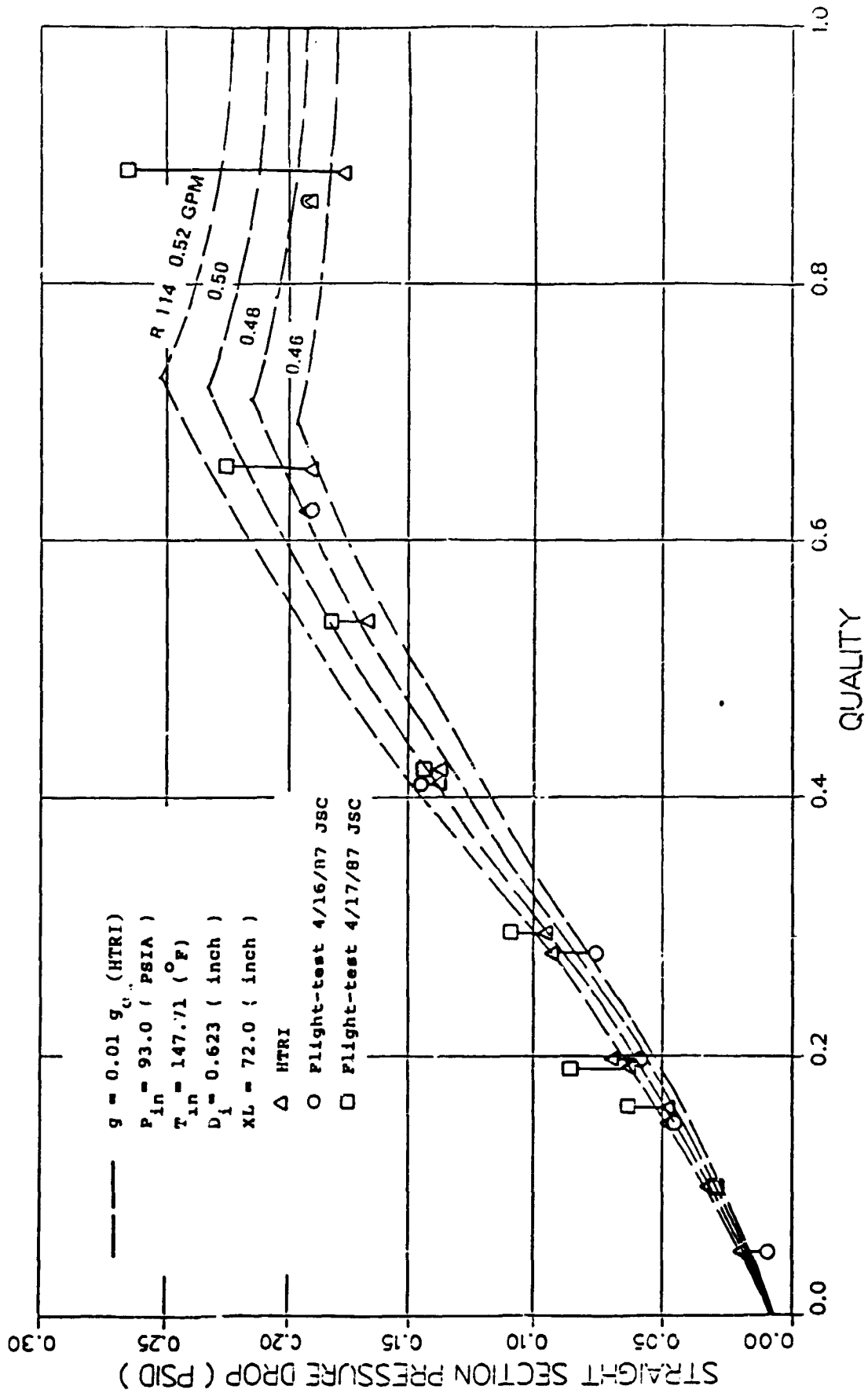


FIGURE 2.1.2.2-1

CURVED SECTION PRESSURE DROP VS QUALITY

REDUCED GRAVITY

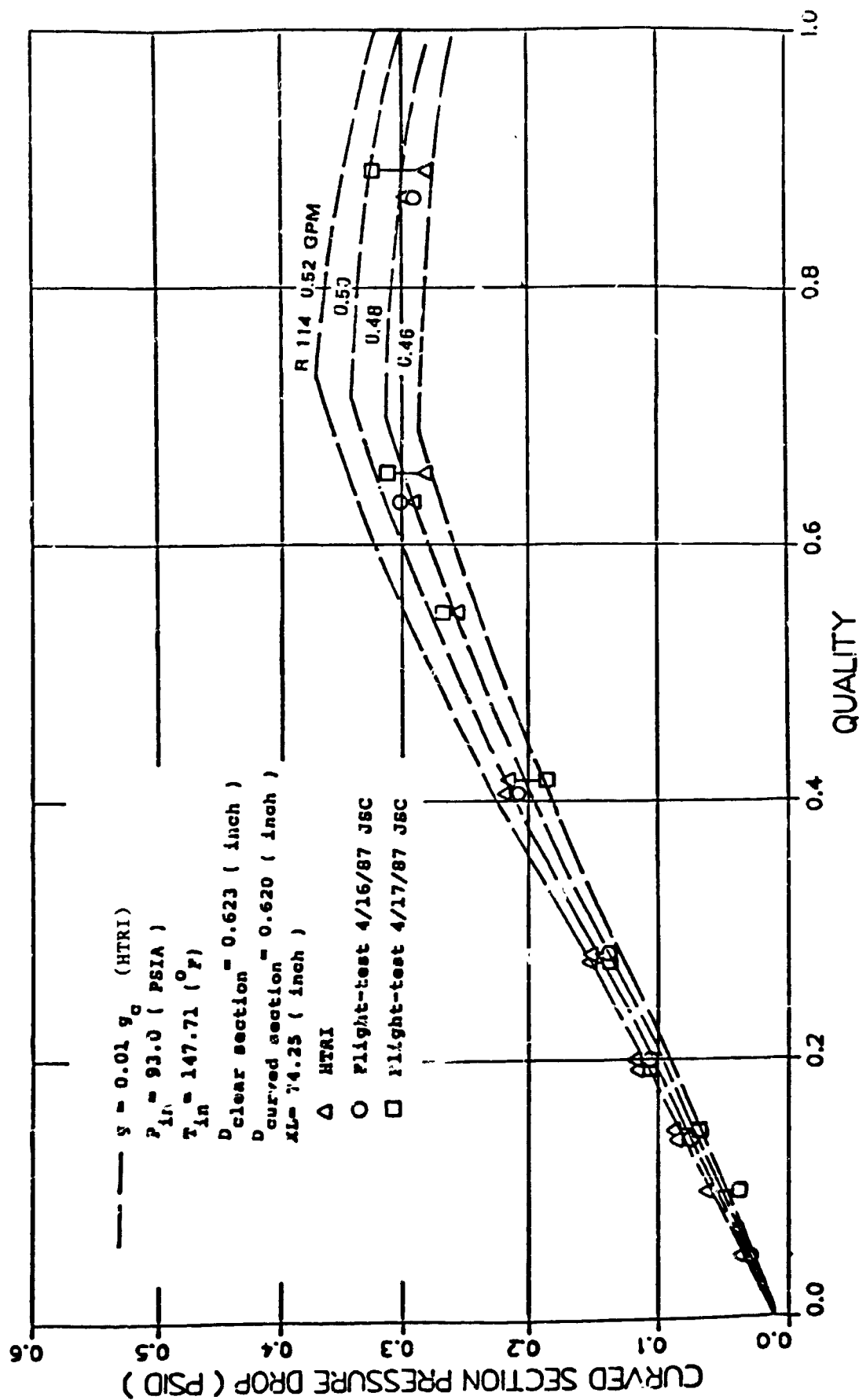


FIGURE 2.1.2.2-2

qualities of 0.3 to 0.6. At the very low qualities where the experimental accuracy of the pressure transducers is limited, the measured pressure drops were lower than the predicted values. In some cases, the experimentally measured pressure drops were lower than calculated pressure drops that would occur for liquid flowing alone in the tube at that same mass velocity which obviously is not feasible. The HTRI method tended to under-predict the pressure drops in the high quality regions.

For a given total mass flow rate, the pressure drop is expected to increase with increasing quality, as long as a liquid film annulus is maintained on the tube wall. At very high qualities (higher than those tested in this experiment), it is presumed that the liquid would not continuously wet the wall but be carried as a droplet mist and the pressure drop would decrease with increasing quality. Under these conditions, a homogeneous flow model would be appropriate.

Since the HTRI model tended to under-predict pressure drop at high qualities, it was adjusted so that an annular type formulation was used for the high quality pressure drops. The results are plotted in Figure 2.1.2.2-3 and 2.1.2.2-4. The correlations used in these figures are the same as those used for the pretest predictions, however, the transition point between the annular and mist correlations has been adjusted. For the purposes of this report, this technique will be called the wet wall modified FTRI method. The correlation includes a two phase multiplier applied to the pressure drop of the liquid flowing alone in the tube. This formulation is appropriate whenever an annular liquid film is present and represents an active shear transport mechanism. From observations of the high speed films generated in these tests a turbulent liquid film persisted even at the highest qualities tested near 90 percent.

STRAIGHT SECTION PRESSURE DROP VS QUALITY

REDUCED GRAVITY

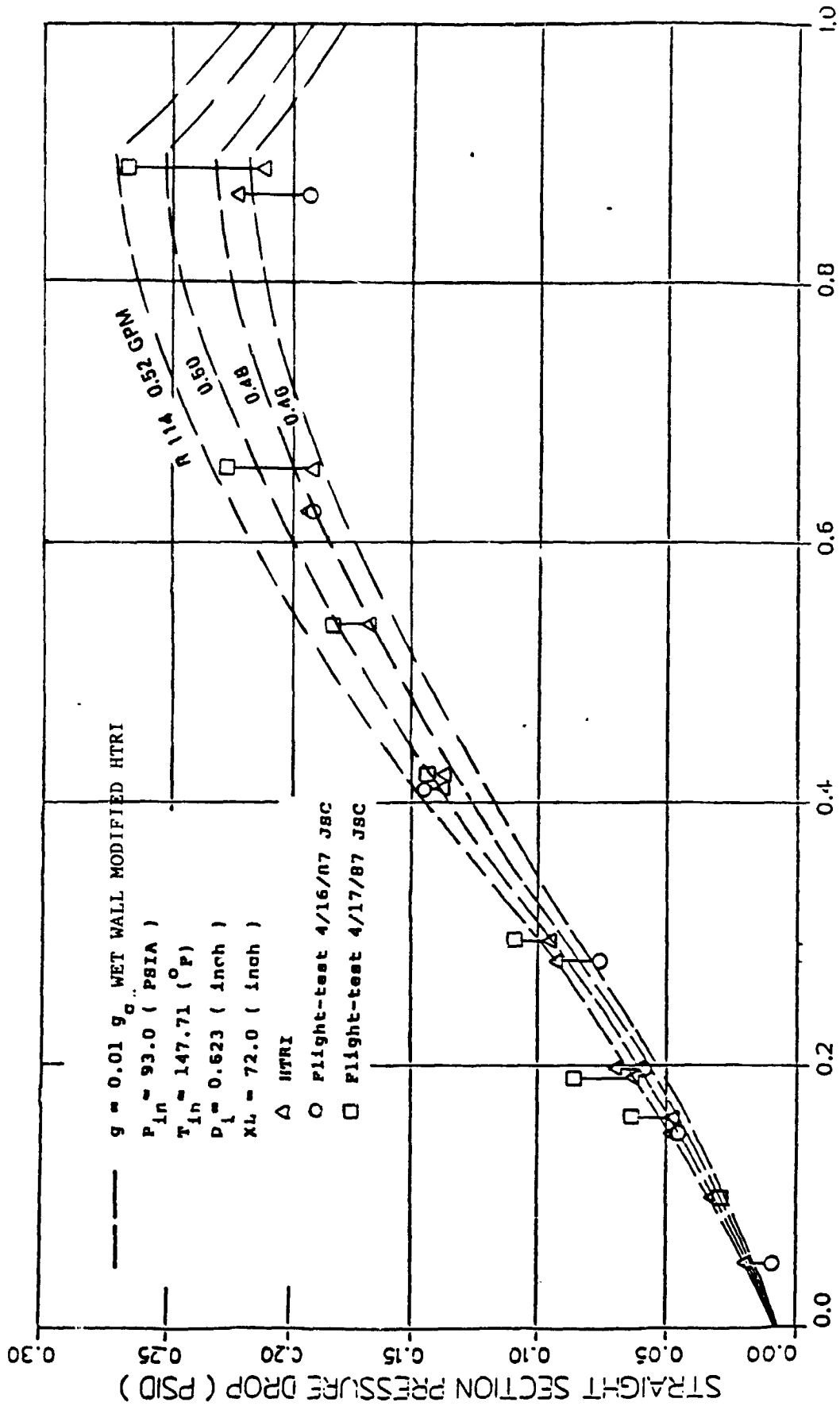


FIGURE 2.1.2.2-3

CURVED SECTION PRESSURE DROP VS QUALITY

REDUCED GRAVITY

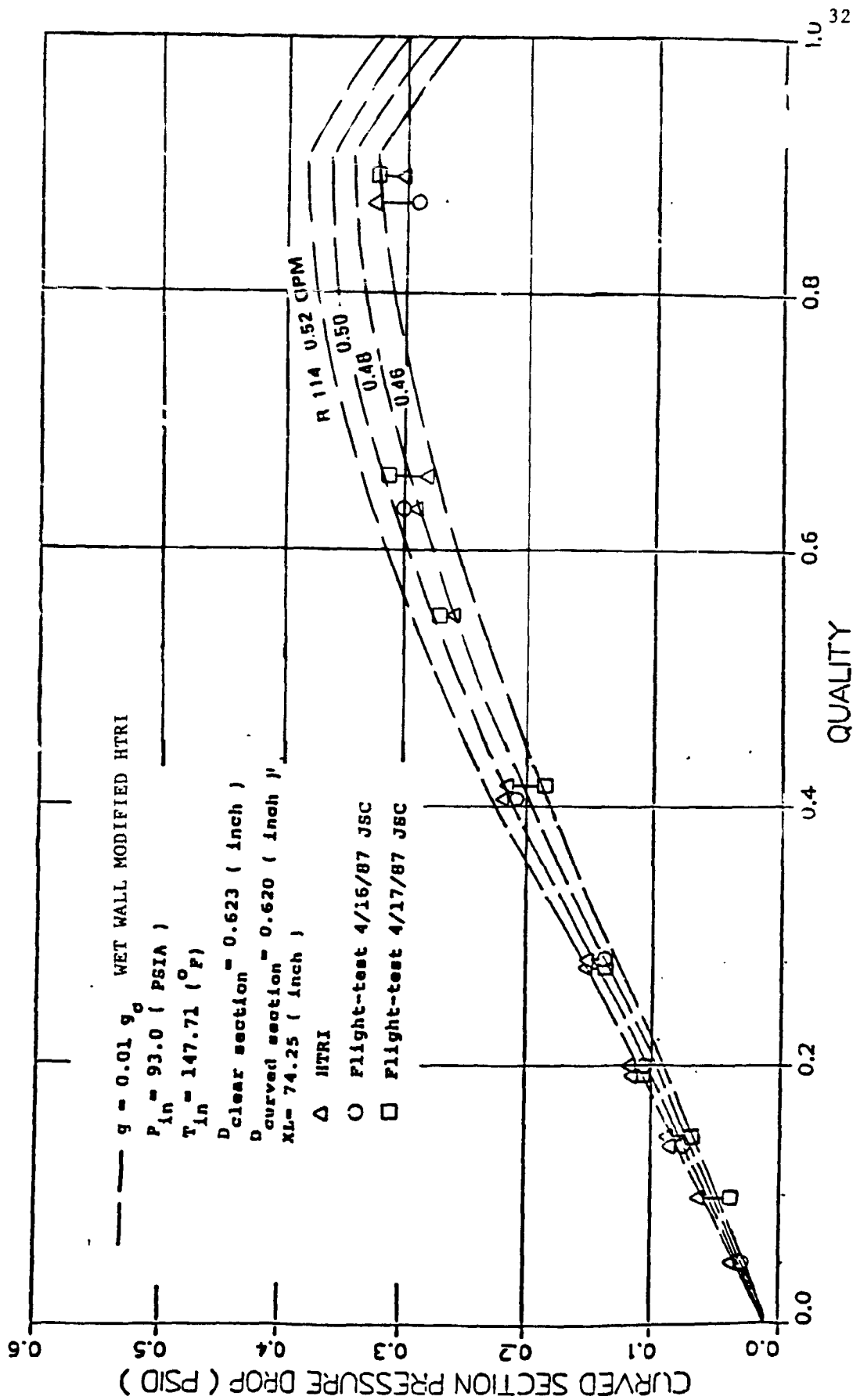


FIGURE 2.1.2.2-4

The test predictions for the curved section include the frictional pressure drop of the straight sections preceding and following the curved section as well as the frictional pressure drop in the 110° arc flex line. Chisholm type B and C correlations (Reference Appendix C) were used for the curved section and the HTRI method was used for estimating the straight sections. The measured pressure drop shows a higher degree of repeatability for the curved section compared to the straight section.

A statistical analysis was performed for 45 representative data points taken for the straight section. Several pressure drop predictive techniques (Appendix D) were employed over the range of qualities and flow conditions observed. Figure 2.1.2.2-5 shows a compilation of all the acceptable (less than 0.1 g) reduced gravity pressure drop data along with the deviation from prediction for the following predictive methods.

- o Wet Wall Modified HTRI
- o Lockhart - Martinelli
- o Modified Lockhart - Martinelli
- o Friedel
- o Chisholm B-type
- o Homogeneous
- o Taitel and Dukler Stratified
- o Chisholm Stratified
- o HTRI (unmodified)

Figure 2.1.2.2-6 shows the mean sample errors and standard deviation for these methods using the 45 data points. Flow charts of some of these formulations are given in Appendix D.

Of these methods, only the Friedel (Reference 7) and HTRI are sensitive to the gravity level. The HTRI method correctly predicts that the pressure drops will increase during zero-gravity while the

STRAIGHT SECTION - 45 DATA POINTS

	$\left[\frac{DP_{PRED} - DP_{TEST}}{DP_{TEST}} \right]$		AVG	σ
1) WET WALL MODIFIED HTRI	-0.035			0.278
2) LOCKHART-MARTINELLI	0.950			1.225
3) MODIFIED LM	0.656			1.059
4) FRIEDEL	-0.040			0.614
5) CHISOLM B-TYPE	0.516			0.967
6) HOMOGENEOUS	0.402			0.368
7) TAITEL & DUKLER STRATIFIED	-0.491			0.233
8) CHISOLM STRATIFIED	-0.596			0.237

CONCLUSION: METHODS 1) AND 4) ARE GOOD PREDICTIONS.

REDUCED GRAVITY TEST DATA PREDICTIONS SUMMARY

FIGURE 2.1.2.2-6

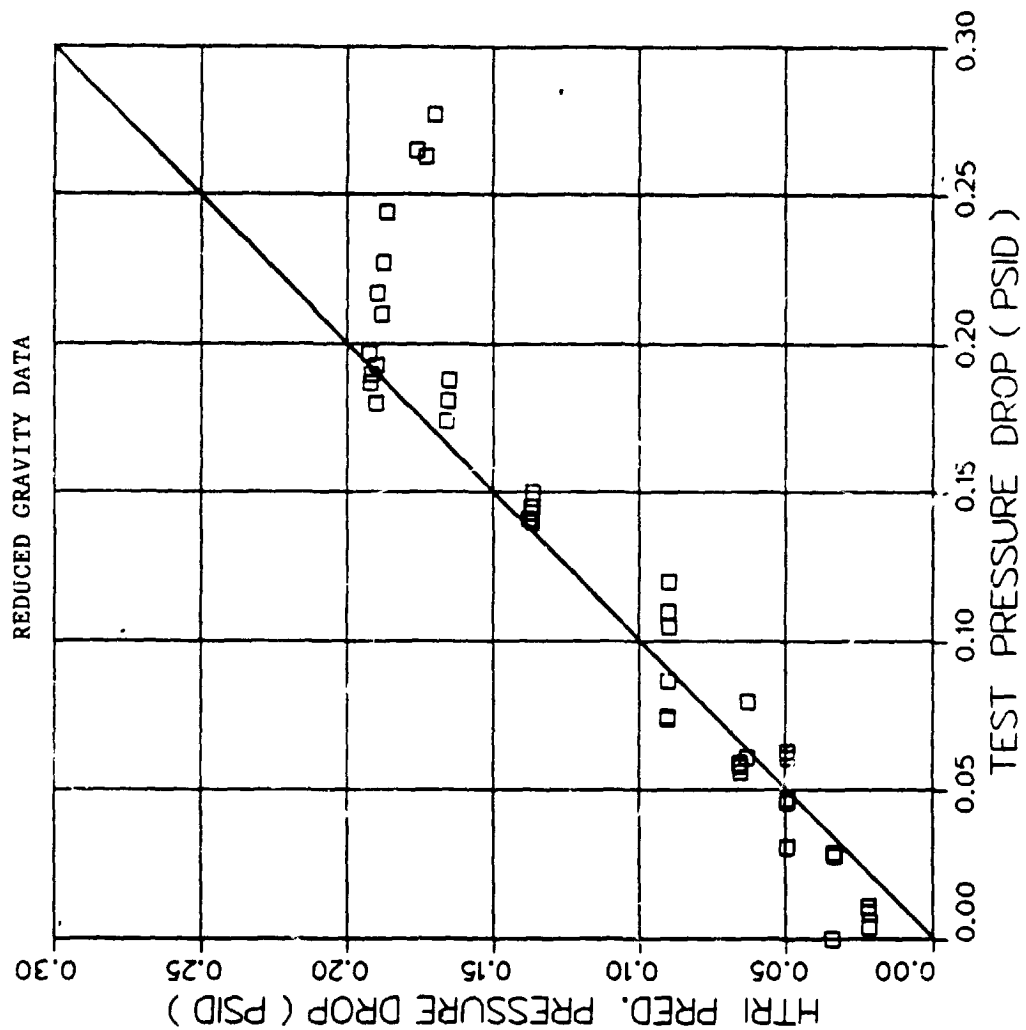
Friedel pressure drop prediction decreases slightly in reduced gravity. As can be seen in Figure 2.1.2.2-6, the wet wall modified HTRI and Friedel methods correlate with the data best. The wet wall modified HTRI model under-predicts on an average of 3.5 percent with a standard deviation of 28 percent. The Friedel method also under predicts but has larger standard deviations. Scatter plots showing the predicted pressure drop versus measured test pressure drop for the HTRI, Friedel and wet wall modified HTRI models are shown in Figures 2.1.2.2-7,8 and 9. It can be seen that the wet wall modified HTRI model provides good correlation for the complete range of quality tested.

During the reduced-gravity testing, two flow regimes, slug and annular, as well as the slug/annular transition were observed. At low qualities, Taylor bubbles followed by fairly quiescent liquid slugs in an intermittent slug type flow were seen. At the higher qualities, annular flow was observed. The transition line between these two flows has been identified and shown and plotted in Figure 2.1.2.1-7. The modified Dukler flow regime map is the best map available for predicting the slug to annular transition in reduced-gravity. The measured pressure drops were in very good agreement with existing predictive models for both the annular and intermittent flow. It is recommended that the wet wall modified HTRI or Friedel correlations be used for predicting pressure drops in the straight section and the Chisholm B and C (Appendix C) type equations be used for predicting the pressure drops in curved sections and flow discontinuities.

2.1.3 Condenser Test Section

The Sundstrand condenser design uses multiple parallel flow channels tapered in the direction of axial flow to maintain shear flow vapor velocities over the length of the condenser (Figure 2.1.3-1). By maintaining shear flow conditions, a stable condensing front is established and noncondensable gas is swept through the condenser and back to the cold end of the RFMD. Also

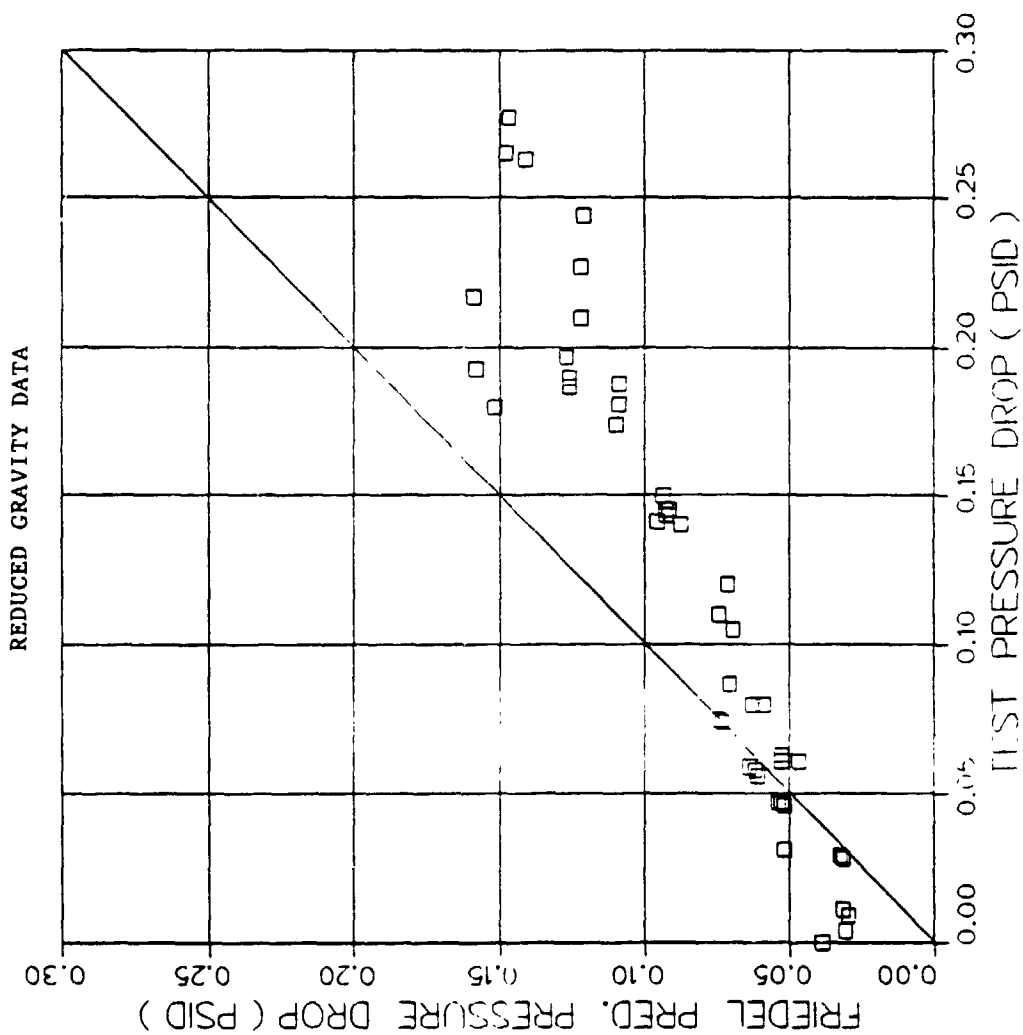
STRAIGHT SECTION TEST DP VS PRED. DP 4/16, 4/17 FLIGHT TEST



REDUCED-GRAVITY STRAIGHT SECTION HTRI
PREDICTED PRESSURE DROP VS. TEST DATA
PRESSURE DROP SCATTER PLOT

FIGURE 2.1.2.2-7

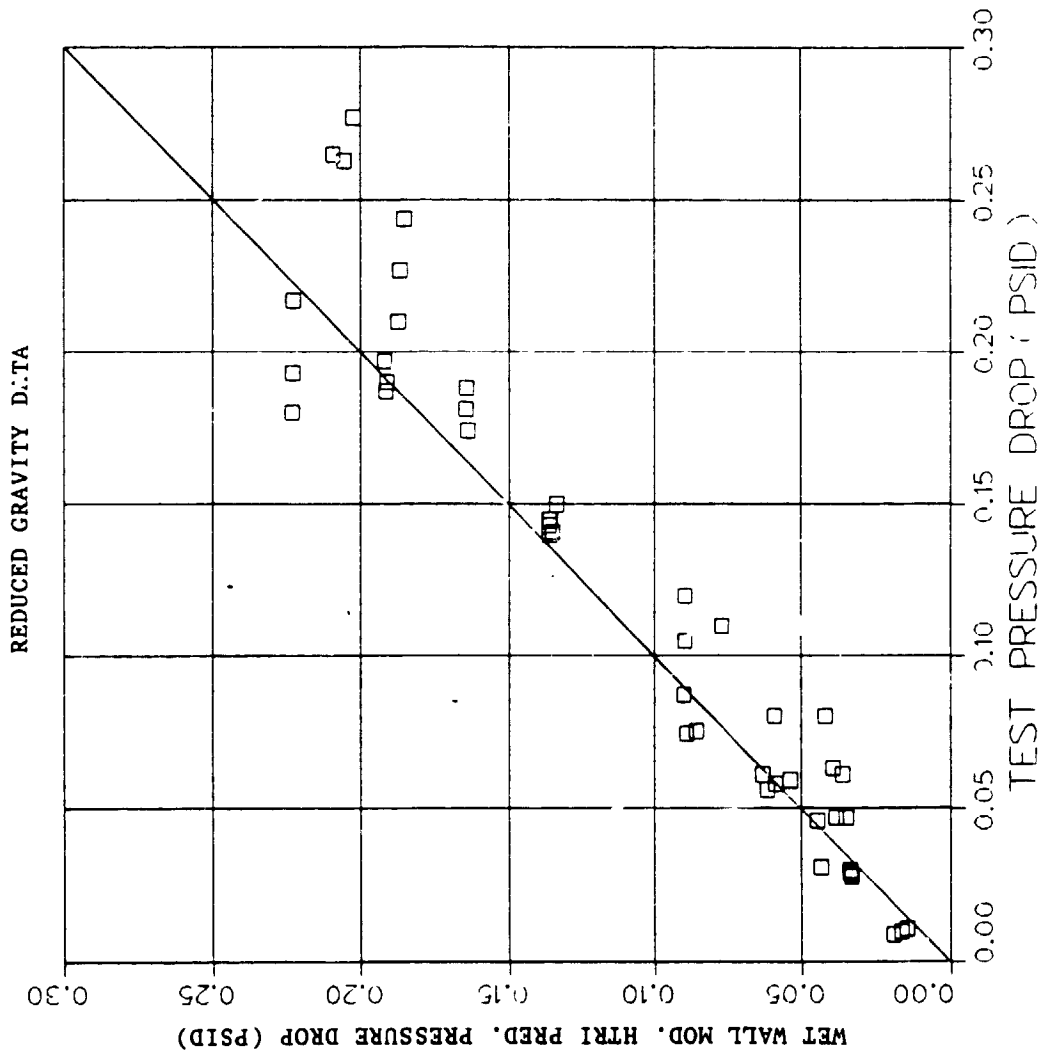
STRAIGHT SECTION TEST DP VS FRED. DP 4/16, 4/17 FLIGHT TEST



REDUCED-GRAVITY STRAIGHT SECTION FRIEDEL
PREDICTED PRESSURE DROP VS TEST DATA PRESSURE
DROP SCATTER PLOT

FIGURE 2.1.2.2-8

STRAIGHT SECTION TEST DP VS PRED. DP 4/16, 4/17 FLIGHT TEST



REDUCED-GRAVITY STRAIGHT SECTION WET-WALLED
MODIFIED HTRI PREDICTED PRESSURE DROP
VS TEST DATA PRESSURE DROP

FIGURE 2.1.2.2-9

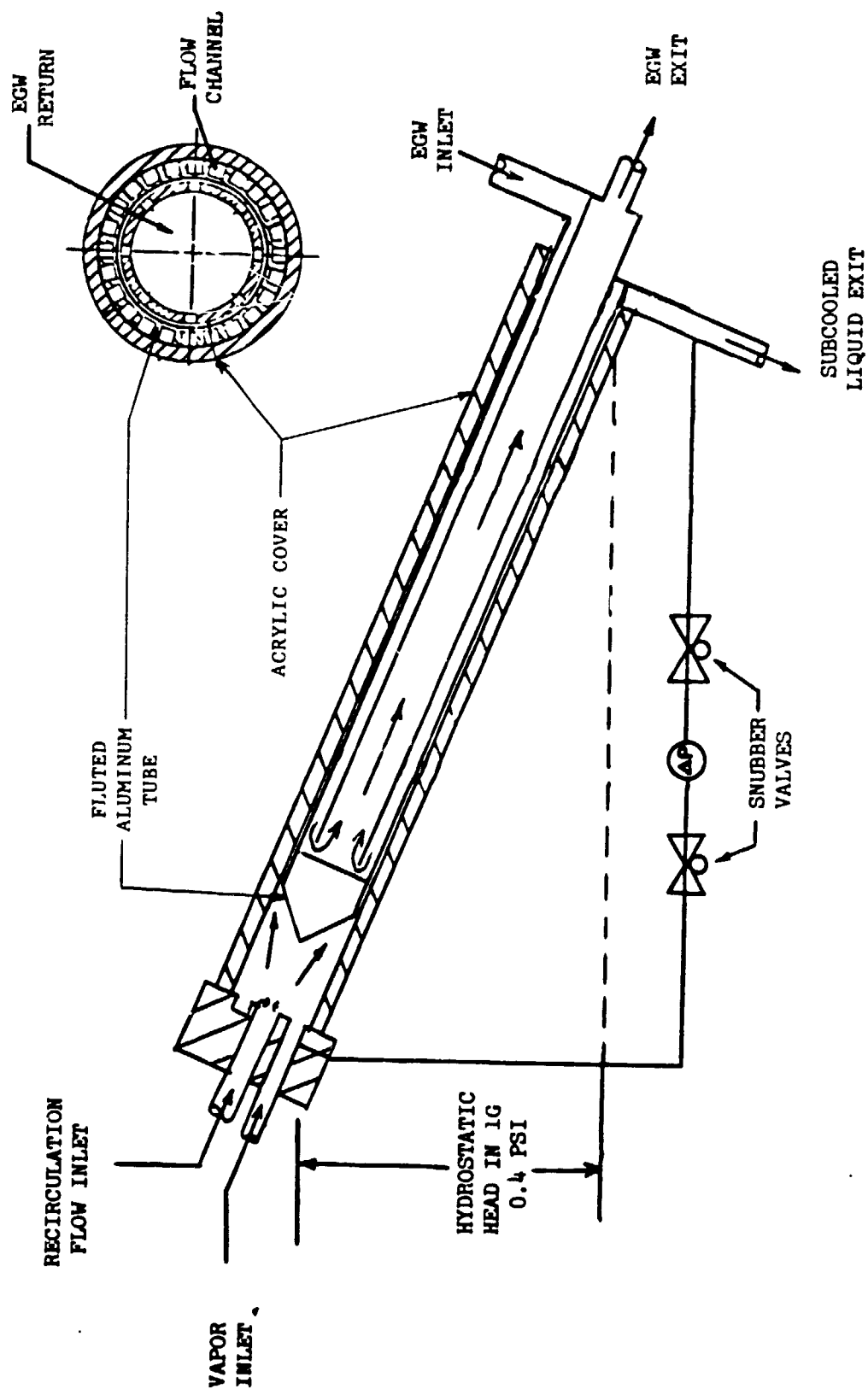


FIGURE 2.1.3-1

CONDENSER TEST SET-UP

the positive pressure drop associated with the shear flow condenser eliminates flow instabilities such as oscillatory flow and run back from occurring within the condenser.

Preflight predictions of the condenser performance in reduced gravity were carried out using an extensive analytical model of the condenser. The model considers the frictional pressure drops, the momentum pressure gain associated with the higher velocity vapor condensing to a liquid film and the hydrostatic pressure drops that occur in a gravitational field. Heat transfer and pressure drop are computed for local conditions in each of 20 axial length increments used in the modeling program.

The pressure drop in the condenser is a very strong function of the active condensing length within the condenser. At design point, most of the condenser is predicted to operate in the annular flow regime with condensation occurring over the entire axial length. If the coolant flow is increased or its temperature decreased, condensation will be completed earlier in the condenser with a significant amount of subcooling heat transfer being done. When the condensing length is shorter than the design condition, the overall condenser pressure drop is significantly reduced because of the lower liquid velocities as compared to vapor velocities.

Pressure drops and heat transfer performance parameters were recorded during the flight profiles and the ground testing. The data taken in the reduced-gravity environment was complicated by liquid which accumulated in the lower sections of the vapor line between the RFMD and condenser during the high-gravity portion of the flight. Upon entry into reduced gravity this accumulated liquid volume was released and flowed in an intermittent type pattern into the condenser inlet. This represented an apparent decrease in the inlet quality to the condenser with an increase in its overall mass flow. Visual observations of the condenser during the flight are presented in Appendix A.

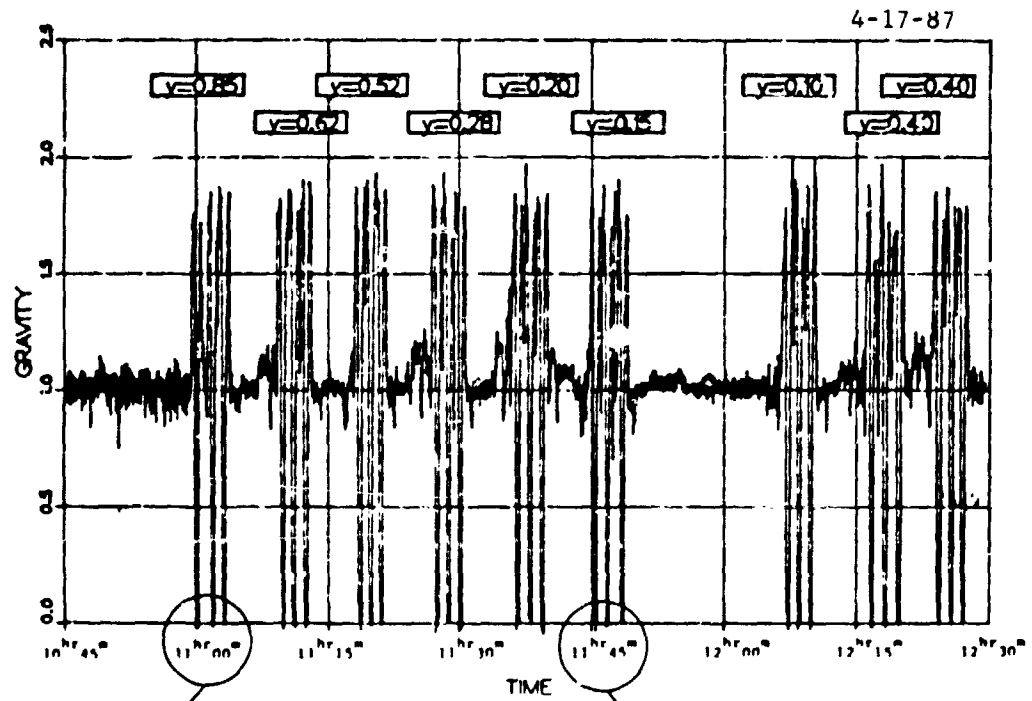
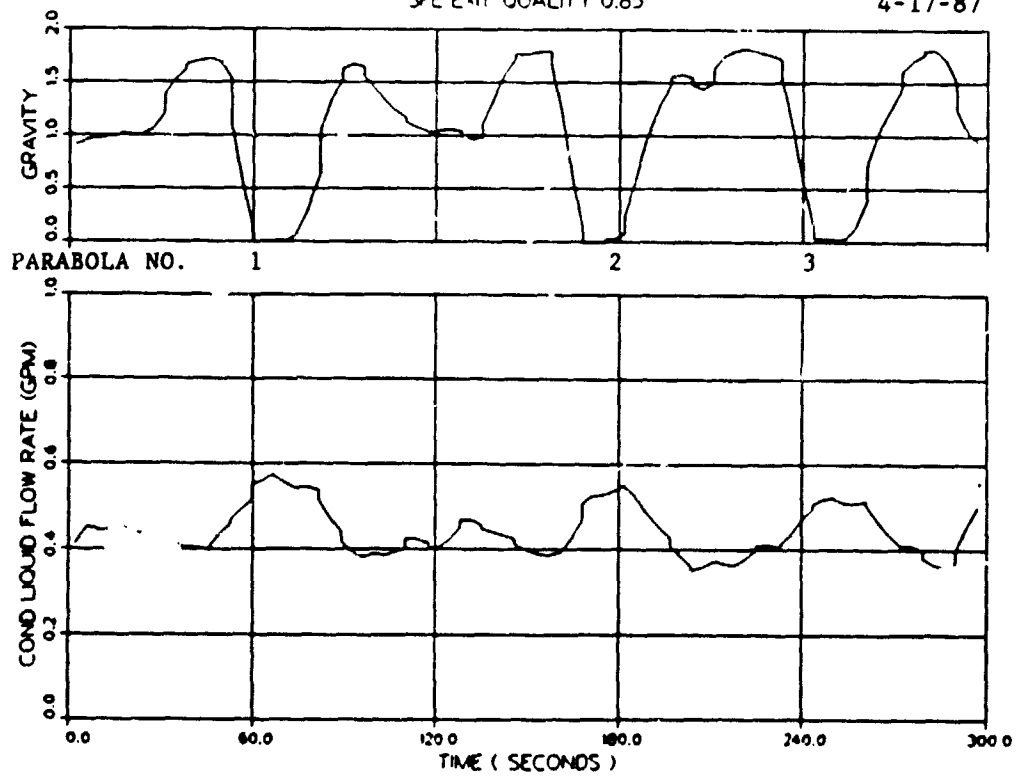
2.1.3.1 Liquid Carry-over

An analysis was performed to estimate the amount of liquid carry-over for use in the data correlation. The volume of the liquid carry-over was estimated by integration of the condensed liquid flow rate versus time for various parabolae at different evaporator qualities. This process is illustrated in Figure 2.1.3.1-1. Figure 2.1.3.1-1b shows the increased condensate liquid flow rate during periods of reduced gravity for zero-gravity parabolas numbered 1, 2 and 3 on April 17. The first three parabolas performed on April 17 were run at the 85 percent evaporator outlet quality condition. The amount of liquid carry over generally decreased from one parabola to the next as the liquid volume within the vapor line was flushed through the condenser. Figure 2.1.3.1-2 summarizes the results of the analysis to determine the amount of liquid carry-over into the condenser.

Four possible sources for the liquid accumulation volume have been identified. The first potential source of the liquid carry over would be a thermodynamic wetting of the vapor as it flows from the RFMD through the back pressure regulating valve (BPRV) into the condenser. Some fluids fall into the saturation dome and upon adiabatic pressure drop undergo spontaneous condensation or wetting. This characteristic occurs if the saturation line has a negative slope when plotted on the enthalpy pressure diagram. R114 does not exhibit this wetting characteristic and therefore the saturated vapor exiting from the RFMD will superheat upon adiabatic pressure drop. It is noteworthy that this phenomena of adiabatic superheating upon pressure drop also occurs in ammonia.

The second source of the liquid carry over was identified to be the BPRV servo flow. This continuous flow of 0.02 gpm would result in

(a) GRAVITY VS TIME

(b) COND LIQUID FLOW RATE VS TIME
SFE EXIT QUALITY 0.85

CONDENSER FLOW VARIATION

FIGURE 2.1.3.1-1

OBTAINED BY INTEGRATION OF DIGITAL FLOW RATES

DATE		APRIL 16, 1987					APRIL 17, 1987																																																						
SFE QUALITY		0.15					0.84					0.85					0.15																																												
PARABOLA NO.		7					8					9					23					24					26					1					2					3					16					17					18				
CARRY-OVER VOLUME IN ³		32.2					10.7					3.1					21.0					18.0					11.1					19.2					14.0					11.9					10.9					8.5					8.4				
ESTIMATED LINE VOLUME -																																																													
RFMD TO BPRV 6 IN ³																																																													
BPRV TO CONDENSER 26 IN ³																																																													

ESTIMATE OF LIQUID CARRYOVER

FIGURE 2.1.3.1-2

approximately 5 cubic inches being accumulated in the inlet plumbing for every minute of the normal or high gravity conditions. This represents a significant fraction of the carry-over liquid observed (Figure 2.1.3.1-2). The amount of liquid carry over due to the BPRV servo flow would be proportional to the time spent between reduced-gravity parabolas until the volume limit that the plumbing could accommodate in stratified flow is reached. Once that limit was reached, slugging would start to occur, and no more liquid would accumulate.

A third potential source of the liquid carry over volume could be due to incomplete demisting of the condenser vapor flow. Liquid droplets could be carried out with the vapor stream through the higher velocity flow passages within the KFMD. In the relatively large vapor line (3/4 in diameter), the flow would tend to stratify and accumulate. It would be expected that the carry over volume for this mechanism of liquid transport would be effected by the overall vapor flow rate. More liquid droplets would be carried during a high heat load condition where the vapor velocities are higher. The April 17th data shows a higher carry-over mass flow for the high quality, higher vapor flow condition. This is not evident from the April 16th data because the test stand was run for an extended time at low heat load prior to the test allowing a longer accumulation of time.

The fourth potential source of the liquid carry-over volume could result from condensation in the vapor transport line. Previous heat loss models showed that only approximately 25 watts of heat loss were expected in the vapor transport line. This small heat loss results in a condensation rate of $0.6 \text{ in}^3/\text{min.}$, a small fraction of the total carry-over volume observed. Even if the heat loss estimates are off by a significant factor, the carry-over liquid volume due to condensation would be small. Therefore, this mechanism can be dismissed.

It should be noted that this additional liquid flow observed during the flight test did not effect the condenser or system performance except for the increased condenser pressure drop.

2.1.3.2 Simulation of Condenser Test Results

Using the reduced gravity test data with the carry over volume taken as an additional liquid burden on the condenser, an analytical simulation of the condenser operation was performed for parabola number 24 on April 16th. Figure 2.1.3.2-1 summarizes the results.

The analytical model was adjusted to match the conditions for ethylene glycol (EGW) flow rate and the inlet temperatures for both R114 and EGW. The condenser heat transfer was 3300 watts based on the coolant mass flow, specific heat, and temperature rise. Using the total R114 flow rate, the observed R114 inlet temperature and outlet enthalpy based on the exit temperature, 5000 watts of heat rejection was estimated. This poor heat balance is due to inaccuracies in measured flow rates, the transient effect of the liquid carry-over and the transient effect of the changing coolant flow rate which dropped during the reduced-gravity conditions due to cooling cart pump cavitation. It can be seen from Figure 2.1.3.2-1 that the measured pressure drops between the test condition and the simulation number one are in fair agreement despite the poor heat balance.

The measured pressure drop on the R114 side of the condenser was lower than predicted due to a radial clearance between the acrylic condenser cover and the aluminum fluted tube (Figure 2.1.3-1). The radial clearance between the parts was due to the clearance required for assembly of the condenser and the thermal expansion caused by the temperature difference between the acrylic which is close to the R114 temperature and the aluminum which is at ethylene glycol temperature. During operation, the radial clearance could

APRIL 16, 1987 DATA SFE - EXIT QUALITY = 0.84

PARABOLA #24	TEST	SIMULATION WITH COVER CLEARANCE	SIMULATION WITH COVER CLEARANCE
<u>EGM SIDE</u>			
• FLOW RATE GPM	3.842	3.842	3.842
• INLET TEMP °F	89.15	89.2	89.15
• OUTLET TEMP °F	95.75	95.83	95.75
• HEAT ADDITION $Q_w = m C_p \Delta T_w$, WATTS	3300	3318	3300
<u>R114 SIDE</u>			
• PRESSURE PSI	84.83	84.83	84.83
• VAPOR FLOW GPM	0.4	0.4	0.4
• LIQUID FLOW GPM (CARRYOVER)	0.08	0.08	0.08
• INLET QUALITY	0.833	0.833	0.833
• PRESSURE DROP (PSID)	<u>1.18 + .95</u>	<u>1.76</u>	<u>1.47</u>
• HEAT REJECTION, Q_f WATTS			
$Q_f = m (H_{in} - H_{out})$			
	4997	4997*	4997*

* BASED ON WATER HEAT REJECTION

SIMULATION OF CONDENSER REDUCED GRAVITY TEST

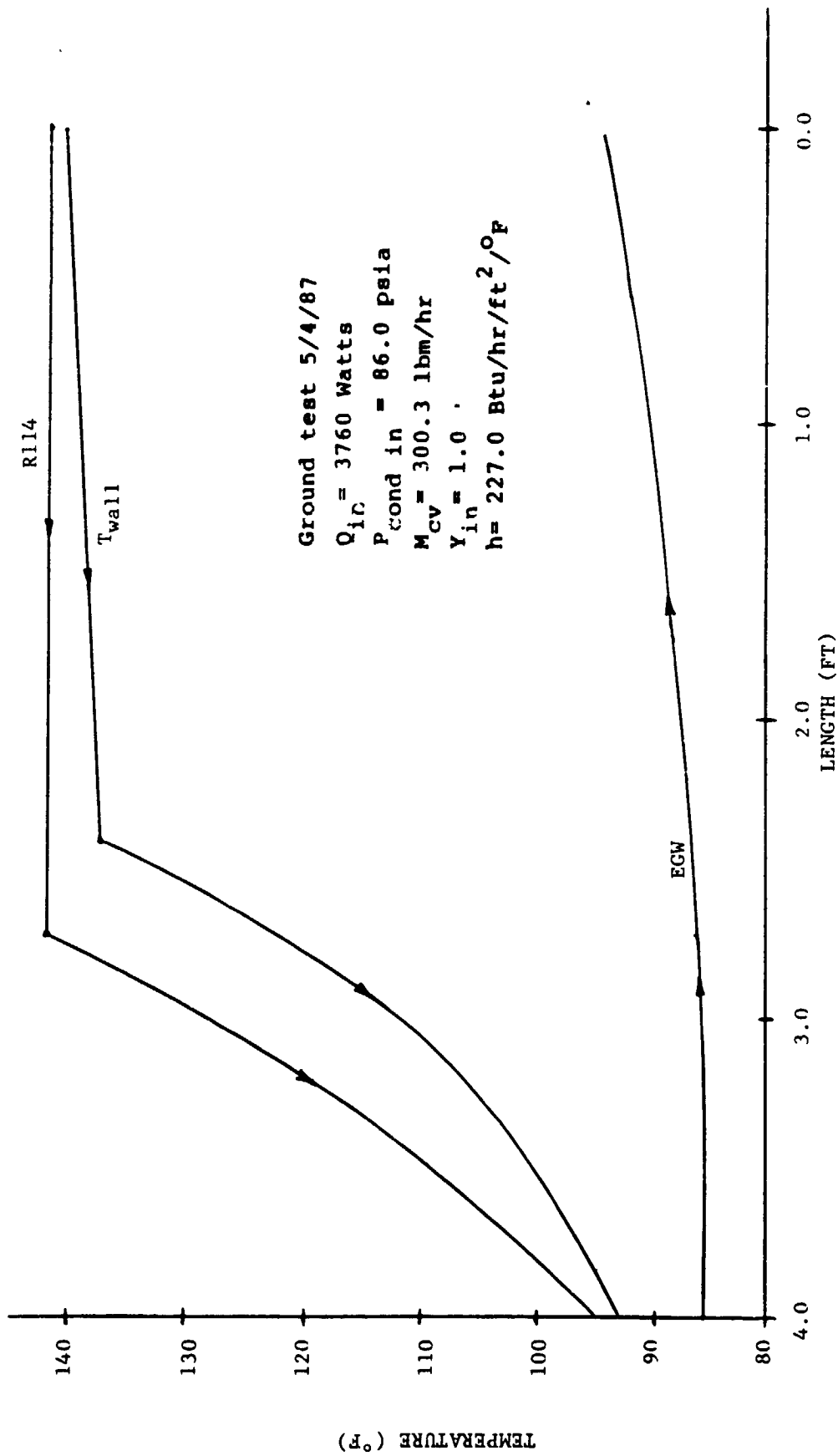
FIGURE 2.1.3.2-1

be as much as 0.0075 inches and this would result in a pressure drop over-prediction. The clearance was corrected for in the simulation number two by altering the condenser flow passage from a rectangle to a "T" shape to compensate for the clearance. This pressure drop correlates well with the data.

The majority of the resistance to heat flow exists on the coolant side of the heat exchanger. Based on the coolant flow rate and temperatures measured in the flight experiment a heat transfer coefficient of 193 BTU/hr/ft²/°F is expected. This value was calculated using the standard Dittus-Boelter type equations for single phase flow in tubes (Reference 8). As a check of the validity of the analytical tools the heat transfer coefficient in the condenser model was then adjusted until the measured thermal performance of the heat exchanger was simulated. By comparing the heat transfer coefficient necessary in the simulation to that expected during testing, the validity of the thermal model can be tested. For the 85 percent quality case tested, a "simulation" heat transfer coefficient of 227 BTU/hr/ft²/°F was necessary. This is in fairly close agreement with the value of 193 BTU/hr/ft²/°F calculated from the test conditions for that flow geometry.

A similar comparison was performed for the ground test conditions of high heat load. The heat transfer coefficient during the test run was calculated to be 186 BTU/hr/ft²/°F for the measured flow and temperature heat sink. A simulation value of 234 BTU/hr/ft²/°F was necessary to correlate the test. Profiles of the R114 temperature, EGW coolant temperature and wall temperature are shown as a function of length for the ground test in Figure 2.1.3.2-2.

In conclusion, the condenser test results were complicated by two factors. These were liquid carry-over resulting from liquid which pooled in the vapor lines during the gravity condition which was released into the condenser in reduced-gravity and unsteady coolan.



CONDENSER TEMPERATURE DISTRIBUTION

FIGURE 2.1.3.2-2

(EGW) flow to the condenser due to pump cavitation. This resulted in transient operation of the condenser for every reduced-gravity test point. The liquid pooling problem would not present difficulties during continuous zero-gravity operation. Despite these problems, simulation of the test results allowed reasonable pressure drop correlations to be obtained.

2.1.4 System Operation

The primary objectives of the KC135 flight tests were to expand the two-phase flow regime and shear flow condenser data bases. In accomplishing these objectives, the components of the Sundstrand Two-Phase Thermal Management System (TPTMS) concept were demonstrated to be unaffected by the variable gravity environments experienced during the KC135 flight profiles.

The following section contains a brief overview of the TPTMS response to the KC135 flight profiles and a discussion of the three transient tests performed to demonstrate the system response to abnormal operating conditions.

2.1.4.1 Sundstrand TPTMS Response to a Reduced-Gravity Flight Profile

During the reduced gravity test flight, the system was subjected to a gravity field which varied from reduced-gravity to about two-gravities. The reduced gravity flight profile shown in Figures 2.1.1-2 shows the magnitude and duration of the gravity level during the flight. Any system which is flown on a reduced gravity flight similar to this must operate independently of the gravity level.

Figures 2.1.1-3 to 2.1.1-5 show the test stand installed on the KC135. As can be seen, height differences exist between test stand

components as dictated by the physical layout of the hardware. Height differences in liquid lines cause pressure changes in the system which are gravity dependent. Throughout the flight test, the TPTMS continued to operate with no adverse effects due to the changing gravity field or airplane attitude.

As the transition is made from hyper-gravity to reduced gravity, the system reacts to the lack of gravity heads due to height differences. The accumulator begins to fill with liquid (Figure 2.1.4.1-1) because the level probe is no longer pumping against the gravity head created by the height differences between the RFMD and accumulator. This trend is reversed when the reduced gravity period ends and the transition to hyper-gravity is made. The overall trend of Figure 2.1.4.1-1 shows an increase in accumulator position which is a result of the increasing heat load displacing liquid in the system plumbing.

As the accumulator fills, the height of the fluid annulus in the RFMD is reduced. The reduction in RFMD liquid level causes a slight drop in flow to the evaporator and a slight drop in pressure (Figure 2.1.4.1-2a and 2.1.4.1-3). The drop in pressure is small since a majority of the evaporator pitot outlet pressure is a result of the regulated vapor pressure. The evaporator pitot flow decreases proportionally with RFMD liquid level. In addition, the SFE mass flow changes with heat load because the cavitating venturi is unchoked (Figure 2.1.4.1-2b).

The liquid pressure at the inlet of the cavitating venturi and SFE increases as the zero-gravity period begins (Figure 2.1.4.1-4). The pressure increases slightly because the measurements were taken at a high point on the loop. In a gravity field, the liquid pressure in a hydraulic system decreases with height so an increase in pressure will be indicated at high point when the gravity is reduced.

ACCUMULATOR POSITION VS TIME

4-16-87

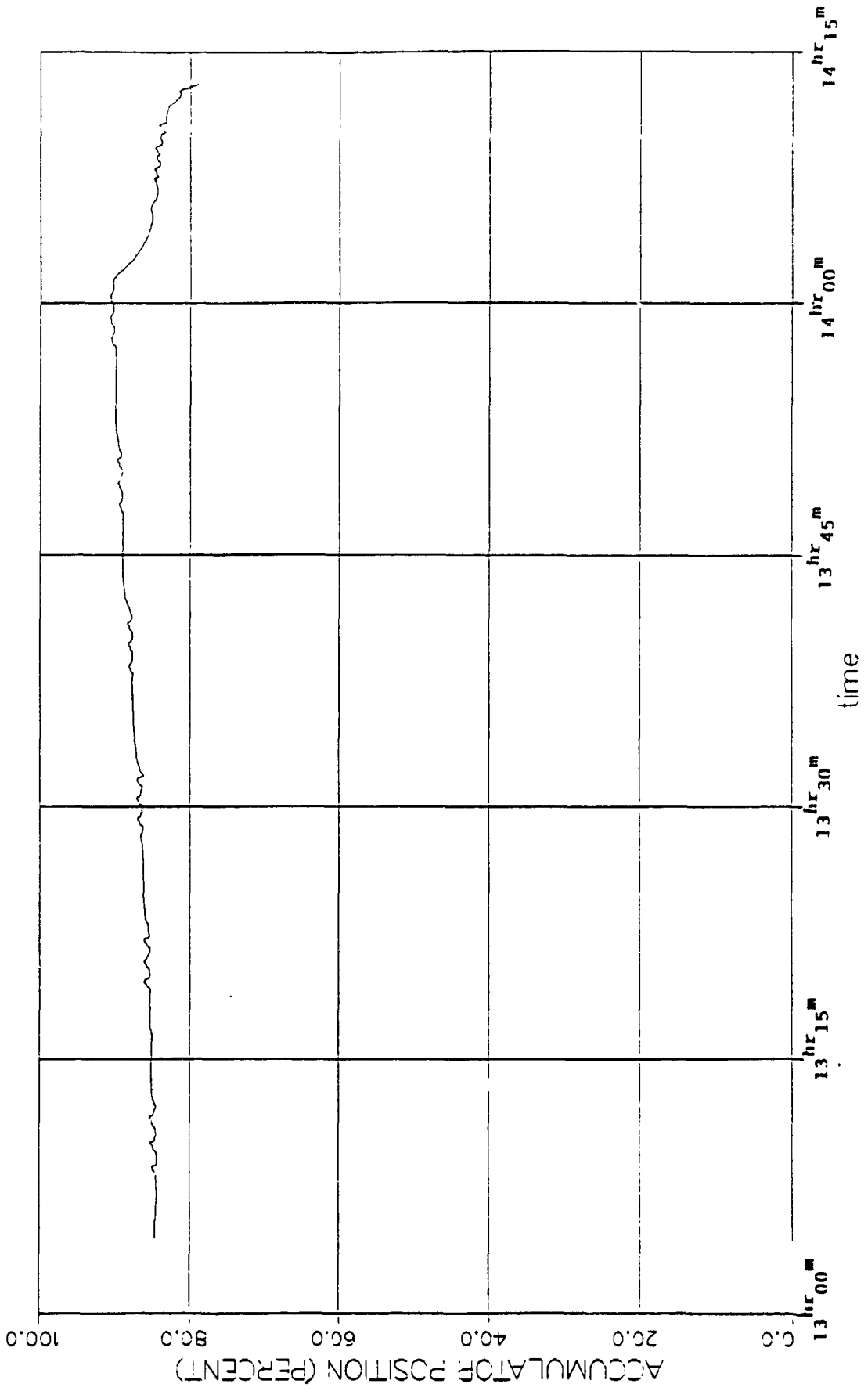


FIGURE 2.1.4.1-1

SFE LIQUID FLOW RATE VS TIME

SFE EXIT QUALITY 0.85

4-17-87

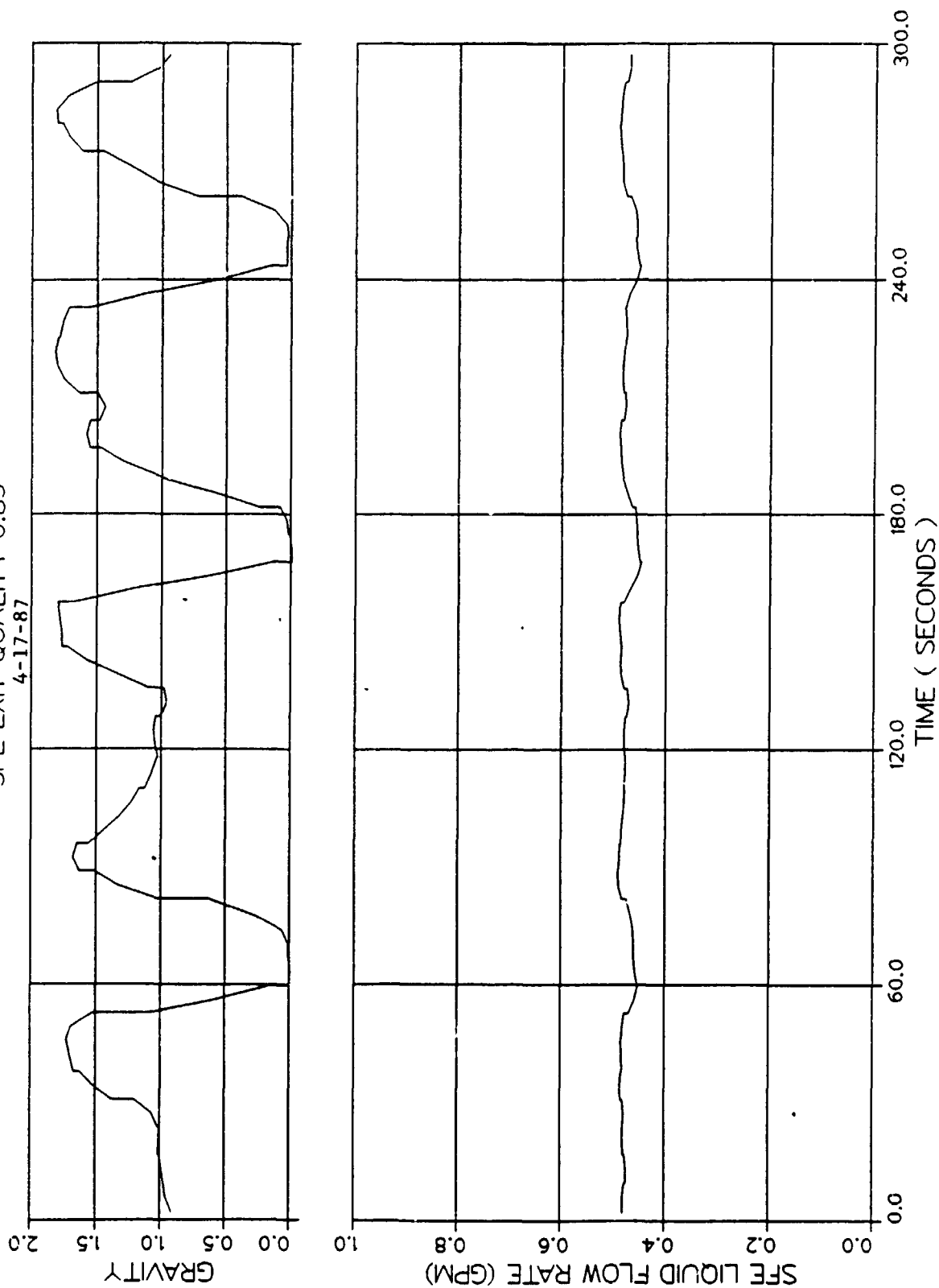


FIGURE 2.1.4.1-2a

SFE LIQUID FLOW RATE VS TIME

4-16-87

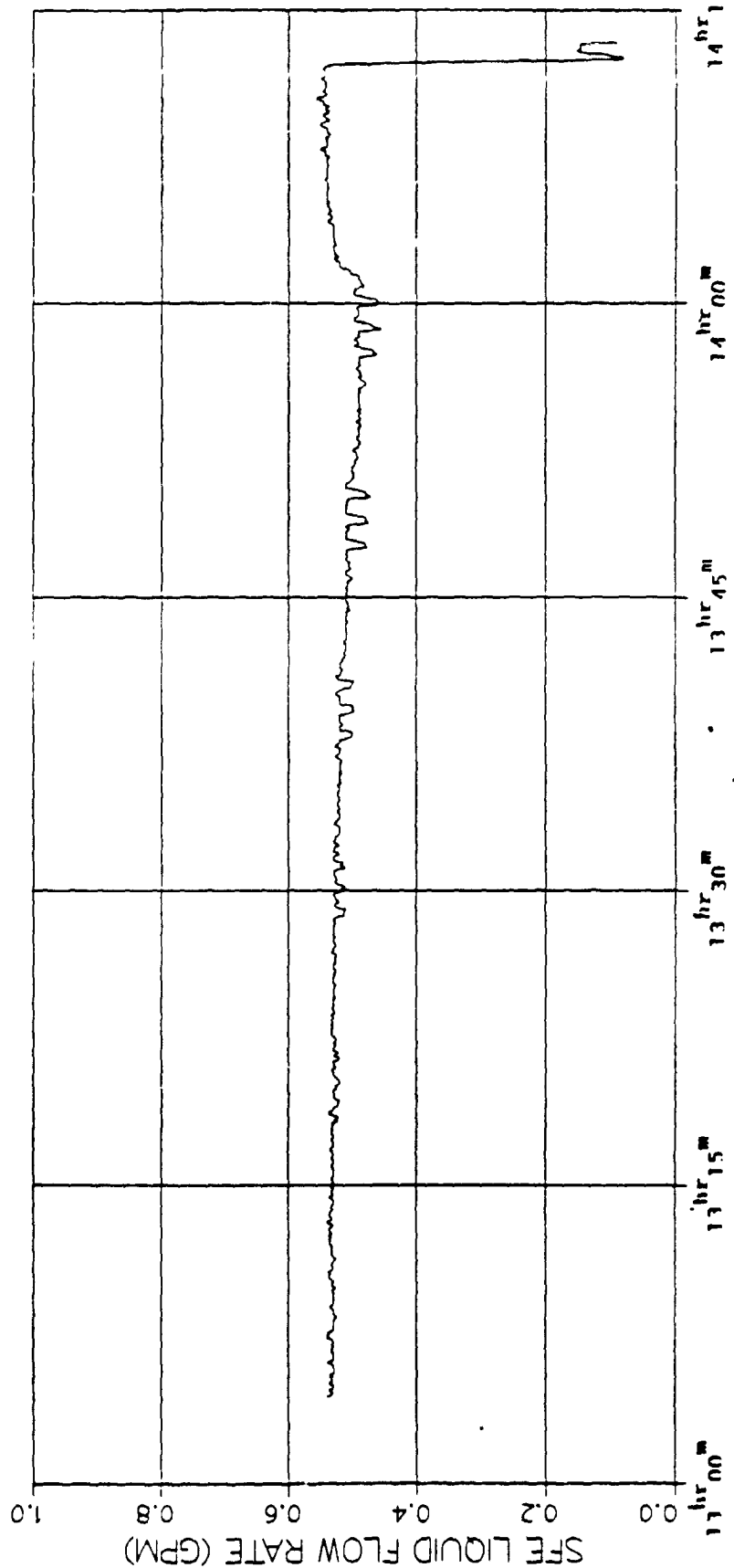
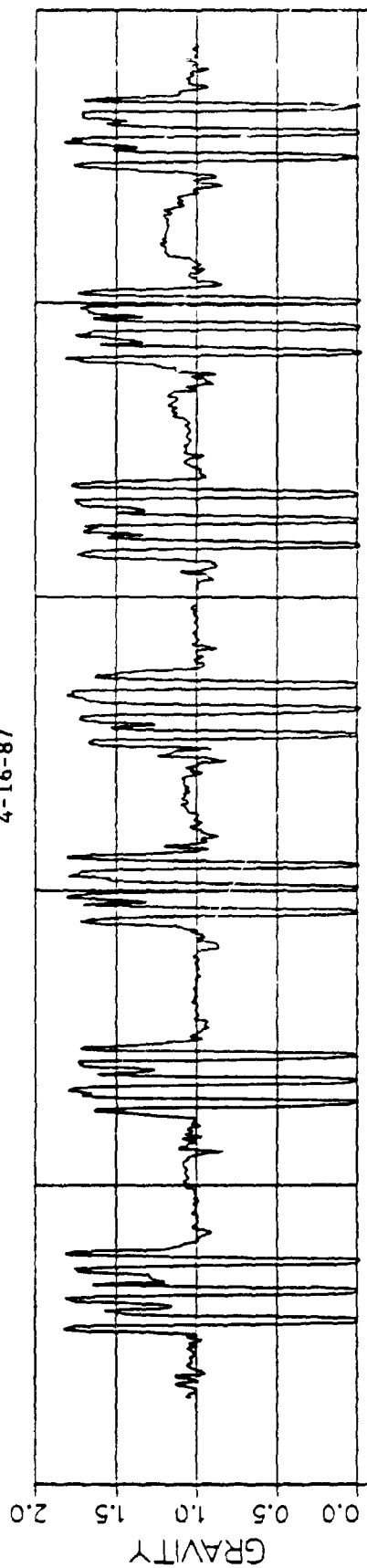


FIGURE 2.1.4.1-2b

EVAP. PUMP OUTLET PRESSURE VS TIME

SFE EXIT QUALITY 0.15

4-17-87

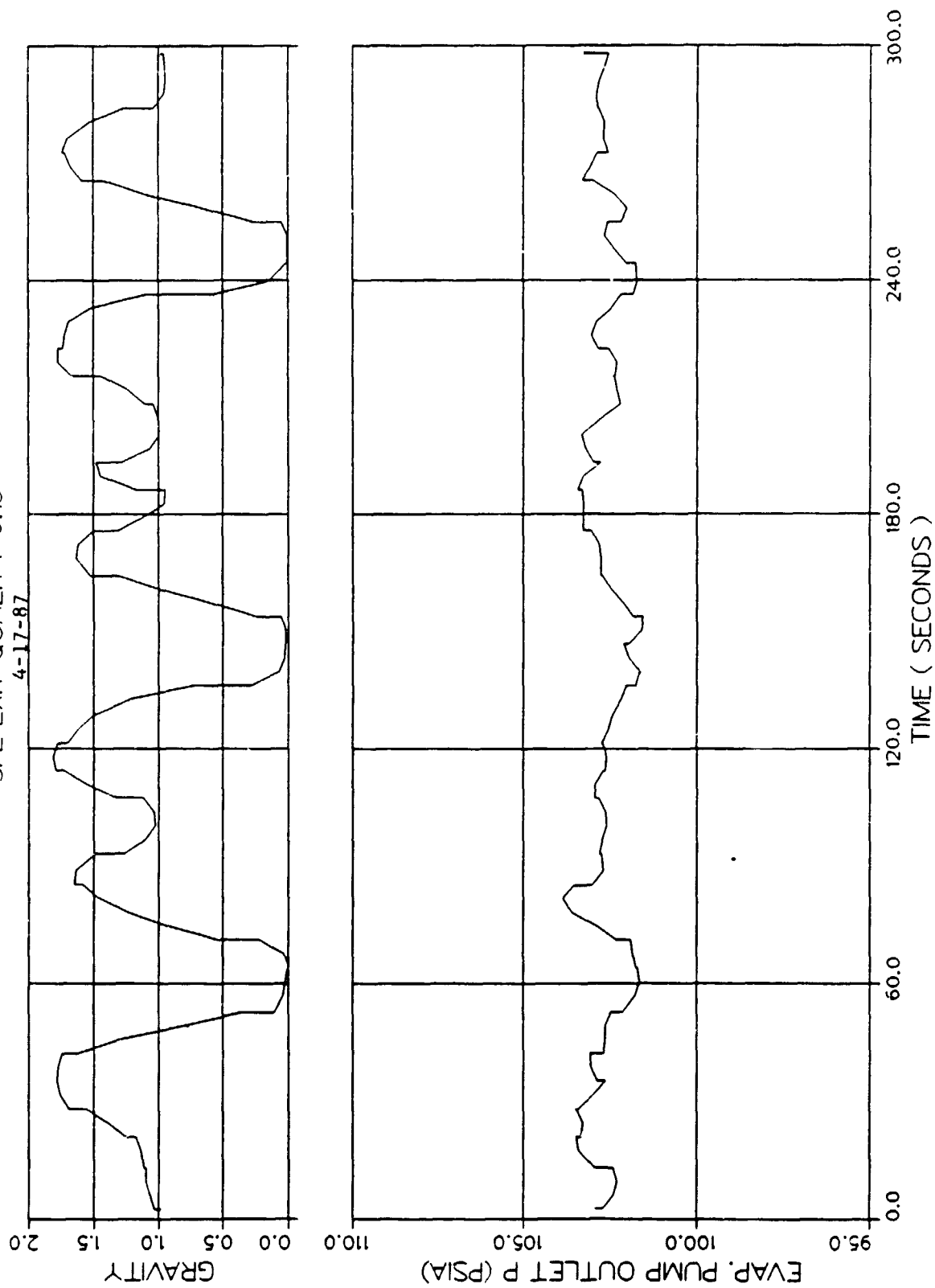


FIGURE 2.1.4.1-3

C. V. INLET PRESSURE VS TIME

SFE EXIT QUALITY 0.84

4-16-87

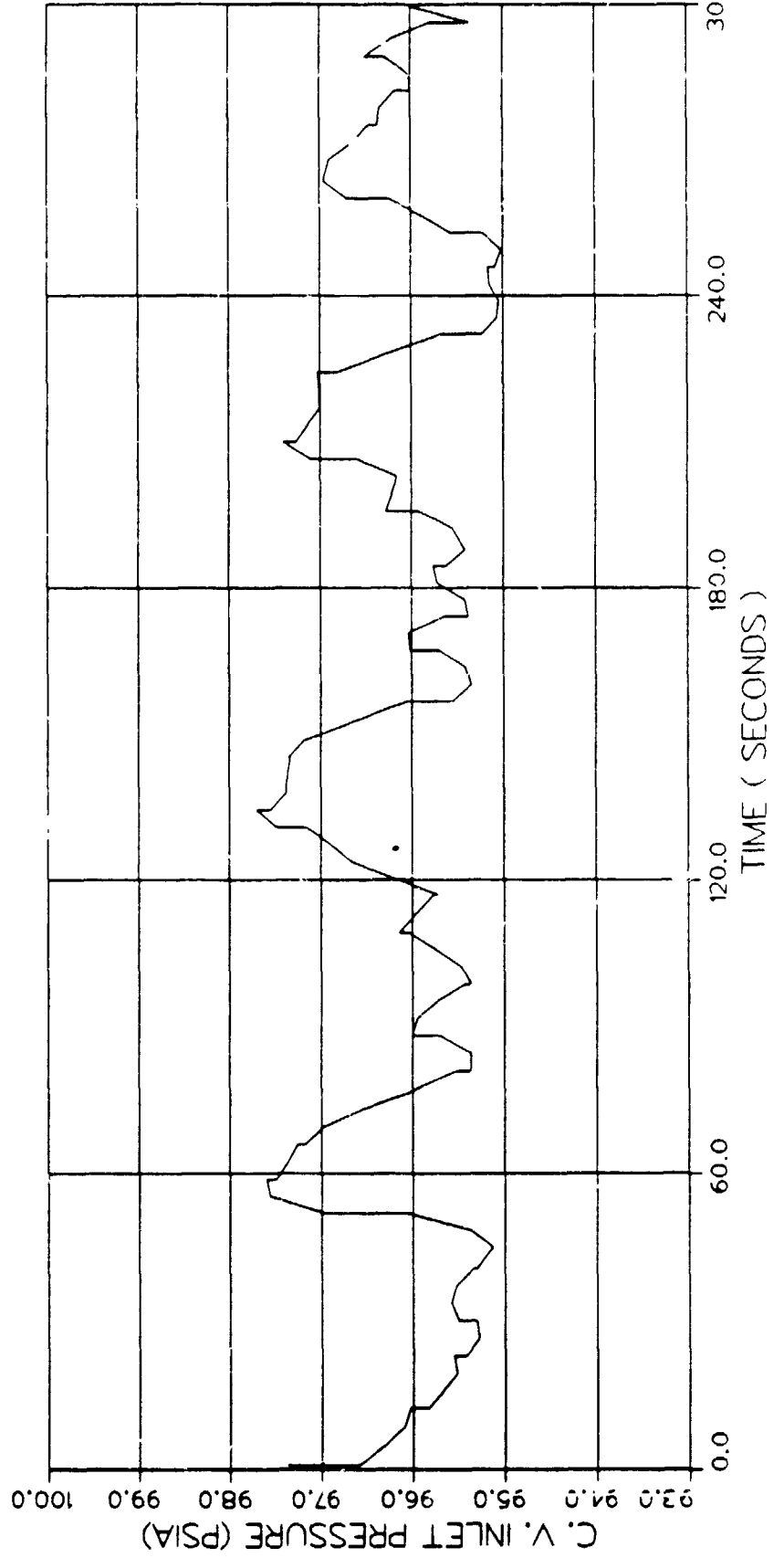
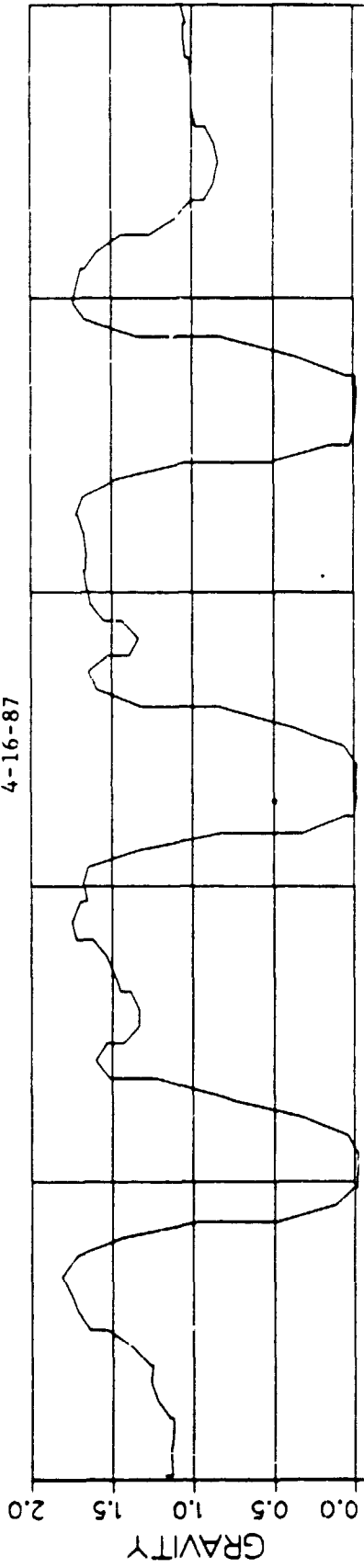


FIGURE 2.1.4.1-4

The Swirl Flow Evaporator (SFE) performance improved in the reduced gravity field. The coil surface temperature went up in the high gravity field and down in the reduced gravity field. Figure 2.1.4.1-5. At low qualities, the change in surface temperature was minimal and at high qualities the change was ambient $\pm 1^{\circ}\text{F}$. The reduction in temperature, during the reduced gravity period, is attributed to the improved fluid contact with the coil as expected. Conversely, the increase in temperature during the hyper-gravity period is due to partial stratification of the liquid and vapor in the SFE which reduces the effectiveness of the evaporator.

2.1.4.2 System Transient Tests

Three system level reduced gravity transient tests were performed during the flight test: loss of system heat rejection, reduced gravity RFMD shutdown and reduced gravity RFMD startup. These tests demonstrate the ability of the TPTMS to accommodate potential operating modes which could be encountered in zero-gravity operation.

The loss of system heat rejection was performed to demonstrate the effects of temporary loss of cooling from the TPTMS condenser. The test was performed by reducing the coolant flow to the condenser to zero while the test stand was being operated at about half the maximum design heat load (1900w). The condenser coolant was shutdown just prior to performing three consecutive reduced gravity maneuvers (Figure 2.1.4.2-1). As expected, the RFMD drum pressure increased (Figure 2.1.4.2-2) and the condenser interface was driven out of the condenser raising the temperature of the flow exiting the condenser (Figure 2.1.4.2-3). The mass flow rate to the SFE was not significantly affected (Figure 2.1.4.2-4). Upon completion of the three reduced gravity maneuvers, the coolant to the condenser was restarted and the system quickly returned to normal operation.

SFE COIL SURFACE TEMP. VS TIME

4-16-87

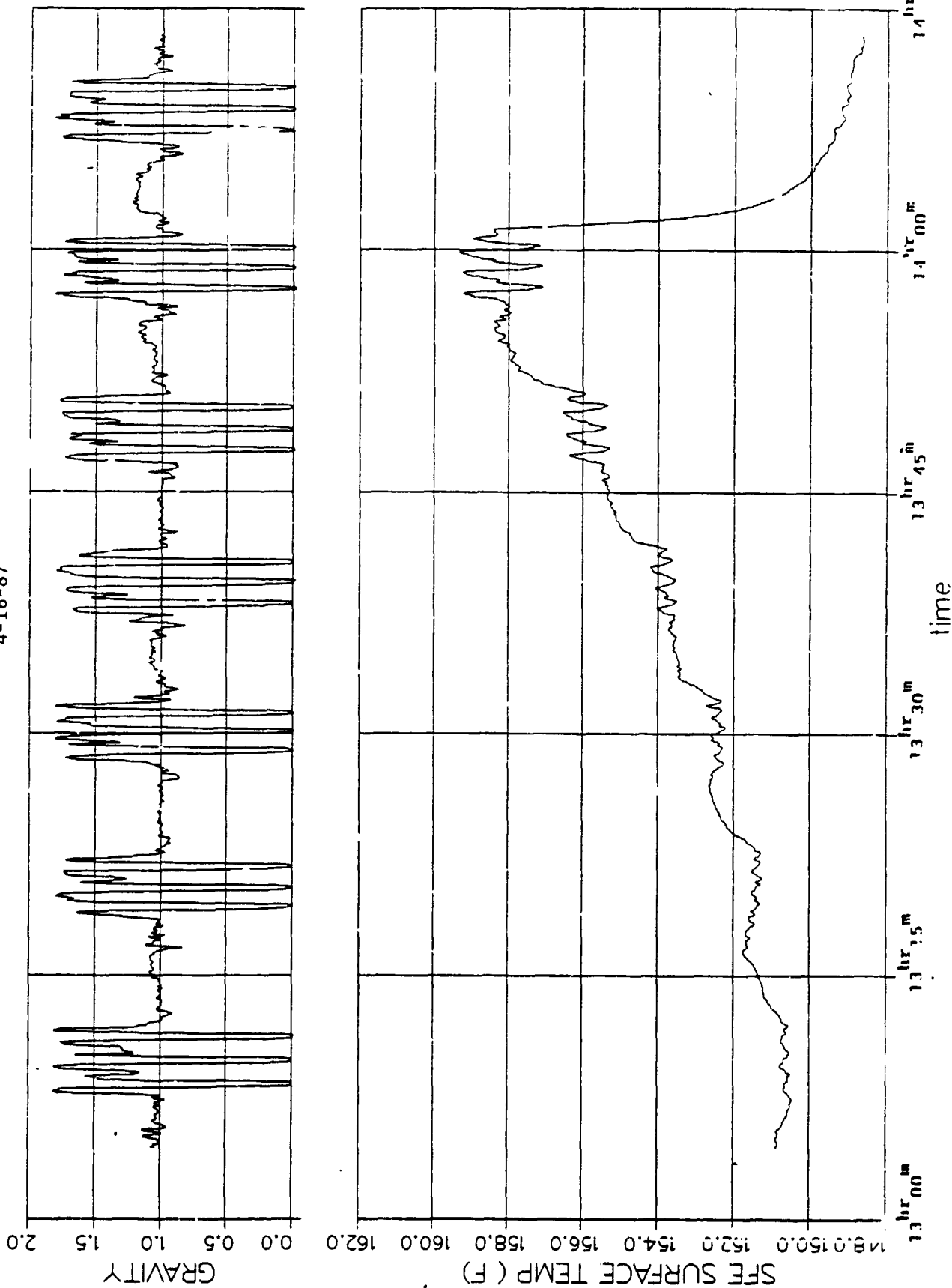


FIGURE 2.1.4.1-5

COND WATER FLOW RATE VS TIME COOLANT SHUT DOWN 4/17/87

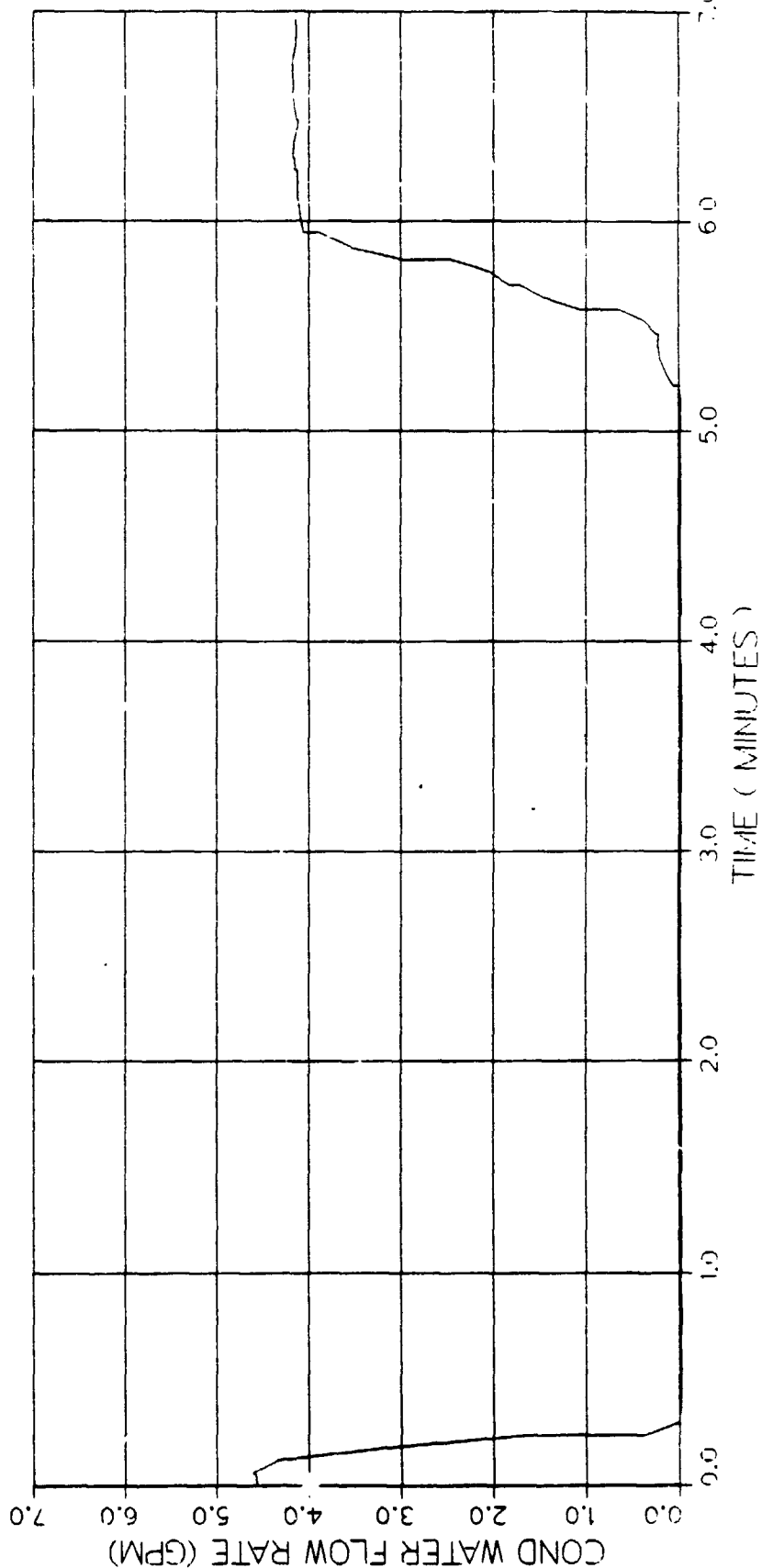
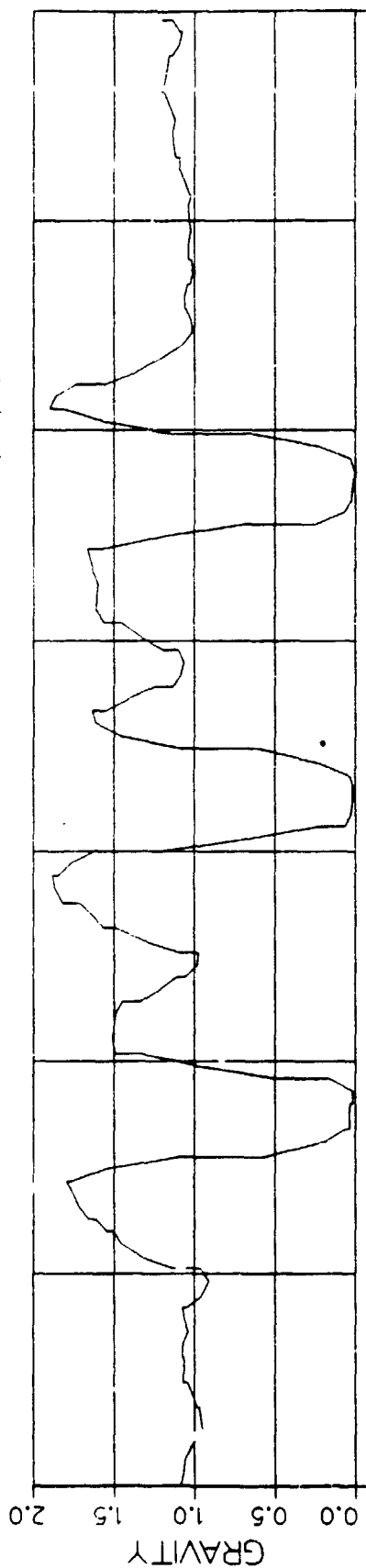


FIGURE 2.1.4.2-1

EVAP. PUMP OUTLET PRESSURE VS TIME COOLANT SHUT DOWN 4/17/87

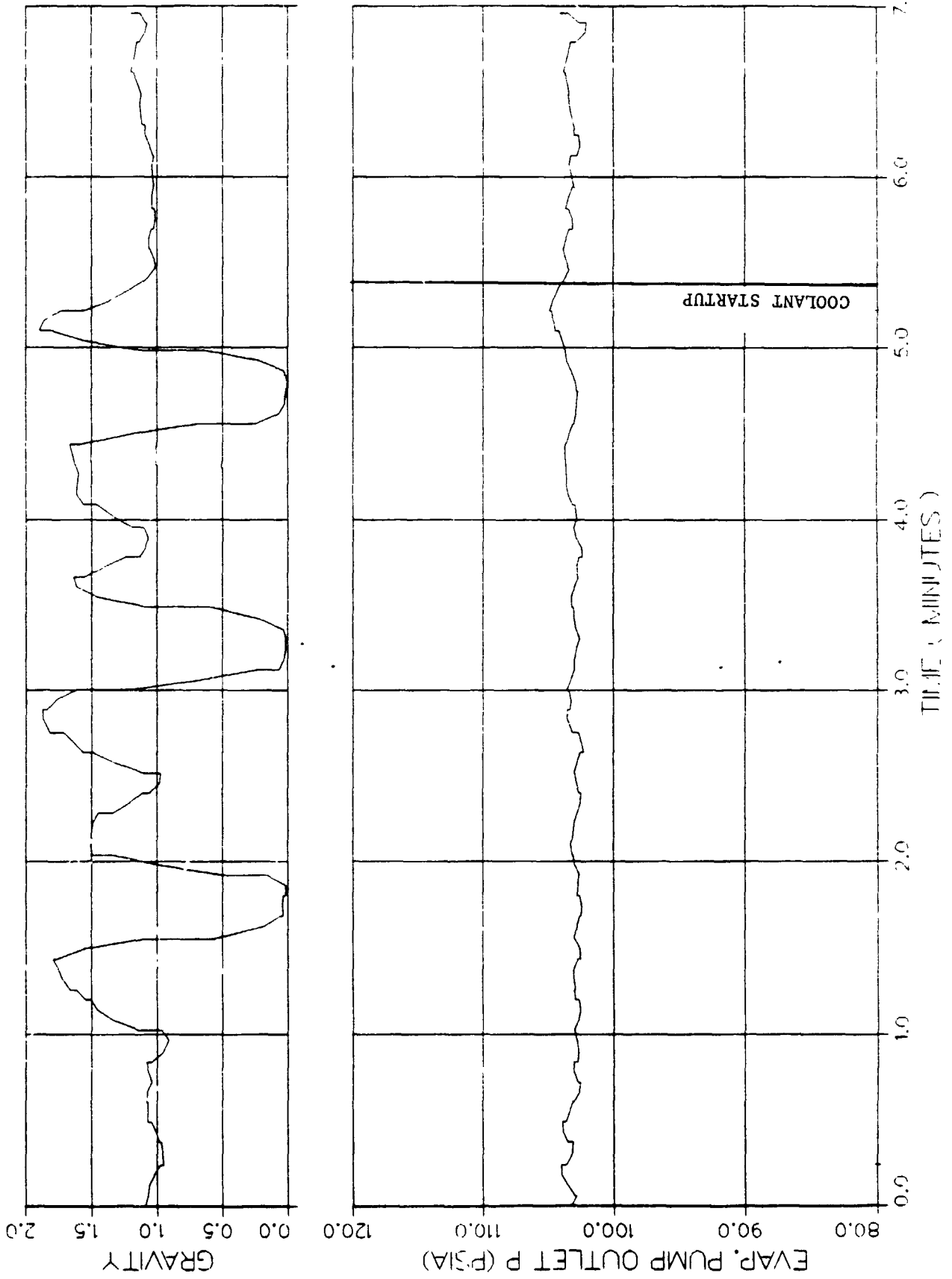


FIGURE 2.1.4.2-2

CONDENSER LIQUID EXIT TEMP. VS TIME
COOLANT SHUT DOWN 4/17/87

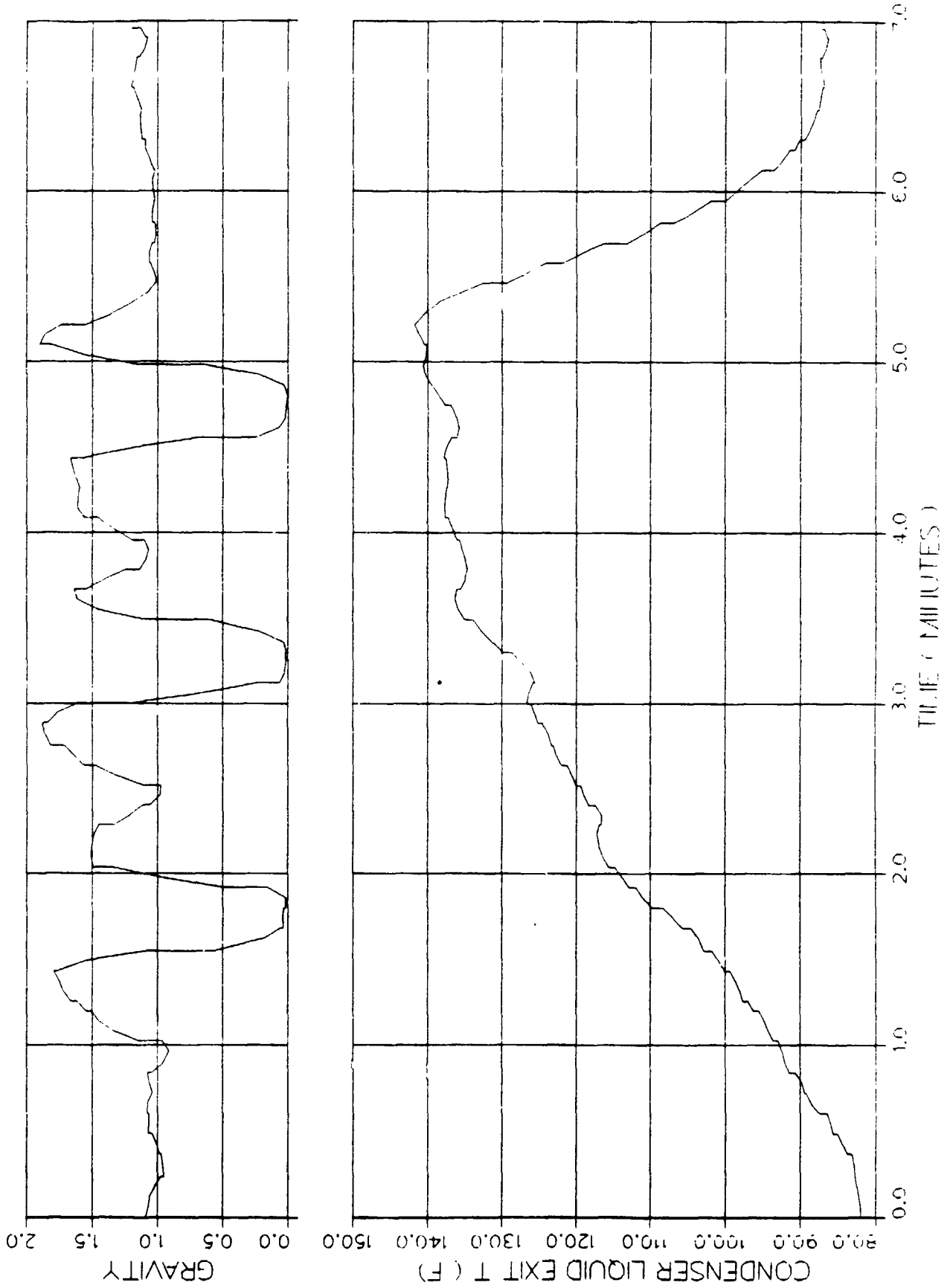
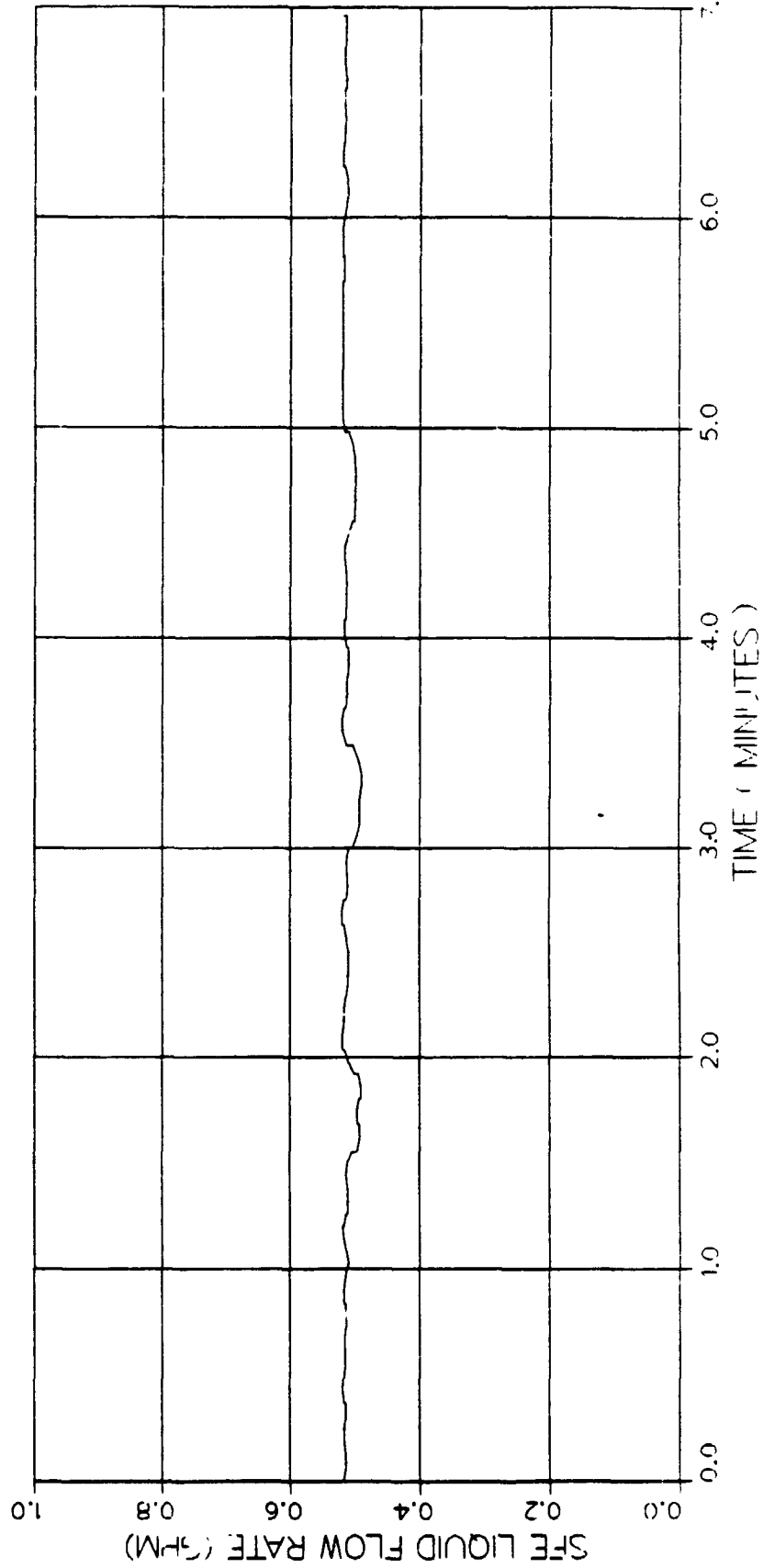
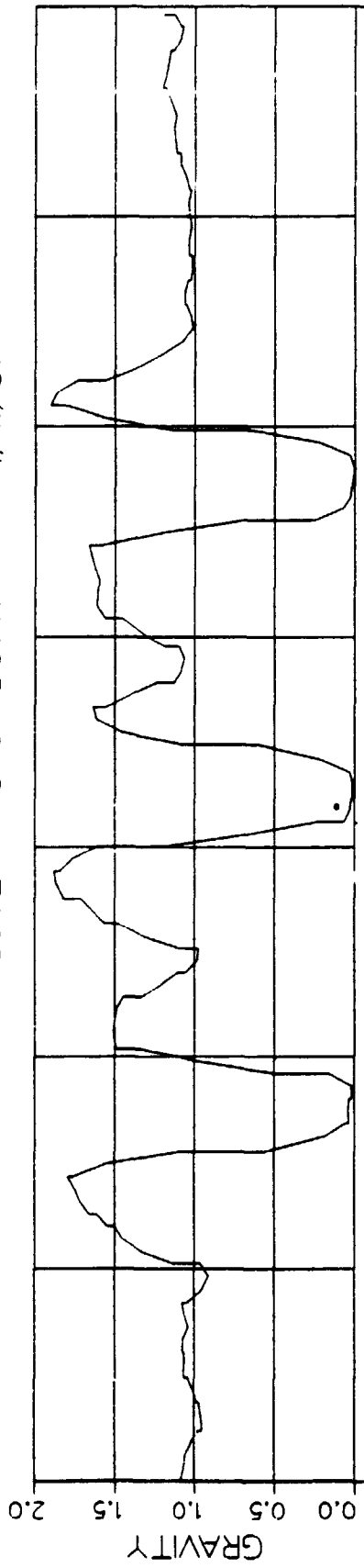


FIGURE 2.1.4.2-3

SFE LIQUID FLOW RATE VS TIME COOLANT SHUT DOWN 4/17/87



ORIGINAL PAGE IS
OF POOR QUALITY

FIGURE 2.1.4.2-4

The purpose of the reduced gravity RFMD shutdown and startup tests was to demonstrate the ability of the RFMD to perform in a reduced gravity environment and monitor the system response. The test was performed by shutting off the RFMD motor power at the beginning of a reduced gravity period and restarting the RFMD at the beginning of the next reduced gravity period (Figure 2.1.4.2-5). As expected, when the RFMD was shutdown the SFE liquid flow rate went down (Figure 2.1.4.2-6) and the evaporator pump outlet pressure was reduced (Figure 2.1.4.2-7). When the RFMD was restarted, the system quickly reestablished normal operating conditions.

The entire test stand was inadvertently shutdown when one of the KC135 crewmen disabled a power supply. The power supply was reconfigured in about ten minutes and a hot system restart was executed. The system restart was normal and without incident.

The system level reduced gravity transient tests were all successful. They demonstrated that the system operates as expected adverse conditions and can be expected to perform well for continuous use in reduced gravity.

2.2 Ground Test Results

2.2.1 Overview

Ground testing was performed both before and after the KC135 reduced gravity flight tests. Preflight tests verified the acceptability and suitability of the flight test plan. Post flight ground tests provided one gravity data which was equivalent to the reduced gravity data. Ground testing utilized the same test setup, photographic techniques, and test conditions that were utilized in reduced gravity. Photographs of the ground test setup are shown in Figures 2.2.1-1 and 2.2.1-2.

RFMD RPM VS TIME
RFMD SHUT DOWN 4/17/87

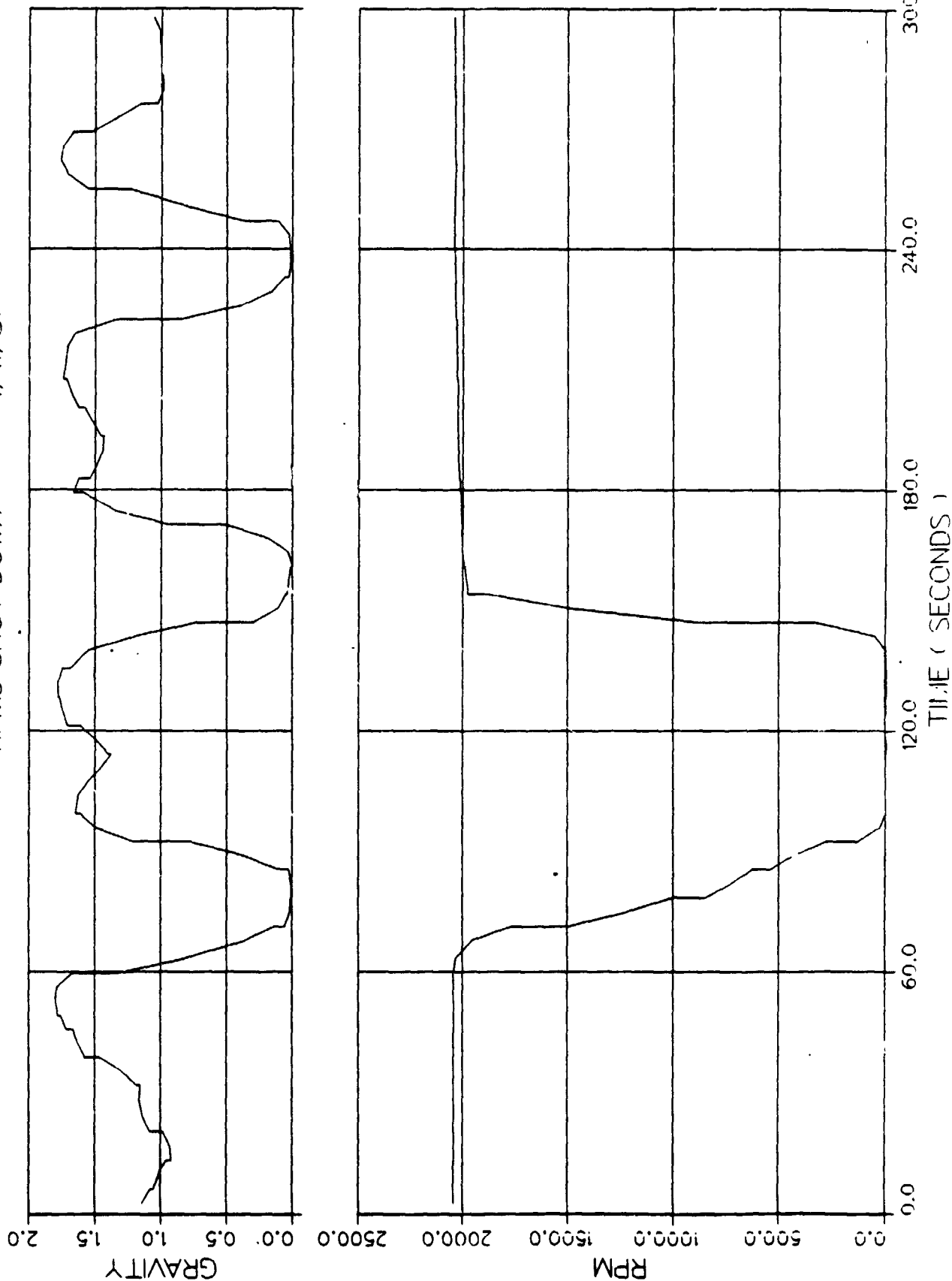


FIGURE 2.1.4.2-5

SFE LIQUID FLOW RATE VS TIME RFMD SHUT DOWN 4/17/87

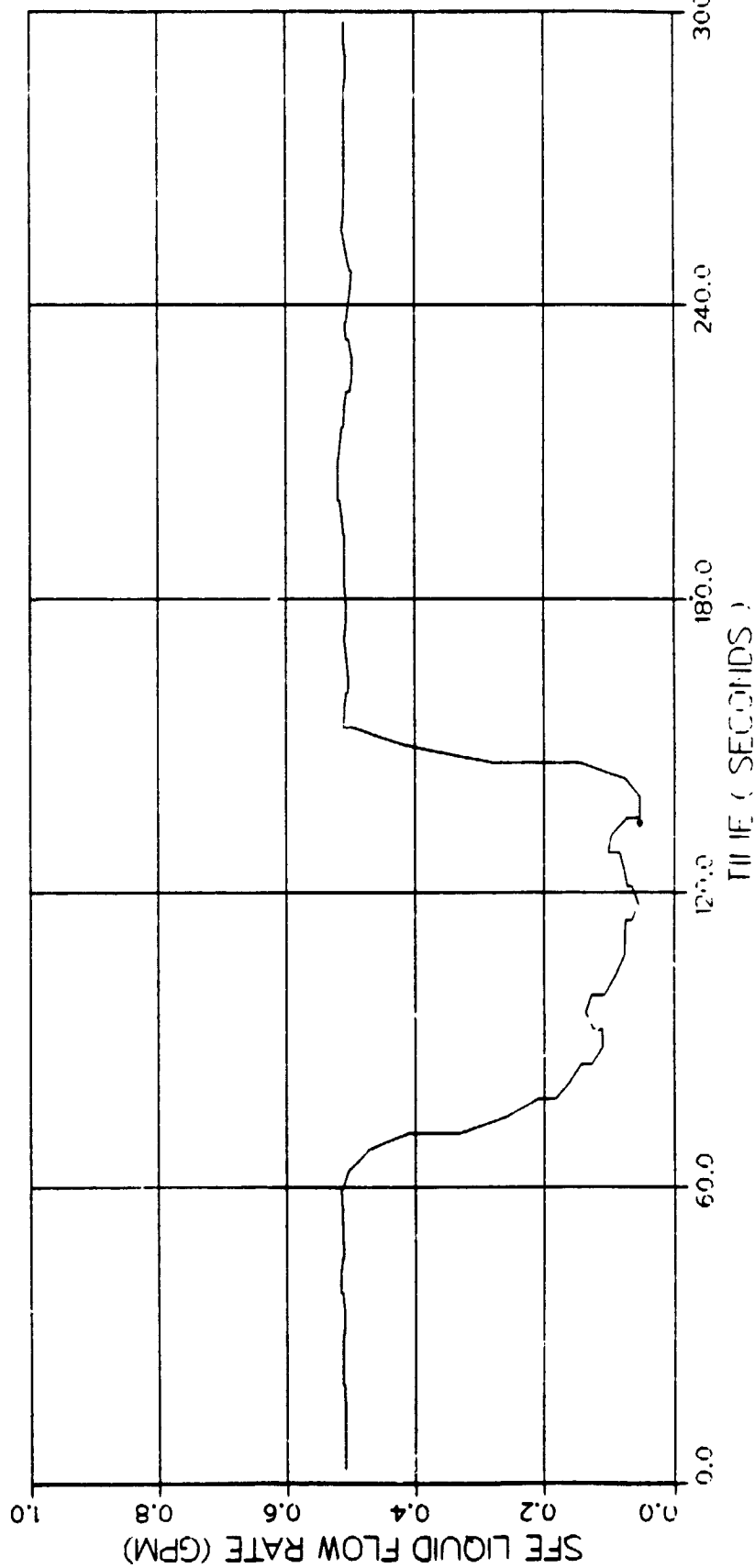
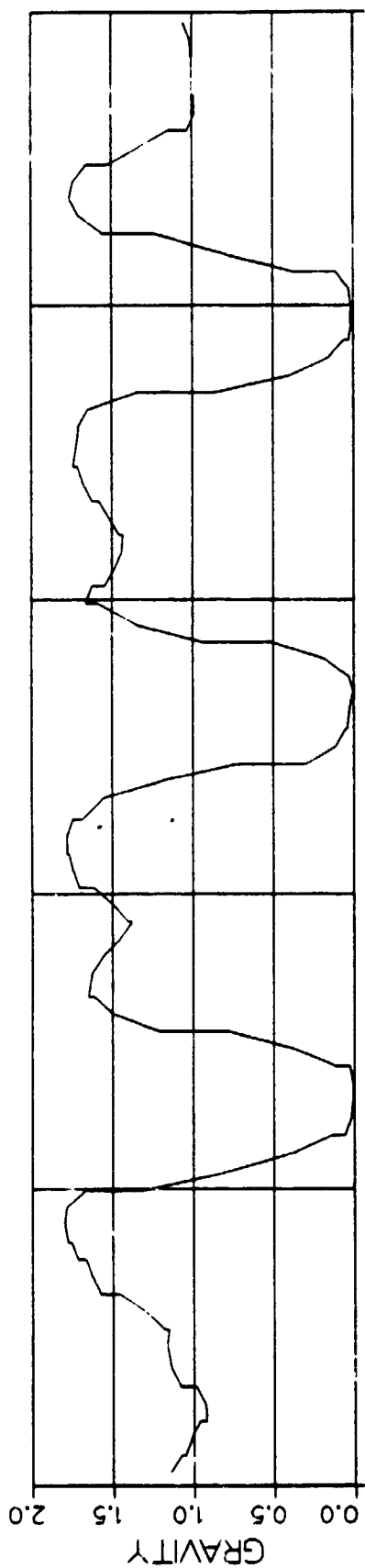
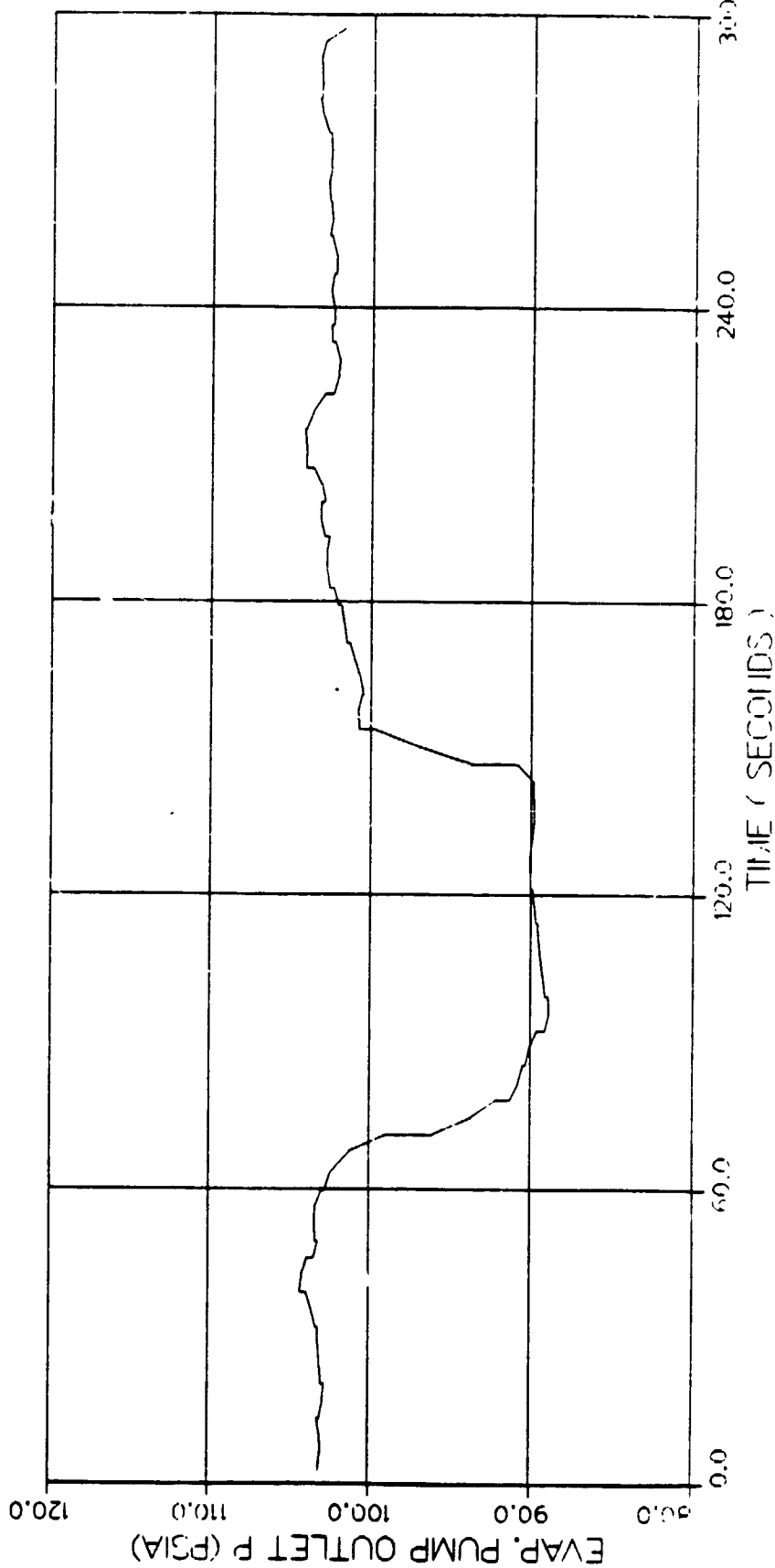
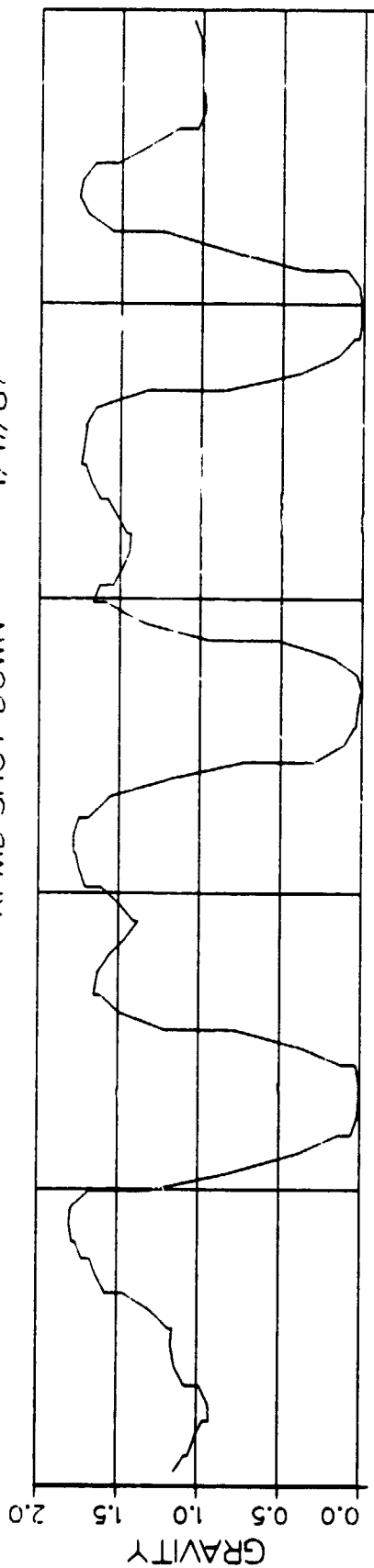


FIGURE 2.1.4.2-6

EVAP. PUMP OUTLET PRESSURE VS TIME RFMD SHUT DOWN 4/17/87



ORIGINAL PAGE IS
OF POOR QUALITY

FIGURE 2.1.4.2-7

ORIGINAL PAGE IS
OF POOR QUALITY



Figure 2.2.1-1 Ground Testing at NASA-JSC

ORIGINAL PAGE IS
OF POOR QUALITY

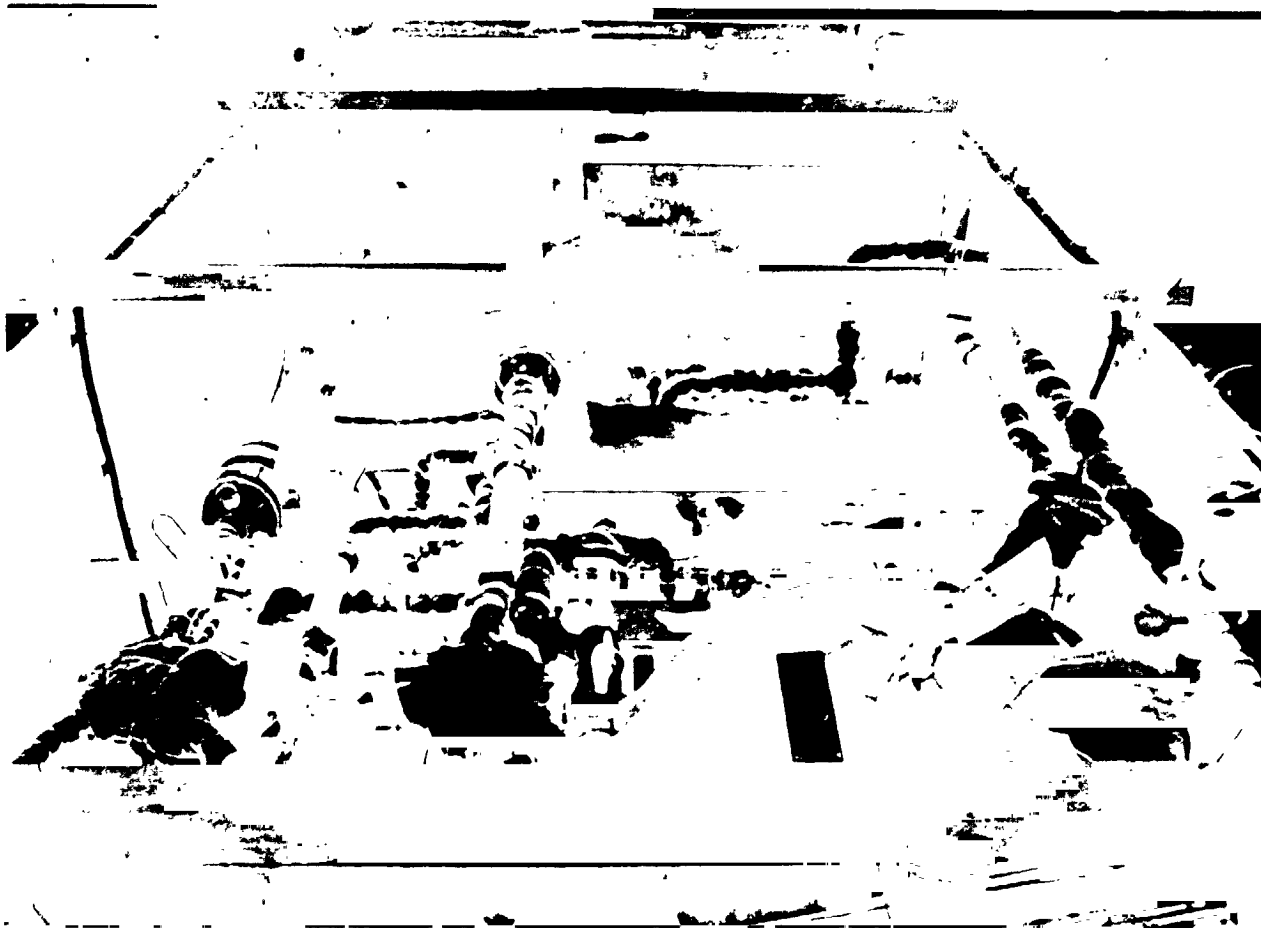


Figure 2.2.1-2 Ground Testing at NASA-JSC

2.2.2 Two-Phase Adiabatic Test Section

2.2.2.1 Two-Phase Flow Regimes

Ground test flow regimes observed both in real time and from high speed films were different from those predicted. These are summarized in Figure 2.2.2.1-1. Stratified flow generally occurred for most of the lower qualities tested, giving way to a semiannular stratified transition at the 80 percent quality. At the higher qualities, annular flow was expected to occur with transition into slug flow at the lower qualities. This can be seen by looking at the Taitel and Dukler, HTRI, Mandhane and revised Baker flow regime maps plotted in Figures 2.2.2.1-2, 3, 4 and 5 for the ground testing.

On the Taitel and Dukler map shown in Figure 2.2.2.1-2 boundaries prescribed by Taitel and Dukler (1976), by Sardesai et al (Reference 12) for in-tube condensation and by Kawaji (1987) (Reference 13), all show that annular flow should exist for the range of qualities tested. The observed test data follows the transition line between annular and stratified wavy with changing quality. Inspection of the HTRI map, Figure 2.2.2.1-3 also shows a discrepancy between observed and predicted one-gravity flow regimes. Annular, semiannular and slug flows were expected. Discussions with HTRI indicated that the map is more appropriate for in-tube condensation where liquid is deposited on the wall and is not necessarily valid for adiabatic flow.

The last two maps presented contain factors to account for fluid property variations, and therefore the figures drawn are specific to R114. The Mandhane map, shown in Figure 2.2.2.1-4 has its flow regimes boundaries drawn specific to the fluid properties, whereas the Baker map, Figure 2.2.2.1-5 has the data points modified by fluid property parameters. Baker's fluid parameter, λ and Ψ , are

<u>QUALITY</u>	<u>OBSERVED FLOW PATTERN DESCRIPTION</u>	<u>FLOW REGIME</u>	
		<u>OBSERVED</u>	<u>PREDICTED BY HTRI</u>
.15	STRATIFIED WAVY/OCCASIONAL SLUG	STRATIFIED WAVY/SLUG	SLUG
.2	STRATIFIED WITH LESS WAVE DEVELOPMENT	STRATIFIED	STRATIFIED/ANNULAR TRANSITION
.3	STRATIFIED WAVY/THIN ANNULAR FILM	STRATIFIED/ANNULAR	
.4	STRATIFIED WAVY/SEMIANNULAR	STRATIFIED/ANNULAR	ANNULAR
.5	THIN STRATIFIED WAVY/SEMIANNULAR	STRATIFIED/ANNULAR	ANNULAR
.6	THIN STRATIFIED WAVY/SEMIANNULAR	STRATIFIED/ANNULAR	ANNULAR
.8	SEMIANNULAR	ANNULAR	ANNULAR

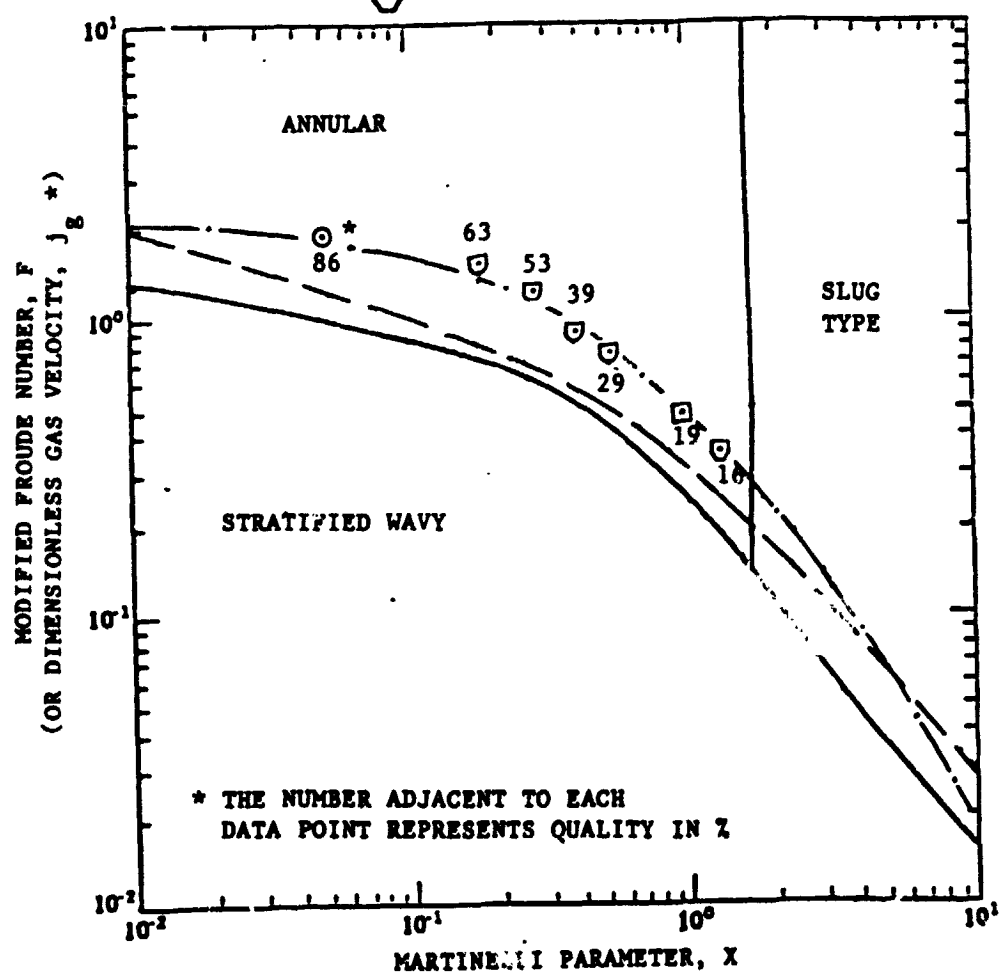
GROUND TEST FLOW REGIMES

FIGURE 2.2.2.1-1

GROUND TEST - TAITEL AND DUKLER FLOW REGIME MAP

OBSERVED FLOW REGIME

- ⊙ ANNULAR
- ◻ STRATIFIED/ANNULAR
- ◻ STRATIFIED
- ◻ STRATIFIED WAVY/SLUG



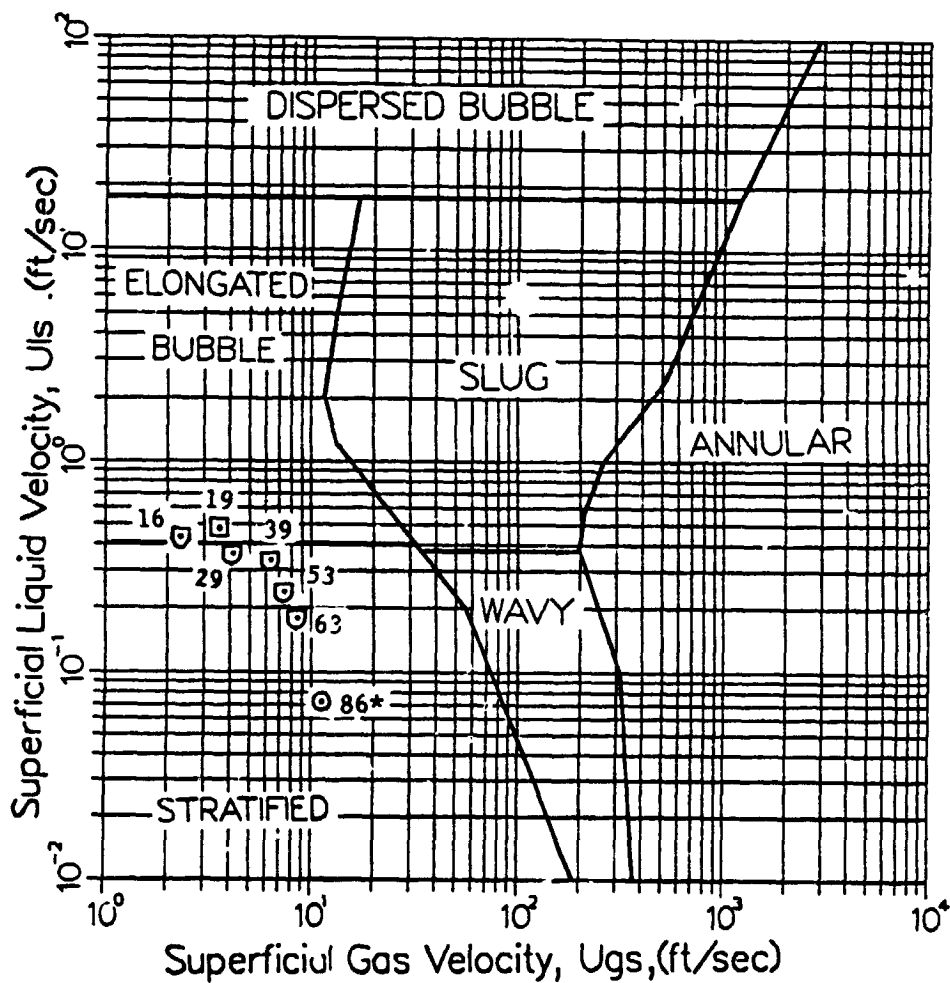
Flow Map Proposed by Taitel and Dukler

- Taitel & Dukler (Reference 4)
- - - Sardesi et al. Transition for Condensation Between Annular and Stratified Flow Regimes (Reference 12)
- Modified Taitel & Dukler
($f_l = 3f_g$, Proposed by Kawaji et al (Reference 13))

FIGURE 2.2.2.1-2

ORIGINAL PAGE IS
OF POOR QUALITY

MANDHANE (1974) TWO-PHASE FLOW REGIME MAP WITH PHYSICAL PROPERTY CORRECTION (R-114, 150 F)



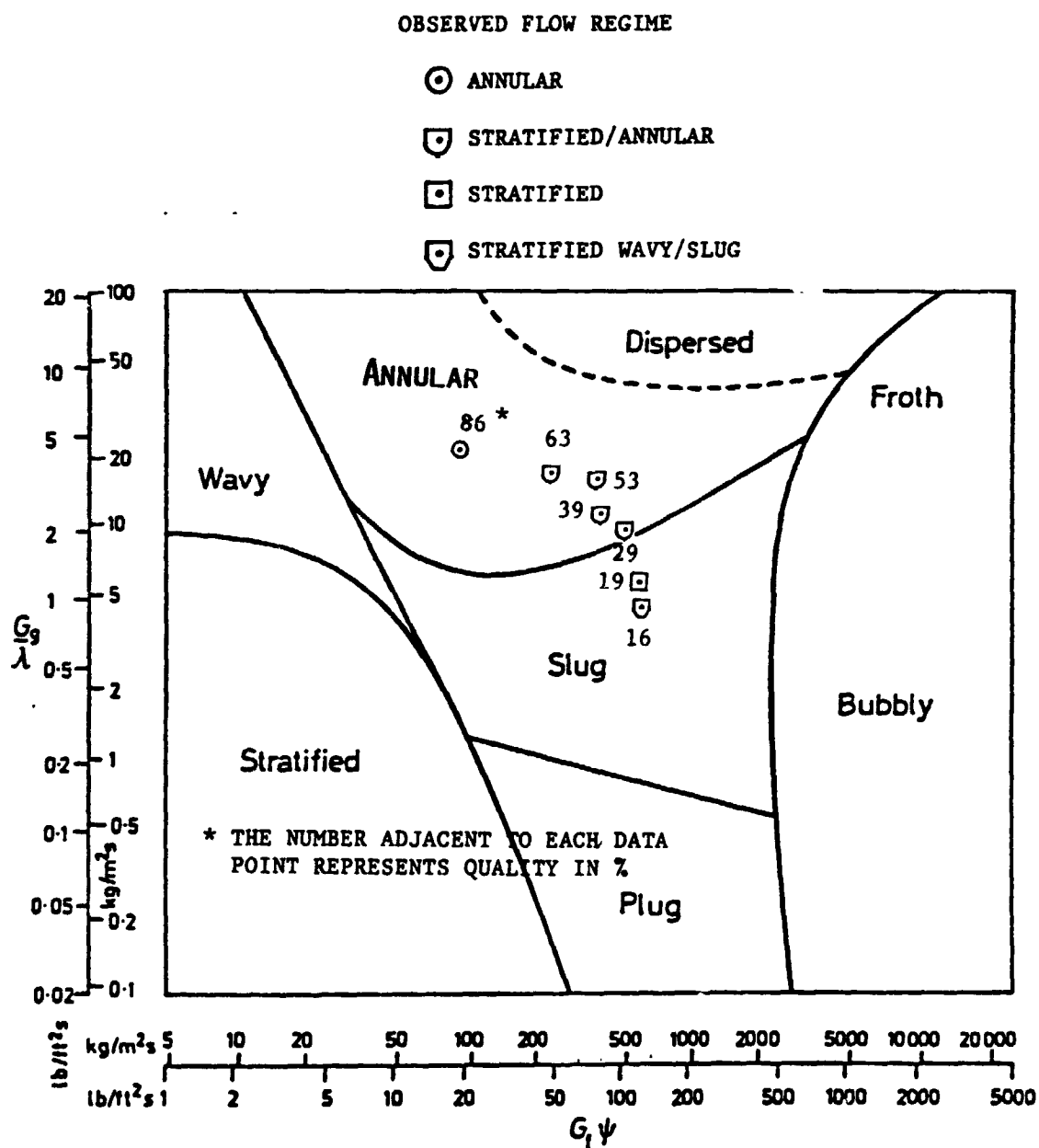
OBSERVED FLOW REGIME

- ANNULAR
- ◻ STRATIFIED/ANNULAR
- ◻ STRATIFIED
- ◻ STRATIFIED WAVY/SLUG

* THE NUMBER ADJACENT TO EACH
DATA POINT REPRESENTS QUALITY IN %

FIGURE 2.2.2.1-4

REVISED BAKER FLOW REGIME MAP FOR GROUND TEST



Flow pattern map for horizontal flow (Baker)

FIGURE 2.2.2.1-5

defined in Section 2.1.2.1 and the Mandhane map is modified by the X' , Y' parameters. These are defined by:

$$X' = \left(\frac{\rho_g}{\rho_a} \right)^{0.333} \left(\frac{\rho_g}{\rho_w} \frac{\sigma_w}{\sigma} \right)^{0.25} \left(\frac{\mu_g}{\mu_w} \right)^{0.2}$$

$$Y' = \left(\frac{\mu_g}{\mu_w} \right)^{0.2} \left(\frac{\rho_g}{\rho_w} \frac{\sigma_w}{\sigma} \right)^{0.25}$$

Where ρ , σ , and μ represent the density, surface tension and viscosity, the subscripts g and l represent the gas and liquid phases, and the subscripts a and w represent the values for air and water at atmospheric conditions. For the R114 at the average test conditions, these property correction factors are quite large, with $X' = 5.26$ and $Y' = 1.25$.

The Mandhane map correctly identifies the stratified flow regime but fails to identify the annular flow pattern. The Baker map correctly identifies the annular and slug flow patterns but fails to identify the stratified flows. Both of the property specific maps do not accurately predict the test data, however, as previously described, the Baker map provided a good fit for the reduced gravity tests.

The discrepancy between observed and predicted flow regime maps in ground testing resulted from several factors. The primary reason is lack of data for single component fluids with density ratios close to that of R114. Most data has previously been generated for two components such as air-water and oil-gas mixtures. The HTRI flow regime map which seems to fit the reduced-gravity data fairly well needs modification for adiabatic flow because of its derivation from horizontal in-tube condensation data. In general, the horizontal flow regime maps tested do correlate the observed data, however, the HTRI and Sardesai show the best agreement.

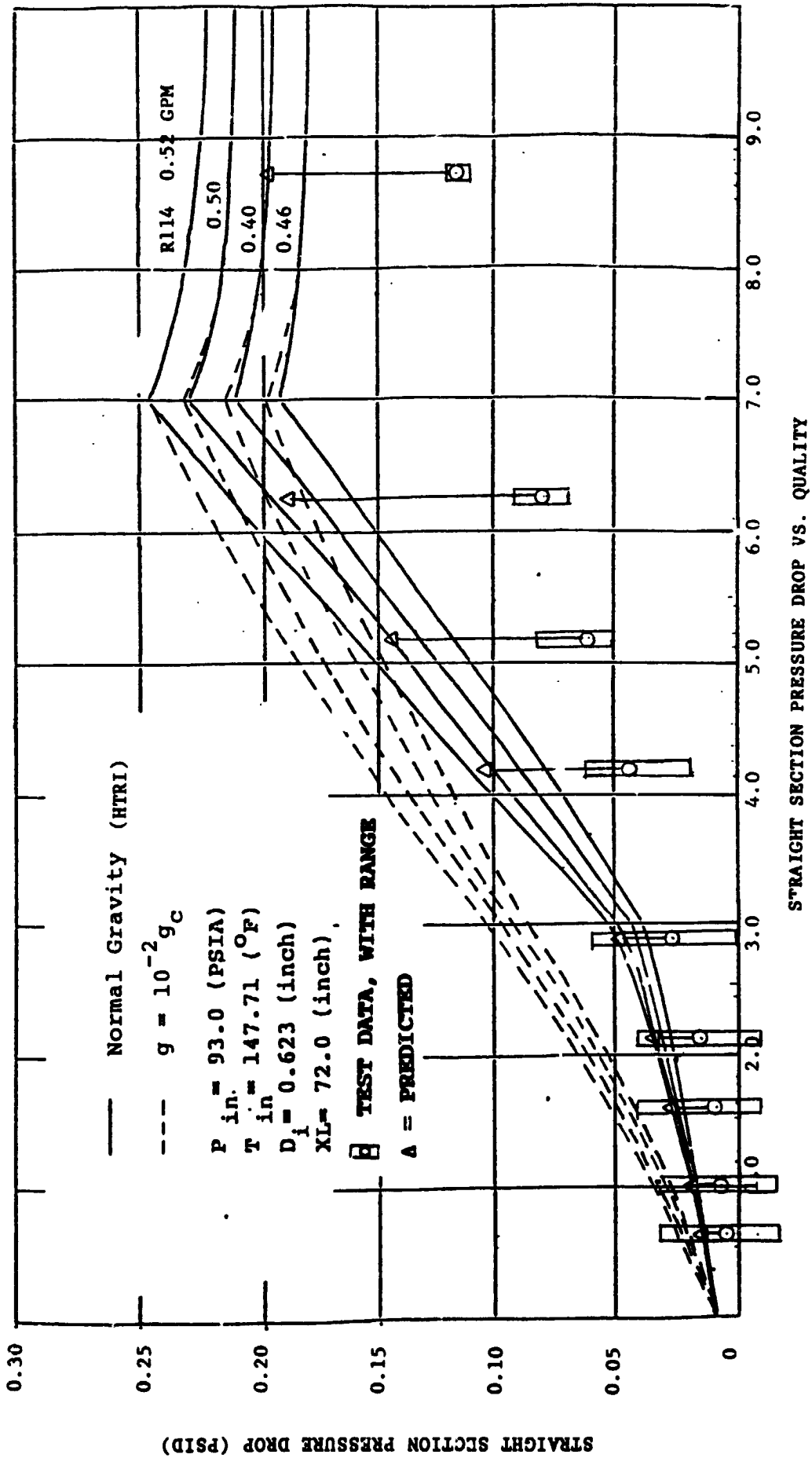
2.2.2.2 Pressure Drops

The straight adiabatic section pressure drop measurements generated during ground testing are shown plotted versus the pretest predictions using the HTRI method in Figure 2.2.2.2-1. The measured pressure drops are generally lower than those predicted. This under-prediction can be attributed to the choice of flow regimes used in the predictive model. In the HTRI model, a stratified type flow was presumed to exist with qualities less than 0.3, and a completely shear driven flow was presumed to exist at qualities above 0.7 quality. In a region between 0.3 and 0.7 qualities, a proration of the two predictive methods was used.

The flow regime transition zones for pressure drop correlation were altered to correlate with the observed rather than predicted flow regimes, resulting in better agreement between the predicted pressure drops and the test data. This predictive method will be referred to as the Transition Modified HTRI method in this report. Using this method, the revised pressure drop predictions shown in Figure 2.2.2.2-2 have been generated.

The measured straight section pressure drops were compared to predictive values using nine different correlating techniques. The data and predictions are listed in Figure 2.2.2.2-3. As expected, the best agreement occurred with the stratified flow correlations. The transition modified HTRI method and the Taitel-Dukler and Chisholm stratified methods give excellent agreement. Scatter plots for the original HTRI predictive method, transition modified HTRI method and the Taitel and Dukler stratified model are shown in Figures 2.2.2.2-4, 5 and 6. The improvement obtained by modifying the HTRI transition boundaries can be seen by comparing 2.2.2.2-4 and 5.

APRIL 9, 1987



GROUND TEST

FIGURE 2.2.2.2-1

STRAIGHT SECTION PRESSURE DROP VS QUALITY

GROUND TEST (FLOW PATTERN TRANSITION MODIFIED HTRI)

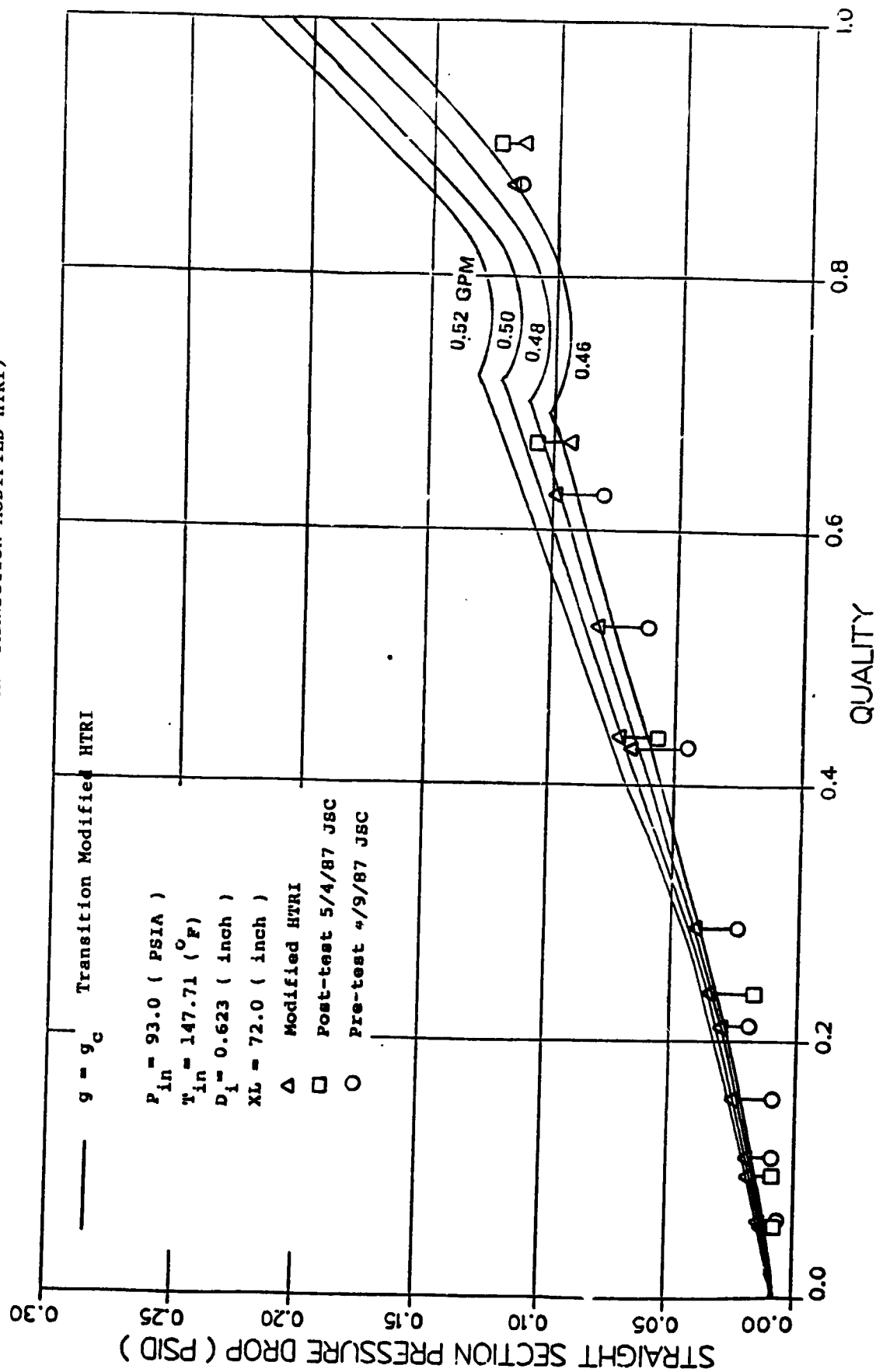
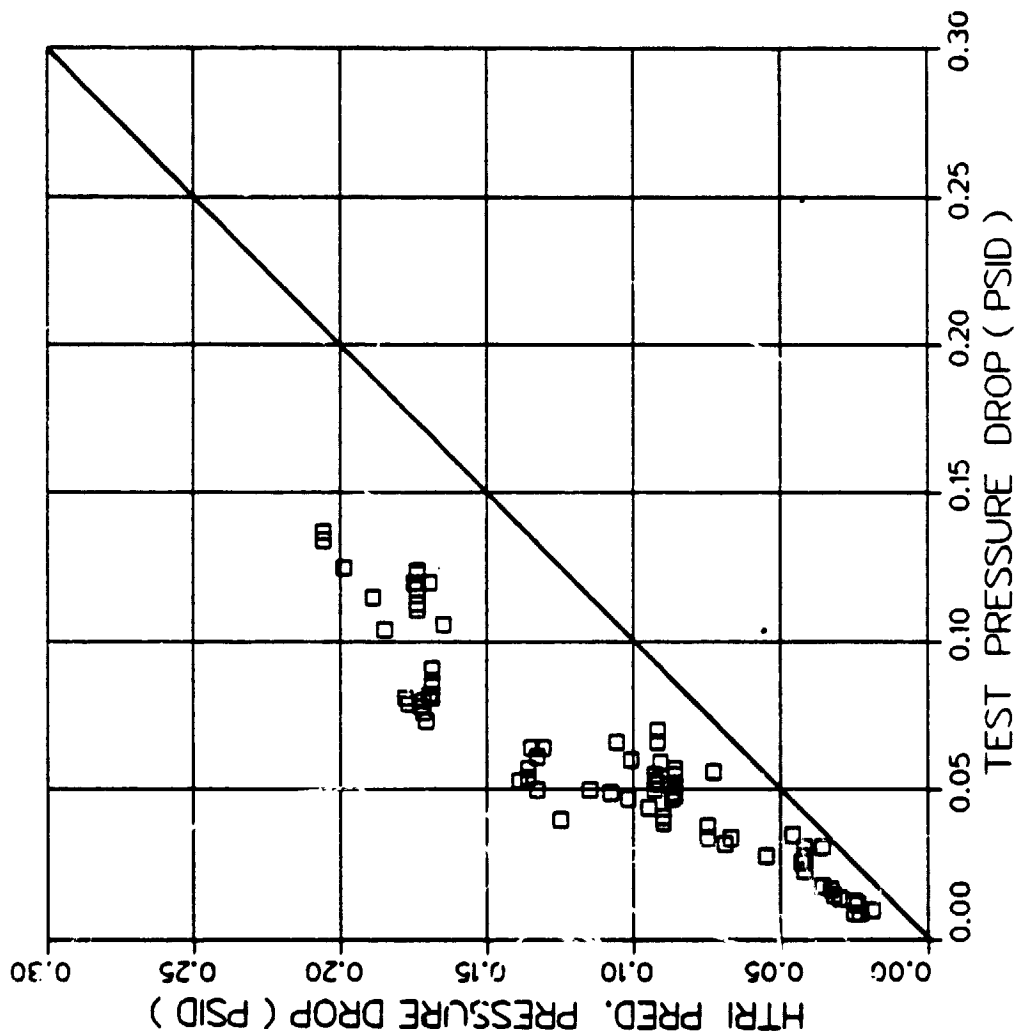


FIGURE 2.2.2.2-2

DATA AND PREDICTIONS

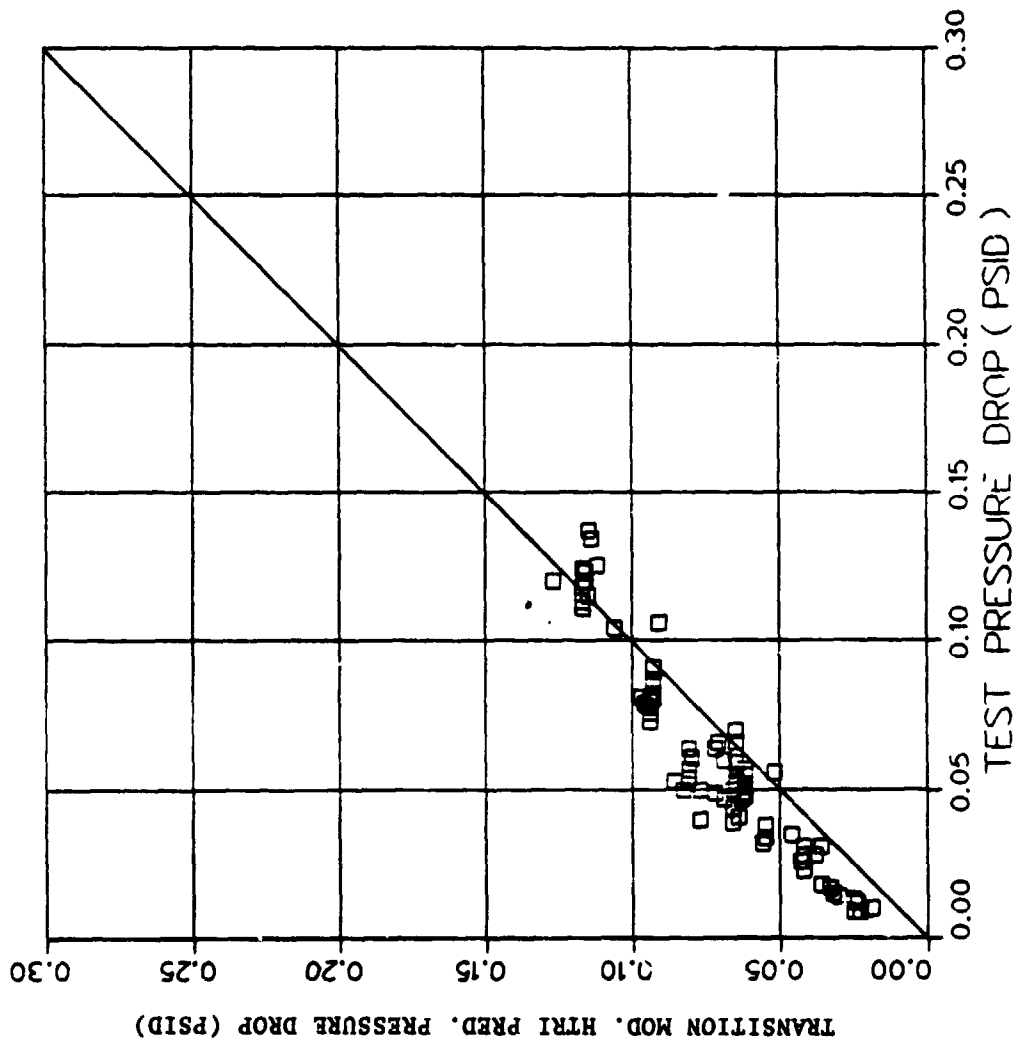
STRAIGHT SECTION TEST DP VS PRED. DP 4/9, 5/4, 5/7 GROUND TEST DATA



ONE-GRAVITY STRAIGHT SECTION HTRI PREDICTED
PRESSURE DROP VS TEST DATA PRESSURE DROP
SCATTER PLOT

FIGURE 2.2.2.2-4

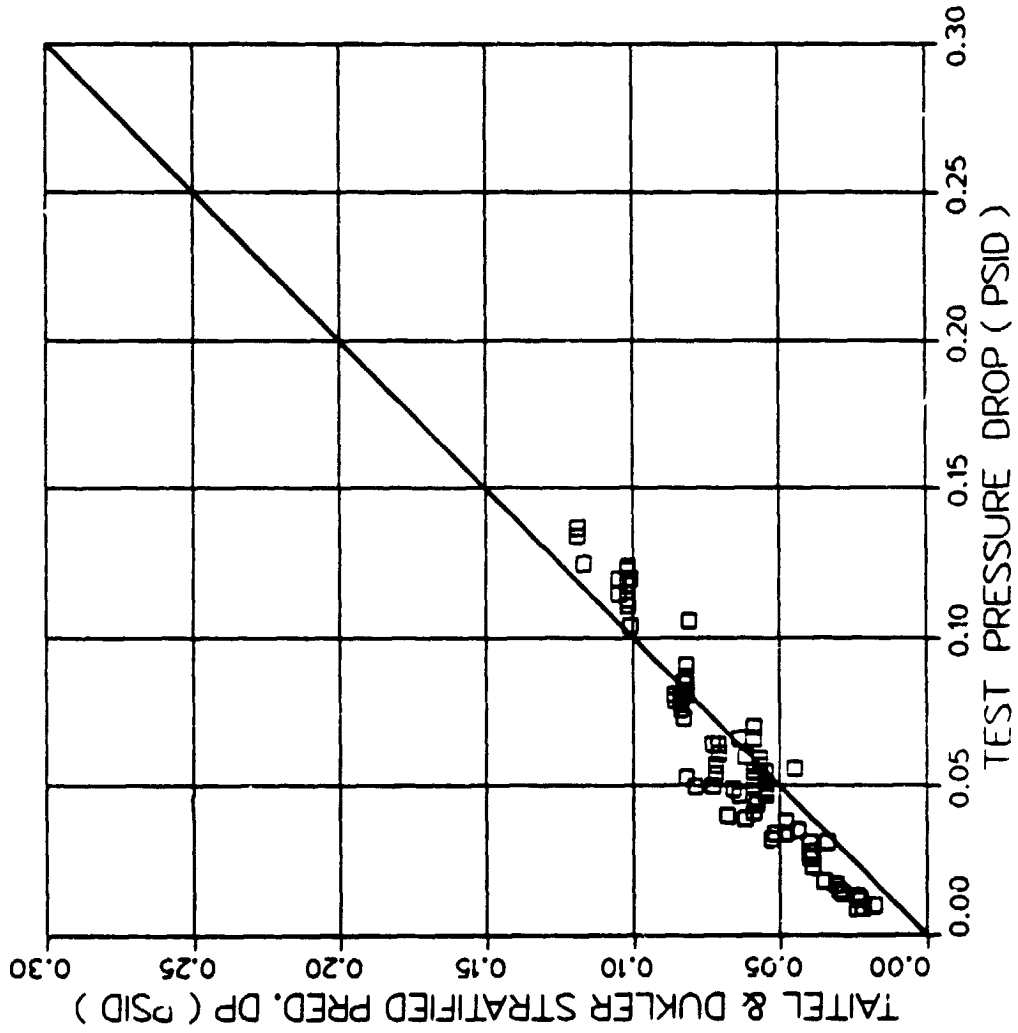
STRAIGHT SECTION TEST DP VS PRED DP
4/9, 5/4, 5/7 GROUND TEST DATA



ONE-GRAVITY STRAIGHT SECTION TRANSITION
MODIFIED HTRI PRESSURE DROP VS TEST DATA
PRESSURE DROP SCATTER PLOT

FIGURE 2.2.2.2-5

STRAIGHT SECTION TEST DP VS PRED. DP
4/9, 5/4, 5/7 GROUND TEST DATA



ONE-GRAVITY STRAIGHT SECTION TAITEL AND DUKLER
PREDICTED PRESSURE DROP VS TEST DATA
PRESSURE DROP SCATTER PLOT

FIGURE 2.2.2.2-6

The pressure drop was also measured over a longer, approximately 20-foot test section, which included fittings, valves, the adiabatic clear sections and the adiabatic curved section. The pressure drop for this section has a larger value and is expected to have less error than that of the adiabatic test sections. No pretest predictions were given for this test section, however, the data has been compiled and is shown in Figure 2.2.2.2-7. The pressure drop versus quality is plotted for both the reduced-gravity and one-gravity conditions. As previously noted the flow rate changed from approximately 0.54 gpm at the lowest qualities to around 0.46 gpm at the highest qualities. The curves show a uniform trend; the reduced-gravity pressure drops are higher than the one-gravity pressure drops at any quality, but have the greatest percentage increase in the low quality condition. It is expected that if the flow in one gravity were not stratified the increase in pressure drop during transition to zero-gravity would be decreased.

TEST SECTION DELTA PRESSURE VS QUALITY

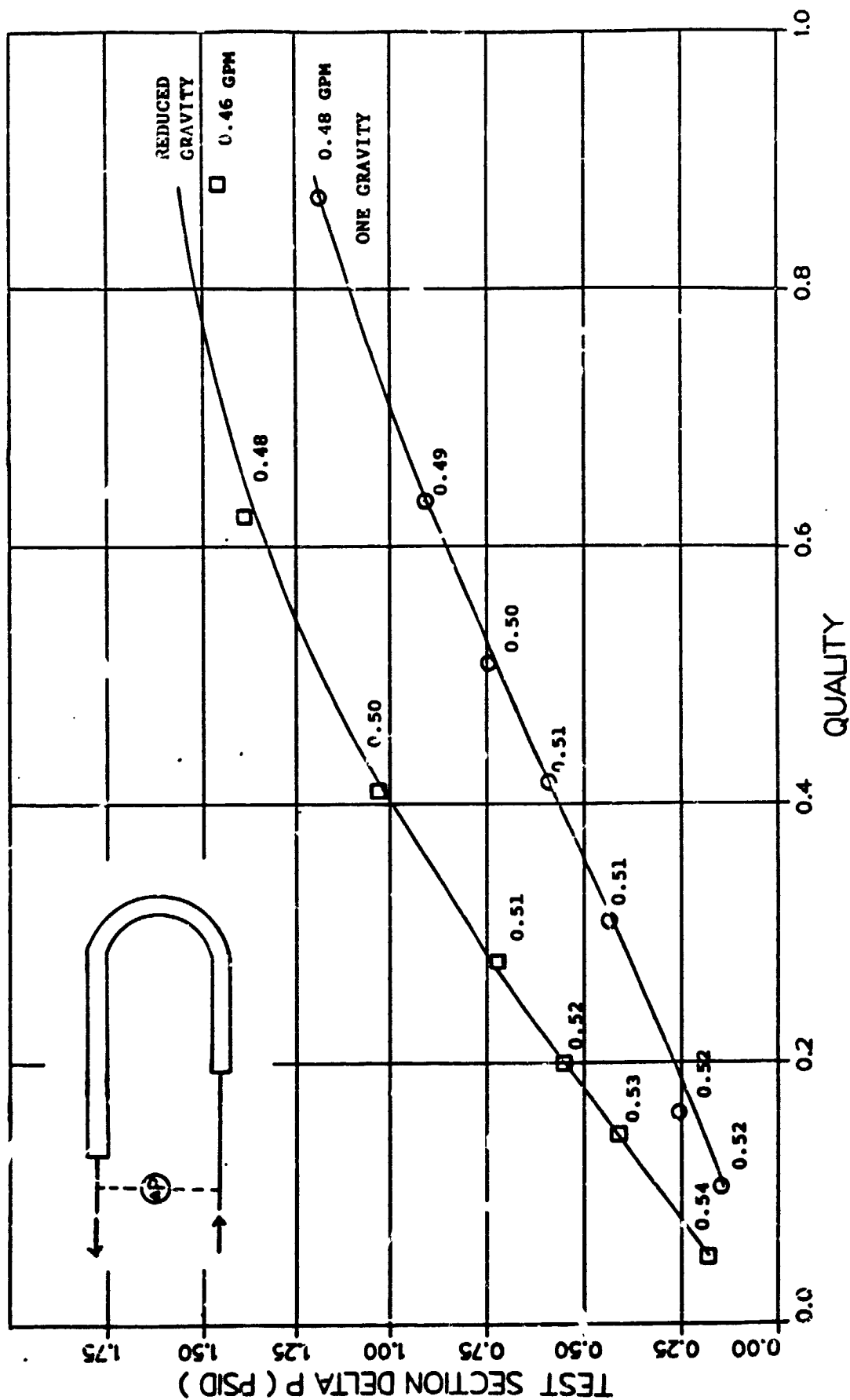


FIGURE 2.2.2.2-7

3.0 Test Conclusions

A test loop was designed, fabricated and successfully tested in normal and reduced gravity conditions meeting the objectives of the Two-Phase Thermal Control System Component Development Program. The test loop operated without any problems during the test flight in one-gravity, two-gravity and reduced-gravity environments. The two-phase flow regimes and pressure drops were recorded for various qualities. The data was analyzed and follows a predictable trend. The TPTMS system demonstrated durability and reliability in system tests which included loss of heat rejection, reduced-gravity RFMD shutdown and reduced-gravity RFMD startup. In addition, an unexpected power failure during the tests had no adverse effect on the test loop. The test loop was easily restarted and the testing continued uninterrupted.

3.1 Two-Phase Adiabatic Test Section

The reduced-gravity flow regimes were predictable, with slug and annular flows occurring during the reduced-gravity test. The test demonstrated the predictability of the transition between slug and annular flow. The transition between bubble flow to slug flow and annular to mist were not observed in this experiment. The modified Dukler flow regime map (Figure 2.1.2.1-6) provides the best agreement with the observed transition between slug and annular flow in reduced-gravity.

The reduced-gravity pressure drops closely followed the predicted trends. The straight section reduced-gravity pressure drop was accurately predicted by using the wet wall modified HTRI and Friedel correlations. The curved section reduced-gravity pressure drop was accurately predicted by the Chisholm B and C type correlations.

The one-gravity flow regimes did not match predictions. Stratified flow, wavy stratified and stratified/annular flow was observed whereas annular and slug flow were expected. The initial predictions for the straight section pressure drop were performed using the HTRI method which led to an over-prediction of the pressure drop, primarily because of inappropriate selection of flow regime. The HTRI method is based on horizontal condensing flow rather than adiabatic flow. When the flow regime boundaries were modified to match the test observations, very good correlation between the flow regimes and pressure drop predictions and the test results was achieved. The transition modified HTRI method provides the best correlation between the predicted and the observed flow regimes in one-gravity. The stratified Chisholm, Stratified Taitel and Dukler and transition modified HTRI provide the best pressure drop predictions for the straight section whereas the Chisholm B and C type provided the best pressure drop predictions for the curved section.

The pressure drop in zero-gravity is higher than in one-gravity by about twenty percent averaging the data for all qualities and flows.

3.2 Condenser

The condenser provided adequate heat rejection for the test loop during the test flight. The data collected on the condenser was difficult to analyze because transients experienced during the gravity transitions caused liquid carry-over from the vapor line. Analysis of the test data was performed on a point-by-point basis due to the transient conditions. When the specific conditions of a test point are analyzed, there was very good correlation for both pressure drop and overall heat transfer coefficient. The original condenser model over-predicts the pressure drop because it did not take into account the gap between the condenser cover and the fluted tube. When this is done, the condenser model pressure drop predictions greatly improve.

C - 2

4.0 Recommendations For Further Investigation

The reduced gravity two-phase flow pressure drop and flow regime data collected during this experiment confirms the validity of the predictive methods for the test setup configuration, thus, meeting the objectives of the test. The two-phase data in this report was generated using a single plumbing run and one evaporator. A large thermal management system will be made up of many heat loads requiring a variety of two-phase mass flows in different size lines. The effect of heat load, line size and mass flow must be understood to accurately size such a complex system. Further reduced-gravity testing should employ a test matrix which includes heat load, line size and mass flow variations. This would provide enough data to generate a complete reduced-gravity flow regime map which could be used for pressure drop prediction and line size selection.

Preliminary indications of a fifth flow regime (frothy-annular) in reduced-gravity should be investigated further. This should include detailed visual observations of the film footage to compare void fraction and film thickness in reduced and normal gravity at the same mass flux and quality. Further reduced-gravity testing could include film thickness measuring devices such as conductivity probes to evaluate the differences.

Although the test stand itself performed very well during the flight experiment, some components could be modified to improve the performance. The cavitating venturi could be resized to provide choked flow control on subsequent experiments. The condenser data was particularly difficult to analyze because of varying coolant (EGW) mass flows and liquid carry-over in the vapor line. Liquid carry-over can be reduced or eliminated by plumbing the condenser inlet at the same height as the RFMD vapor exit. The varying coolant (EGW) mass flows can be eliminated by modifying the heat

rejection cart to prevent pump cavitation in reduced-gravity. When more predictable condenser operating conditions are achieved, additional condenser tests could be performed. Finally, a clear section of line could be added to visually check the effectiveness of the RFMD demisters. These changes would improve the overall system operation and result in more complete data being generated.

5.0 Program Description

5.1 Introduction (Background)

In the past, small spacecraft have rejected the internally generated heat and maintained an energy balance via direct radiation to space with active electric heating of certain components to maintain proper thermal environments. As power levels have increased, pumped single-phase liquid loops have been used to collect and transport heat to a space radiator.

Future space platforms, such as the proposed Space Station, will have thermal power levels in the hundreds of kilowatts and transport distances of hundreds of feet. There are significant benefits to the concept of a "thermal bus" to provide the thermal management requirements. This bus would provide minimal variation in temperature and would allow either sources or sinks to be connected at any location without constraints.

A two-phase fluid loop provides the best solution to the design constraints. Heat is transferred by evaporation and condensation rather than sensible heating and cooling of the fluid, and therefore nearly constant temperatures can be maintained. Much lower mass flows are required for the evaporation process relative to sensible heating and cooling, and significant power savings and low distribution weights are realized.

To properly design a two-phase thermal bus for use in a space environment, the ability to accurately predict flow regimes and pressure drops in two-phase lines is essential for proper line size selection. Two-phase flow pressure drops are known to be significantly higher in as compared to earth gravity due to the difference in flow regimes.

Testing of two phase flows in reduced gravity environments has been very limited. In the late 70's, General Dynamics and NASA began a program of experiments flowing air and water through small tubes in reduced gravity environments. Testing was done in both the 2.2 second drop tower at NASA-LeRC and in reduced-gravity flight profiles aboard the NASA-Lewis Lear jet (Reference 9). These experiments show that three basic flow patterns exist in reduced-gravity two phase flow. The first flow pattern can be characterized as bubble, which is a continuous liquid phase with a dispersed bubble pattern within the liquid. For this flow pattern, the bubble size is smaller than the pipe diameter. The second pattern is an intermittent flow pattern. In this flow pattern, liquid slugs are followed by regions of high void fraction. This pulsating type of flow is believed to be the transition between the bubble type flow and an annular flow pattern. The third pattern is an annular flow pattern. In the annular flow pattern, the liquid flows as a thin film on the wall at a slower velocity than the central gas core. Some of the liquid is entrained and carried as a droplets in the vapor core.

Because previous experiments use a relatively short test section and the duration of the test was for a short time, good steady state pressure drop data was not obtained. On a comparative basis, however, the pressure drops measured in the reduced gravity environment greatly exceeded those measured during normal gravity. The greatest enhancement of pressure drops occurred in the lower mass flux regions that would occur in the bubble type flows for reduced-gravity and stratified flows for one-gravity. In the last few months, a new series of experiments have been conducted at the Lewis 100 foot drop tower and on board the Lewis Lear jet. This data taken with an improved test rigs should yield valuable information about the flow patterns in reduced-gravity.

There have been many flight experiments and demonstrations of heat pipe technology in the space environment of reduced-gravity. Heat pipes, however, do not truly represent two phase flow as the liquid and vapor flow paths are segregated. The liquid flows by capillary pumping to the evaporator section of the heat pipe and is returned in a vapor flow space.

This report describes an experiment which was conducted to measure pressure drops and observe two-phase flow in reduced-gravity. Tests were run on a wide range of qualities which would be generated by a Two-Phase Thermal Management System (TPTMS) in a space application. The results of this test will be used to expand the currently small data base on two-phase flow in zero-gravity and improve the current two-phase line sizing techniques.

5.2 Scope/Objectives

The scope of the Two-Phase Thermal Control System Component Development Program included the design fabrication, and testing of a TPTMS test loop under normal and reduced gravity conditions. The test loop incorporated the following key Sundstrand TPTMS components: RFMD, BPRV, Inventory Accumulator, SFE and Shear Flow Condenser. The test loop facilitated a KC135 flight test where two-phase flow regimes were observed and photographed in reduced gravity, and the pressure drop in a straight and curved length of clear tubing were measured. Similar performance data was obtained for the Shear Flow Condenser.

The key program objectives were to expand the two-phase flow regime data base in a reduced gravity environment and to demonstrate the mechanics of the TPTMS concept are not affected by variable gravity environments.

5.3 Test Stand Description

The Two-Phase Thermal Management System (TPTMS) test loop included the Sundstrand Rotary Fluid Management Device (RFMD), Back Pressure Regulating Valve (BPRV), Inventory Accumulator, Swirl Flow Evaporator (SFE), Condenser, Cavitating Venturi and miscellaneous plumbing. The test loop was instrumented with pressure transducers, temperature probes and flow meters. All the data from the test was collected on a digital data system. The two-phase flow pressure drop data was also recorded on an analog recorder to obtain continuous data.

A schematic of the TPTMS test loop used for the reduced gravity flight test is shown in Figure 2.0-1. Nearly saturated liquid is pumped from the RFMD through a cavitating venturi to the SFE where heat is added via electric heaters. The resulting two-phase flow passes through the clear two-phase test section for observation and photography and is returned to the RFMD. The liquid and vapor are separated in the RFMD. The vapor exits the RFMD and passes through the BPRV to the shear flow condenser. The condenser (Figure 2.1.3-1) has a clear cover so the condensation process can be observed and photographed. The subcooled liquid exiting the condenser is returned to the RFMD where it is resaturated and pumped out to the SFE again.

The fluid temperature to the SFE is held constant by controlling the saturation condition in the RFMD with the BPRV. Flow control to the SFE is provided by the cavitating venturi. Inventory control is accomplished with a level probe in the RFMD which is connected to an accumulator. Noncondensable gases are easily purged through the noncondensable gas vent (Figure 2.0-1). For a more detailed discussion of the Sundstrand TPTMS concept and development status see References 16, 17 18 and 19.

To minimize the program cost, the NASA-JSC supplied the test loop instrumentation, data acquisition systems, data acquisition,

software support, ground data reduction facilities, photographic equipment, lighting and photographers. The instrumentation was calibrated at the NASA-JSC and the calibration points were programmed into the data acquisition system. The instrumentation and data acquisition system were integrated into the test loop and checked out prior to shipment. A list of the instrumentation ranges and accuracies are shown in Figure 5.3-1.

The data acquisition system supplied by NASA-JSC consisted of a Hewlett-Packard computer with a Winchester Mass Storage hard disk drive and various signal conditioning equipment. The data system automatically scanned all fifty-three channels of data about every 2.5 seconds. After each scan, the data was stored on the hard disk drive and a monitor display was updated. The monitor provided real time data for system operation.

System heat rejection was performed by the heat rejection cart (Figure 5.3-2). The heat rejection cart schematic is shown in Figure 5.3-2a. An ethylene glycol/water (EGW) mixture is pumped into the test loop condenser where heat is picked up. The EGW mixture then flows through the air-cooled radiator where the heat is then rejected into the cabin air. The heat rejection cart accumulator was plumbed in the loop to provide room for thermal expansion of the water. Flow to the condenser was controlled by a diverter valve which diverted the excess flow back to the reservoir tank. Heat rejection was calculated by measuring the EGW mass flow and the EGW temperature difference at the inlet and outlet of the condenser, as well as using R114 measurements.

All of the test loop components requiring electric power were operated through the Electrical Control Console (Figure 5.3-3). The control panel consisted of power switches, voltage control dials, a variable frequency power supply and a series of panel meters used to monitor essential system parameters and provide system safeties which were software independent.

TEMPERATURE BULBS

<u>LOCATION</u>	<u>MAXIMUM</u>	<u>NOMINAL</u>	<u>MINIMUM</u>	<u>ACCURACY</u>
T1	200 °F	142 °F	30 °F	±.5°F
T3	200 °F	142 °F	30 °F	±.5°F
T4	200 °F	142 °F	30 °F	±.5°F
T5	SEE BELOW*			
T9	200 °F	142 °F	30 °F	±.5°F
T10	200 °F	142 °F	30 °F	±.5°F
T13	200 °F	142 °F	30 °F	±.5°F
T15	200 °F	142 °F	30 °F	±.5°F
T16	200 °F	142 °F	30 °F	±.5°F

* 0 10 THERMOCOUPLES THAT ARE BUILT INTO THE SWIRL FLOW EVAPORATOR (TYPE T)

0 4 TYPE "T" THERMOCOUPLES TO MONITOR HEATER TEMPERATURE

TEST LOOP INSTRUMENTATION ACCURACIES

FIGURE 5.3-1



PRESSURE TRANSDUCERS

TO ATMOSPHERE	MAXIMUM	NOMINAL	MINIMUM	ACCURACY
P1	130	100	5	± 1.3 PSI
P3	130	100	5	± 1.3
P5A	100	85	5	± 1.0
P5B	100	85	5	± 1.0
P6	100	85	5	± 1.0
P7	100	85	5	± 1.0
P9	100	80	5	± 1.0
P12	100	80	5	± 1.0
P13	120	105	5	± 1.2

TO INTERNAL

$\Delta P3$	25	15	0	± 0.25
$\Delta P4$	15	10	5	± 0.15
$\Delta P6A$	5	1	0	± 0.05
$\Delta P6B$	5	1	0	± 0.05
$\Delta P7A$	12.5	7	0	± 0.125
$\Delta P7B$	25	2	0	± 0.05
$\Delta P8$	25	5	0	± 0.25
$\Delta P9$	15	5	0	± 0.15

0 17 DELTA PRESSURE TRANSDUCERS
 0 1 ABSOLUTE PRESSURE TRANSDUCER - 10PSIA \pm .2 PSIA MAX FOR MEASURING CABIN PRESSURE
 0 THE SWIRL FLOW EVAPORATOR HAS THREE PRESSURE PORTS REQUIRING THREE PRESSURE TRANSDUCERS



TEST LOOP INSTRUMENTATION ACCURACIES

FIGURE 5.3-1

FLOW METERS AND MISC. INSTRUMENTATION

FLOW METERS

	MAXIMUM	NOMINAL	MINIMUM	ACCURACY
Q2 R114	1 GPM	0.3 GPM	0 GPM	1%
Q11 R114	1 GPM	0.6 GPM	0 GPM	1%
Q14 R114	1 GPM	0.6 GPM	0 GPM	1%
Q16 WATER	10 GPM	5.0 GPM	0 GPM	1%
Q17 R114	1 GPM	0.5 GPM	0 GPM	

MISCELLANEOUS

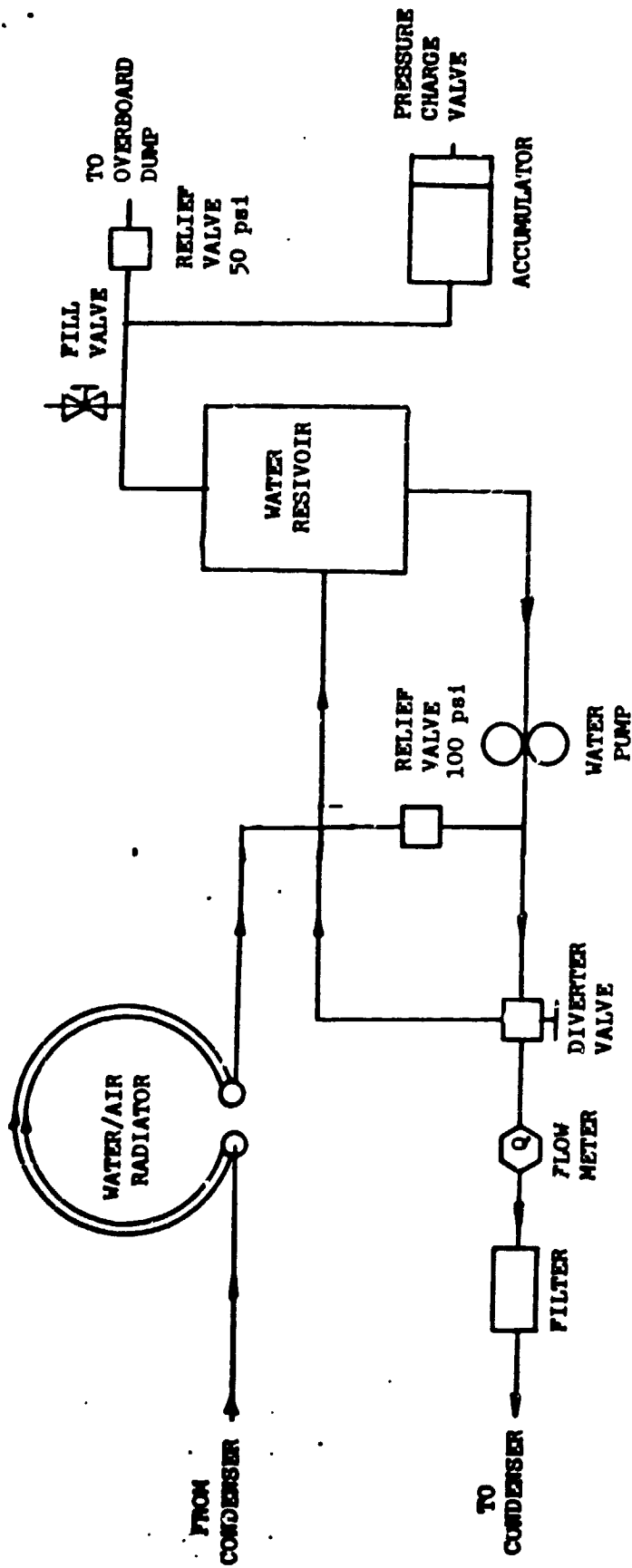
M (MAG. PICKUP)**	4000 RPM	3000 RPM	0 RPM	1%
PS**	FULL	HALF	EMPTY	1%
ACCELEROMETER	3 G	1 G	-2 G	1%
SWIRL FLOW EVAPORATOR HEATER POWER TRANSDUCERS (2)	5000 WATTS		0 WATTS	1%

- 0 DIGITAL TIME DISPLAY (3) - FOR TIME CORRELATION OF TEST SECTION FILM (LCD)
- 0 DIGITAL ACCELEROMETER DISPLAY - FOR TIME CORRELATION OF TEST SECTION FILM
- FOR RFMD BEARING LUBRICATION SAFETY TO BE SUPPLIED BY SUNDSTRAND
- THE PROTOTYPIC RFMD INCORPORATES A SPEED PICKUP AND THE PROTOTYPIC ACCUMULATOR INCORPORATES A BELLOW'S POSITION SENSOR. BOTH SENSORS WILL BE SUPPLIED BY SUNDSTRAND

ORIGINAL PAGE IS
OF POOR QUALITY



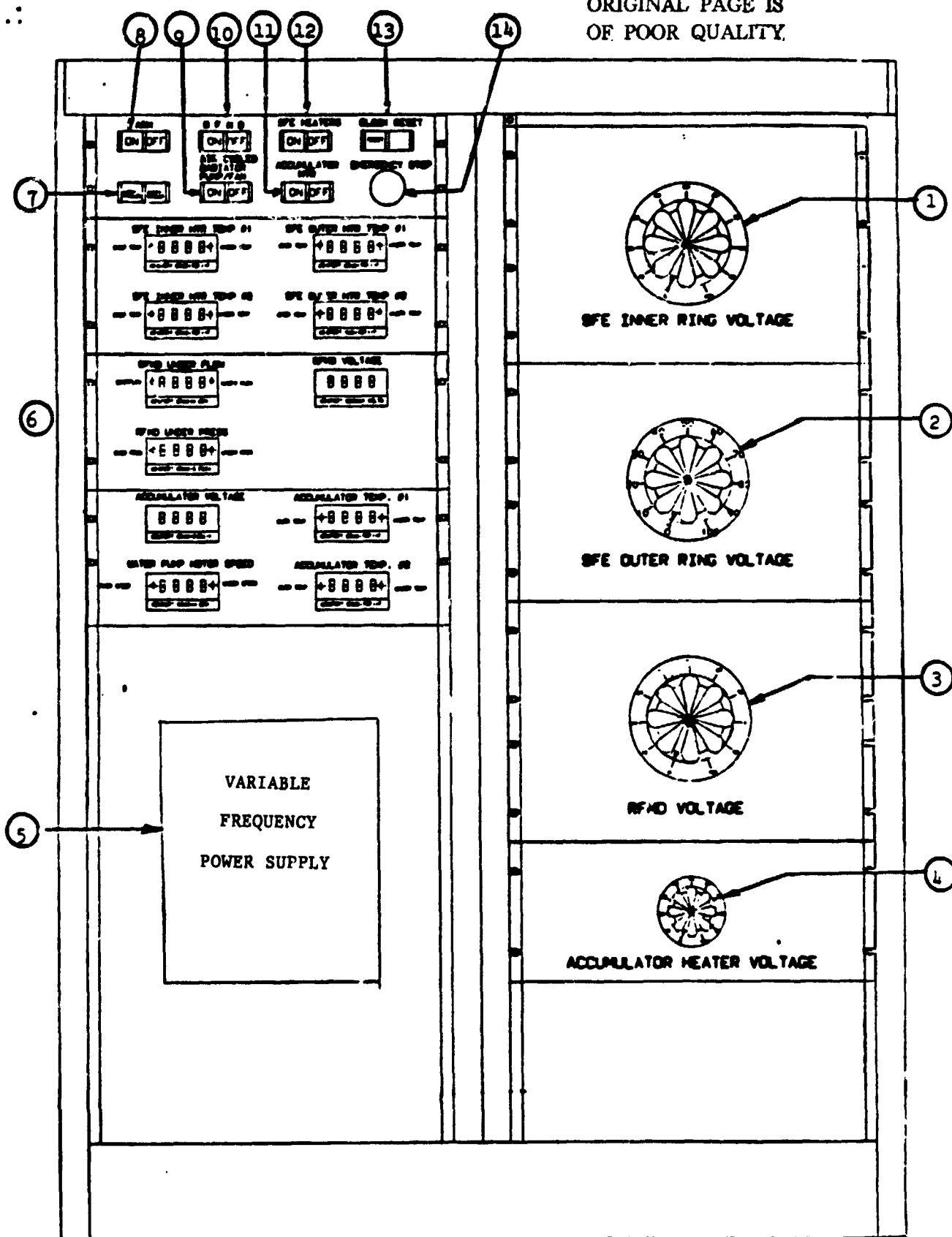
Figure 5.3-2 Heat Rejection Cart



HEAT REJECTION CART SCHEMATIC

FIGURE 5.3-2a

ORIGINAL PAGE IS
OF POOR QUALITY



ELECTRICAL/CONTROL CONSOLE

FIGURE 5.3-3

ELECTRICAL/CONTROL CONSOLE REFERENCE

<u>NUMBER</u>	<u>DESCRIPTION</u>
1	Swirl Flow Evaporator Inner Ring Voltage: 0-120 volts
2	Swirl Flow Evaporator Outer Ring Voltage: 0-120 volts
3	Rotary Fluid Management Device Motor Voltage: 0-120 volts
4	Accumulator Heater Voltage: 0-110 volts
5	Variable Frequency Power Supply: 0-400 Hz
6	Panel Meters (11)
7	Safety Enable/Disable Switch
8	Arm Switch
9	Air Cooled Radiator Pump/Fan Power Switch
10	Rotary Fluid Management Device Power Switch
11	Accumulator Heater Power Switch
12	Swirl Flow Evaporator Heaters Power Switch
13	Clock Reset
14	Emergency Stop

TABLE 5.3-3 (CONTINUED)

The RFMD input power was controlled by a variable frequency power supply with voltage control. The heater voltage for the SFE and inventory accumulator were controlled by a Variac located on the control panel. The heat rejection cart motor was also controlled from the panel.

The test loop safety system was monitored and operated from the control console. The safety system was armed after startup of the RFMD and cooling cart. When activated, it provided redundant fail safe operation of the test stand so that no single point failure would cause damage to either people or equipment.

The Swirl Flow Evaporator (SFE) employed electric thermofoil heaters which were bonded to the evaporator cold plate. The heater skin temperature was monitored by four thermocouples, two on the inner ring of heaters and two on the outer ring of heaters. Each of the thermocouples was interconnected to a set of panel meters with dual set point (high and low limit) control outputs. If the heater skin temperature rose above a predetermined value, the heaters were automatically shut down by opening the magnetic contactor which supplies power to the heaters. The heater skin temperature was also visually displayed on the control panel using the software independent panel meters.

The RFMD bearings were protected from a loss of lubrication flow. The lubrication safety system employed a flow meter on the condenser end lubrication flow and a pressure transducer which monitored the evaporator pitot outlet pressure. The condenser end lubrication flow and the evaporator pitot outlet pressure were visually displayed on panel meters. Each panel meter had dual set point control output capabilities. If either the condenser end

lubrication flow or the evaporator pitot outlet pressure fell below the specified limit set on the panel meters, the RFMD power was shut down by opening the magnetic contactor. When the RFMD power was cut off, the SFE heater power was also cut off because SFE cooling was no longer provided. The RFMD safety system was redundant because it employs two independent monitoring and shutdown systems. The SFE shutdown was redundant because when the RFMD power is cut the heater power was also cut. Should this fail, the heaters would over temperature and cut off.

All of the test stand electrical systems were guarded by either fuses or breakers. The thirty-six swirl flow evaporator heaters were protected by fuses. All of the other electrical components (motors, power supplies, etc.) were protected by breakers, and each motor starter had overcurrent protection. The fuses, safeties and breakers were used in addition to the breakers provided aboard the aircraft. The entire test stand was also bonded and grounded to protect against static discharge.

The TPTMS test stand is a pressurized system, therefore, a pressure relief valve was required in the event of an overpressure situation. The pressure relief valve was be set at a predetermined limit and was be vented to the overboard dump on the KC135.

The heat rejection system was an integral part of the test stand and required a safety system to insure that it was operating properly. The heat rejection system employed a magnetic pickup interconnected to a panel meter having a dual set point control output which monitored the pump and fan motor. Upon failure of the pump motor, the RFMD was shutdown by opening a motor power magnetic contactor. This action will also shut down the SFE heaters. If the heat rejection system failed, the backup system was the pressure relief valve. It was unlikely that this feature would be used since the system has a high thermal inertia and was monitored

closely during operation by flight personnel. The heat rejection safety system was a manually overridden for the loss of condenser cooling tests. The test stand could be quickly shut down by use of an emergency shutdown button should it be necessary.

The flow in the condenser was to be viewed through a clear condenser cover. It was required that the clear cover be protected from possible breakage by a foreign object and contained in the event of an internal rupture. The test stand employed a rigid, clear cover to provide protection and allow viewing of the condensation process. The space between the clear condenser cover and the protective cover was vented to the overboard dump on the KC135.

5.4 Design Considerations

During the reduced gravity flight test aboard the KC135, the system hardware encountered reduced-gravity, one gravity and two gravities. The system hardware operation was gravity insensitive. The major TPTMS components, the RFMD, SFE, condenser and accumulator, were tested in adverse orientations on the ground to show gravity independent operation. During the reduced gravity test flight, the performance of the TPTMS components was unaffected by the changes in gravity.

The test loop was designed to meet the specifications called out in the "JSC Reduced Gravity Aircraft Users' Guide" (Reference 10). The TPTMS hardware is mounted in an aluminum frame and each mounting bracket was sized per the following shock loads; 9-g's forward, 6-g's up and 2-g's inboard/outboard. The test loop frame and facility hardware have a 20" by 20" bolt down pattern to match that of the plane. The TPTMS plumbing meets the required proof and burst requirements for R114 operation.

The test loop is fitted with a clear two-phase return line for observation and photography of two-phase flow. The two-phase flow generated during the test ranged from a quality of five percent to eighty percent. The inside diameter of the two-phase return line is 5/8 inch (Figure 2.0-2). This size was chosen because it maximizes the observable two-phase flow trends and transitions for the conditions of the test. A smaller diameter tube would not have allowed good observation of bubble interactions, coalescence and flow regime transitions. A larger diameter tube would have resulted in only stratified flow at low qualities on the ground rather than the more interesting slug, bubble and plug flow regimes.

Two pressure drop measurements were taken along the clear two-phase return line (Figure 2.0-2); one was a 180° bend made up of two 45° fittings and a flex hose, the other was a 72-inch long straight section downstream of the bend. The pressure measurement ports for the bend were located upstream and downstream far enough so that the fluid entrance and exit effects did not influence the measurement. The distance allowed the flow to be fully developed where the pressure measurements are taken.

The pressure measurement ports for the straight section were similarly located in a fully developed flow region (Figures 2.0-2). In both cases, the pressure drop is large enough so that it can easily be measured with standard instrumentation and accuracy is retained. The downstream side of the clear two-phase line is located at the edge of the test loop to allow easy photography of the fully developed flow regimes.

Heat was rejected from the test loop by a shear controlled condenser (Figure 2.1.3-1). It was comprised of multiple parallel channels formed by cutting axial grooves in the outer surface of a thick walled aluminum tube. The tube was then assembled inside a

transparent cast acrylic tube to allow observation of the condensing process. Cooling water from the heat rejection cart was pumped through the inside of the aluminum tube to provide the heat rejection process. The axial condenser channels decrease in depth from the inlet to the outlet in order to maintain vapor velocities throughout the entire length adequate to provide shear controlled condensation. The condenser provided adequate heat rejection for the duration of the flight test. The performance of the condenser is discussed in Section 2.1.3.

5.5 Test Plan Overview

The overall test plan was divided into the following sections: System Verification, System Performance Mapping, ground testing at JSC and reduced gravity testing aboard the NASA-JSC KC135 aircraft. The System Verification and Performance Mapping was performed at Sundstrand to develop procedures and provide data which was used as a reference for both ground checkout at the NASA-JSC and as a one-gravity reference for the reduced gravity flight test data. The flight test provided reduced gravity and hyper-gravity data for two-phase flow in various flow regimes. In addition, the flight test provided data which was used to characterize the complete TPTMS operation in reduced gravity.

5.5.1 Ground Testing

The test loop was checked out on the ground at Sundstrand and at NASA-JSC. The purpose of the ground testing was to establish an operating procedure, determine the test loop performance and run flight test simulations. The test conditions were as follows:

RFMD Speed: 2000 rpm

RFMD Drum Pressure: 89 psia

Evaporator Pump Outlet Temperature: 146°F

Evaporator Mass Flow: 338.6 lb/hr (0.5 gpm)

Condenser Recirculation: Off

Working Fluid: R114

The following is a typical set of heat loads run during a checkout test:

Swirl Flow Evaporator
Head Loads (Watts)

FIGURE 5.5.1-1

Total Power	Inner Heaters	Outer Heaters	Exit Quality
240	40	200	0.05
480	80	400	0.1
720	120	600	0.15
950	150	800	0.2
1330	230	1100	0.3
1900	300	1600	0.4
2400	430	1970	0.5
2800	500	2300	0.6
3800	700	3100	0.8

The data collected from these tests was used to confirm proper test loop and facility operation.

5.5.2 Reduced Gravity Test Overview

The reduced gravity tests were performed aboard the NASA-JSC KC135 reduced gravity aircraft. The aircraft flies a series of parabolae to obtain the reduced gravity (Figure 5.5.2-1). Each reduced gravity period lasts approximately twenty-five seconds and is bounded by a period of two gravities. Due to the short duration of each reduced gravity period, the testing was done in increments. Each evaporator heat load was selected, allowed to equilibrate during level flight, and remained unchanged for three consecutive parabolae. Data was collected for the entire duration of the test.

5.5.2.1 Filming During Flight

High speed photography was used to film the two-phase flow in the two-phase clear test section, and the condenser. In addition to the high speed cameras, a video and a still camera were used for documenting the overall test loop operation during the flight.

The planned camera speeds for filming the two-phase flow were as follows:

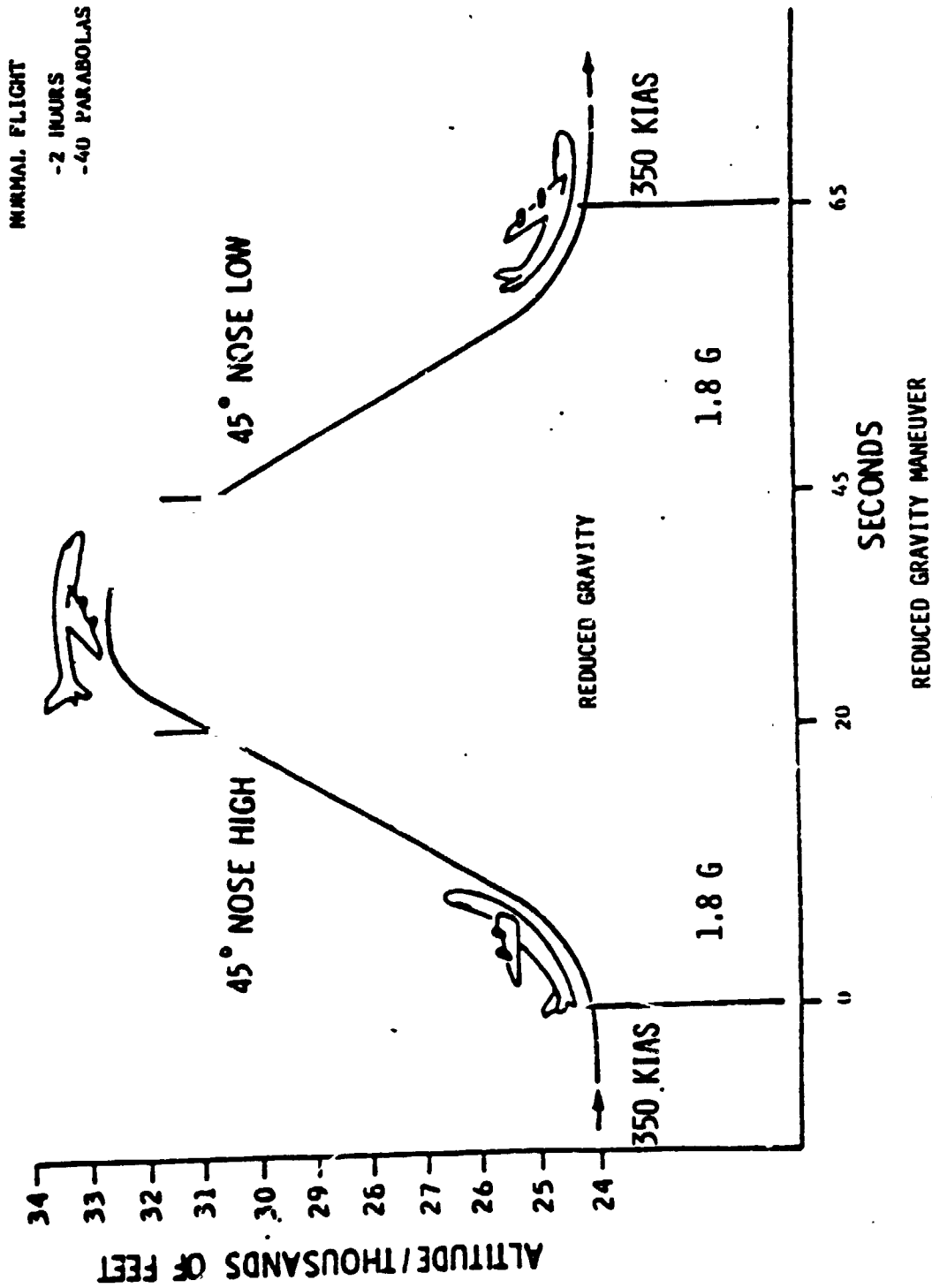
Annular Flow: 4000 to 6000 frames/sec
($Y > \sim .22$)

Slug Flow: 1000 frames/sec
($\sim .10 < Y < \sim .22$)

Plug and Bubble Flow: 400-600 frames/sec
($0 < Y < \sim .10$)

A film log of the ground and flight tests is shown in Appendix E. Some filming was done during the zero-gravity to two-g transition (and vice versa). The gravity transition filming was done at the lower qualities where the most change in flow regime will be seen.

The video camera and still camera used for documenting the test loop operation were mobile units. The cameras were used to show the test loop operation during the flight and the personnel operating the test loop.



KC-135 AIRCRAFT TRAJECTORY

FIGURE 5.5.2-1

5.5.2.2 Reduced Gravity Tests

The test loop and supporting facility hardware were taken to Ellington Field on April 13th for flight test preparations. All of the equipment was setup on the NASA-JSC KC135 reduced gravity aircraft. A final checkout test was performed on the aircraft using the on-board power.

Two days of reduced gravity testing were performed. The first day nine SFE heat loads were run and each heat load was run for three consecutive parabolaes for a total of twenty-seven parabolaes (Figure 2.1.1-2). High speed film of the two-phase flow and condenser were taken for each heat load. Twenty-seven parabolaes were also run the second day. The flight profile was similar to the first day but included loss of heat rejection, reduced-gravity RFMD startup and shutdown tests (Figure 2.1.1-2). No test loop problems were encountered on either day of flight testing.

6.0 References

1. "Johnson Space Center Forced Flow Evaporative Cold Plate Final Report"; June 28, 1985; Contract No. NAS9-17195; DRL No. T-1884; Line Item No. 2; DRD No. MA-182TE.
2. Film Available from NASA-JSC, Houston, Texas. See Appendix E for Reel Numbers and Subjects.
3. Dukler, A.E., J.A. Fabre, J.B. McQuillen, and R. Vernon: "Gas Liquid Flow at Microgravity Conditions: Flow Patterns and Their Transitions," Unpublished Paper (1987).
4. Taitel, Y., and A.E. Dukler: "A Model for Predicting Flow Regime Transitions in Horizontal and Near Horizontal Gas-Liquid Flow," AIChE J 22, pp. 47, (1976).
5. Miller, Chris D.: "Characteristics of Two-Phase, Two Component Flow in Reduced Gravity," NASA-LeRC, (1976).
6. Wallis, G.B.: "One Dimensional Two-Phase Flows," McGraw Hill, (1969).
7. Friedel, L.: "Improved Pressure Drop Correlations for Horizontal and Vertical Two-Phase Pipe Flow," 3R International, 18(7), pp. 485-492, (1979).
8. Dittus, F.W., and L.M.K. Boetler: University of California (Berkeley) Pub. Engrg., Volume 2, pp. 443, (1930).
9. Hepner, D.B., C.D. King, and J.W. Littles: "Zero-G Experiments in Two-Phase Fluid Flow Regimes," ASME Paper 75-ENAS-24 (1975).
10. "JSC Reduced-Gravity Aircraft Users' Guide; Flight Operations Directorate," Aircraft Operations Division, NASA-JSC, Houston, Texas, May 1981.

11. Bell, K.J., J. Taborek, and F. Senaglio: "Interpretation of Horizontal In-Tube Condensation Heat Transfer Correlations With a Two-Phase Flow Regime Map," Chem. Eng. Prog. Symp Series, Volume 66, No. 102, pp. 150-162, (1970).
12. Sardesi, R.G., R.G. Owen and D.J. Pulling, "Flow Regimes for Condensation of a Vapour Inside a Horizontal Tube," Chemical Engineering Science, Volume 36, pp. 1173-1180, (1981).
13. Kawji, M., Y. Anoda, N. Nakamura, and T. Tasaka: "Phase and Velocity Distributions and Holdup in High-Pressure Steam/Water Stratified Flow in a Large Diameter Horizontal Pipe," Int. J. Multiphase Flow, Volume 13, No. 2, pp. 145-159, (1987).
14. Tandon, T.N., Varma, H.K., and Gupta, C.P., A New Flow Regime Map for Condensation Inside Horizontal Tubes, J. Heat Transfer, Trans. ASME, 104, pp. 763-768, (1982)
15. Heat Transfer Research Institute, Report TPG-1, Alhambra, California (1976).
16. Bland, T.J., R.S. Downing and D.P. Rogers: "A Two-Phase Thermal Management System for Large Space Platforms," AIAA-84-1758, (1984).
17. Bland, T.J., R.S. Downing and D.P. Rogers: "A Two-Phase Thermal Management System for the Space Station," SAE Technical Paper 841525, (1984).
18. Niggemann, R.E., W.J. Greenlee, D.G. Hill, W. Ellis and P. Marshall: "A Swirl Flow Evaporative Cold Plate," AIAA 85-0920, (1985).
19. Bland, T.J., Ing-Yong Chen and D.G. Hill: "Development Status of a Two-Phase Thermal Management System for Large Spacecraft," SAE Technical Paper 861828, (1986).

7.0

Appendices

- A. R. Niggemann's Flight Test Narration Transcription
- B. E. Keshock's Flight Test Narration Transcription
- C. Chisholm B and C-Type Method for Pressure Drop Prediction Through Bends
- D. Pressure Drop Predictive Method Flow Charts
- E. Film Log

APPENDIX A

THURSDAY, APRIL 16, 1987

DICK NIGGEMANN'S FLIGHT EXPERIMENT NARRATION

Dick Niggemann is the Chief Research Engineer-Thermal Energy at Sundstrand Corporation in Rockford, Illinois.

Prior to the first test, Thursday, April 16, 1987, 10:06 a.m., the system has been operating for about an hour warming up at about 40 percent quality heat input rate. Condenser is not yet seeing vapor.

At 13 minutes after noon, we are revving the engines and are about to take off. We are airborne at 44 seconds. The system is still running at about 20 percent quality. The primary crew for the experiments are Jeff Dominick, Richard Parish, Dave Hill, Ed Keshock, and myself. Nanette Faget and Fred Best are hitchhiking to follow their densitometer measurements. We're allowed to take our stations now at 15 minutes. During this climb out portion of the flight we are getting slug flow in the first leg of the experiment and its primary stratified wave in the outlet portion. Heat is going up to full power at 12:18. The upstream flow section still seems to have plugs now and then. The downstream seems relatively smooth. We're still on climbing and back to low quality about 5 percent. We're approaching a quality of 5 percent. The flow coming out of the bend appears to rock a little bit, wave back and forth about 18-20 inches and after that it appears to be level. The condenser is not flowing any vapor at this condition. We're attempting to document the difference in the upstream and downstream legs while were still climbing and have plug follow in the upstream leg. We're still climbing and have slug in the upstream segment, and it's still stratified wave in the downstream segment. In the upstream section, we are still climbing. We have a elongated bubble flow. Bubbles occupy about the first third to

the top half of the tube with about 8 to 12 inches bubble lengths. The segments vary between 2 inches and 10 inches long.

We have slug flow now in both ends, we must be level. Or maybe even pointed down, because we have the elongated bubble flow in the downstream segment and it's stratified wavy.

We are about to go into our first parabola at 12:38. In zero g, we get elongated bubbles that are centrally located. The bubbles were generally elongated, but there were some small bubbles floating in between after the turn.

This is quality of .1. I am watching the condenser interface which is in the lower end of the condenser inlet.

This is our second parabola 0.1 quality. This is a very good zero g in the quality of 10 percent. The condensing length goes down to about 38 1/2 on the measurement which is about 11 1/2 inches down from the inlet of the condenser that is on the top end. This is going to be the first maneuver at .15.

O.K. we are going to start pulling it. During the pull out at 2 gs, the interface moved toward the inlet end of the condenser about 2 inches. During pull out, it rearranged and had pulsing flow controlled by the control valve and the interface effectively moved towards the outlet. At 1 g, now were pulling out again so its moved back up towards the inlet. The interface is swinging over approximately a 2 inch amplitude during the pull out from zero g. The interface is realigning itself going downstream the pump cavitated a bit. There appears to be a significant amount of liquid that comes into the condenser during zero g. Liquid level is still towards the inlet end of the condenser cycling between 40 and 38 on the upper edge. At high g we have a very well governed interface, its very visible. Now were pulling zero g, there

appears to be an in rush of liquid from the lines that burdens the lower half of the condenser. Condensing interface is bouncing. Bubbles don't traverse past about 35. This was the second maneuver at .2 and zero g the interface again moved downstream to about 34. That is a judgement call because there are bubbles, whereas at the high g there are no bubbles it's stratified, and at high g the interface does move back upstream. Third zero g, the liquid burden seems to be diminished.

This is the second pull out in quality of .3. The top of the interface is at 36 inches, and we're going into zero g. I am watching the liquid come out of the piping and burden the condensing process a little bit. Its hard to tell where the interface is and how much open area there really is. The interface does move downstream but I think it is because it is carrying the extra liquid burden. This is the first parabola at .4 quality zero gs. Lost all data on that one because we went zero g and I flew. Under pull out, the level is at about 31-32 inches. Liquid continues to pour in. Bubbles are disappearing at about the joint at zero g. The top level is about 32 inches at pull out, g level going to zero. Liquid burden comes in and bubbles disappear about at the mid-span joint, which is about 26 inches.

There is a large stream of liquid that is entering the condenser at a quality of 60 percent. At quality of .8, in level flight the interface is hard to see but its somewhere in the 14 to 15 inch range measured as seen from the top of the tube. Were approaching our first parabola in 80 percent quality the flow section that I am looking at is the opaque section where I can't see anything and across the way I see the outlet of the turn. Were pulling 2 gs and it appears to be a segregated annular flow. The flow appears to be annular. Definitely annular.

This is the third parabola at .8 quality. I am watching the condenser now. Bubbles stop it at about the 12-14 inch level. Still getting a burden of liquid into the inlet end. I think that the burden of liquid which appeared to be a larger amount at the higher qualities may be due to the initial filling of that line with liquid during the 5 percent quality run where the condenser is not flowing as the back pressure valve is closed. I think the line fills with liquid back to the back pressure regulator and may have difficulty emptying in 1 g or 2's, but may start emptying in zero g. I speculate that the low velocity at the low qualities is unable to carry much of that liquid to the condenser, but that more of it is swept along at the higher qualities due to the higher vapor flows. An experiment to determine whether this is the case would be to run a low quality (5 percent) followed by a substantial period of time at running at high qualities to see if the problem disappears.

FRIDAY, APRIL 17, 1987

The second day, Good Friday, April 17, 10:41 a.m. were in the air. We're half way through the tests, the .8 and .6 quality on the condenser and .5 seem to still have liquid coming into the condenser during the zero g portion, but not as pronounced as yesterday, I think. The cameras will tell the truth. We have been photographing the zero g portion of each parabola at every quality. I've been watching the condenser mostly and again for the higher qualities .6, .5 and now .3. Again to my viewpoint, it appears that there is less liquid coming over. On the .3 quality, we had the recirculation on and there seems to be a rather significant churning going on in that space, but I really couldn't tell if more or less liquid came in. We're running .2 quality at this point; were pulling up and it seems to be segregated wave in a downstream. Now were going zero g, and we are getting annular flow. Seems to be quite annular. We're pulling our couple gs now, and it is plug

slug and segregated wave in a downstream portion. Plug slug in the first because apparently we are pulling some slight negatives on that slide. It's clearly annular flow again. Were hitting good zero g now.

Were pulling into the 2 gs at the .15 quality. Interface top is bouncing at 3 inches about 39 1/2 inches on the top and it is just out of the condenser on the bottom end. Going into zero g. We still get a significant amount of burden of liquid into the channel on the zero g.

This is 11:55 a.m. and about 5 minutes ago, we had a lost of 400 cycle power which shut down the test stand. Were doing 10 percent quality. After restarting, which was uneventful, we're in the pull out and we have segregated flow. During the zero g portion, we have a flow with large elongated bubbles flowing in the middle of the channel bullet nosed and boat tailed and then they break up into annular flow in between. But the annular flow has the gas going faster. We just shut the unit off in zero g. The system is coasted down the flow is all but stopped out of the two phase line we are going into our second parabola and we are going to turn the unit on. There are some bubbles emanating from the evaporator yet into the two phase return line, but there just due to the slight upward tug that we are getting. Now were are going into zero g. It was a successful restart. It was beautiful. The zero g start and stop went uneventfully a rather good trip. For Scott Downing's benefit, I did feel the pipes they were cool, and they were not flushing out on during the zero gs. The amount of liquid that was coming through under zero g was documented with a dedicated camera.

Another note, the power outage was caused by a copilot stepping on a connector and breaking it off. The crew fixed it within about 10 minutes.

APPENDIX B

REDUCED-GRAVITY KC135 EXPERIMENT**APRIL 21, 1987****DR. ED. KESHOCK'S PREFLIGHT & FLIGHT NARRATION**

Dr. Keshock is a Professor of Mechanical Engineering at the University of Tennessee in Knoxville, Tennessee.

This is April 2 at NASA Johnson Space Center, and what we're going to be doing today is making some observations of the two-phase flow of Refrigerant 114 in ground tests of the test loop designed by Sundstrand. The system is now pretty much up to equilibrium, and we're going to be running different qualities starting from low quality, going up to a maximum of 80 percent. I'll be reporting my observations of the two-phase flow in the transparent test section.

As the system is coming up to it's first operating condition (5 percent quality), we have a stratified type flow with some waves being developed - noticeable waves being developed because of the slightly higher vapor velocity moving over the liquid interface. These waves are apparent both preceding the bend and probably even more noticeable immediately after the bend. After the bend, it does appear that these waves do die out some as they go further downstream and out of the field of view. The waviness at this quality seems to be quite pronounced. The tube seems to be about one-half filled with the liquid phase - maybe even a little bit more. In a way, under one-gravity conditions, this is not an unusually interesting type flow, other than for the waves developed at the interface, but I suspect that the change to zero-gravity conditions might provide some very different behavior; that is, the liquid may be distributed about the tube in a quite different manner. Anyway, that remains to be seen. unusually interesting type flow, other than for the waves developed at the interface, but I suspect that the change to zero-gravity conditions might provide

some very different behavior; that is, the liquid may be distributed about the tube in a quite different manner. Anyway, that remains to be seen.

The flow velocity, from just eyeballing it, seems to be about 1-1/2 ft. per second. This is just a velocity as indicated by the wave movement at the interface. Just from what I see here, the filming speed that you can get by with would probably be quite low. The normal film projection speed is about 24 frames per second. It looks as though doubling or even tripling that speed would be very ample for this flow regime. It should easily show in detail the wave action at the interface of this flow. Concerning the film speed, just be unusually conservative. Then instead of 72 frames per second or triple the normal photography rate, say one uses a camera speed of 100 frames per second. I think that speed would be very adequate (for these conditions, i.e. 5 percent quality). This first flow condition is at 5 percent, and after this, the quality is going to be increased to 10 percent.

The quality has now been increased to 10 percent. The most noticeable difference in the flow is that there is less liquid occupying the - and than it's apparent even with the naked eye. There is still waviness in the flow. The flow velocity appears to have increased. Oh maybe, the wave velocity might be about 30 inches per second rather than 20 -- at least, that's what it appears. Occasionally, one can observe the bridging of the diameter of the tube (by the liquid flowing along the tube bottom) preceding the bend. You occasionally get a slug type flow condition which, however, quickly comes back down and goes into a wavy stratified flow. Immediately after the bend, one sees no evidence of any bridging of the tube diameter. However, further downstream of the bend, maybe about 4 feet downstream of the bend, where the transition piece is located, you do have bridging of the tube diameter again, forming an intermittent bridging or even an occasional slug-type flow.

We're up at 15 percent quality now. It's still a stratified type flow, also bridging of the tube diameter occurs - Waviness is still apparent, but there's less liquid in the tube. It seems to be filling about one-half the tube -- not a dramatic difference from what was observed earlier. If anything, the waves are not as pronounced. The surface is more ripply. Rather than having numerous waves of a fairly large amplitude, there are waves, but of smaller amplitude and more rippling of the interface. It seems to be apparent that there's a higher vapor velocity.

The quality has now been adjusted up to 20 percent. It hasn't been (at that operating condition) too long, but it appears as though there is a difference evident already. The interface is ripply, with larger waves or surges spaced about maybe 3 or 4 feet apart, just periodically surging along the top of the interface. But the rest of the interface is ripply with low amplitude (interfacial) waves, in other words. It appears as though these larger disturbances can be characterized more as surges. They don't bridge the tube diameter by any means, but they appear to be waves rolling (and building up) along the interface because of the higher vapor velocity. There doesn't appear to be any influence of the bend. The liquid depth is not appreciable at the exit of the bend, but it appears to be about the same on the other side. One has the same surging activity after the bend as preceding the bend.

The quality is now at 30 percent. There's still some of the surging that I described earlier at 20 percent. The distance between these surges is a little bit larger - it looks to be about 5 feet instead of 4 feet. There's not a great change - still a rolling-up of these waves that form the surge. They seem to roll up and almost reach the top and then die down again. There's the same sort of

activity beyond the bend as before the bend, although immediately after the bend (at the bend exit), one notices no surges. Of course, that appears to be a region where the liquid level is low, and then from that point on, the waves begin to develop and form (build up to their maximum amplitude) about 6 feet down from the bend - about where the photographs are being made. Also, there are ripples and small wavelength disturbances - small perturbations on the interface, rather than large waves. The vapor velocity seems to be coincident with that of the surges. If I had to estimate the velocity, I'd say, it would be about 3 or 4 feet per second, but that's just a rough estimate, and the vapor velocity would (no doubt) be larger than that.

We're up at 40 percent now, and there is a noticeably lesser amount of R114 at the bottom of the tube. There's still a ripply interface and also the regular periodic surges which are about 4 feet apart. The waves don't roll up as high, but it's the same sort of action that exists there. There doesn't seem to be much evidence of an annular flow. Also, there doesn't seem to be much influence of the bend upon the flow either. One seems to see these waves or surges exiting the bend itself, which seems to indicate that a surge enters the bend and continues through the bend. One thing that seems to be apparent (or at least it appears this way to the naked eye) is that immediately after the bend the liquid thickness at the bottom of the tube is non-appreciable. Then as one goes downstream of the bend, there appears to be a buildup of waves, which gives the appearance of having a thicker liquid larger at the bottom of the tube. I'm sure that's just because of the increased height of the waves that make it appear to be so. So what it amounts to is that the waves become a little larger amplitude as one goes to the end of the test section, whereas right at the bend-exit the amplitudes are low, and so it appears that the thickness of the liquid film at the bottom is smaller. (The eye isn't able to follow the wave action. Instead, it tends to blur the wave action. Thus, numerous large amplitude waves appear to the eye as a thick(er) liquid layer.)

Now we're at 50 percent quality. There doesn't seem to be any evidence of these surges now. We have just a generally wavy, ripply type interface. The one difference that I do see now is that there seems to be a region of waviness and rippliness, and then a dying out of those waves and a smoother interface as it approaches the bend. After the bend, we seem to have some liquid redistribution within the bend, so that some of the top portion of the tube is wet with liquid. Predominately though, there is a stratified liquid layer at the bottom of the tube with, very high frequency, low amplitude ripples on the interface.

. . . It's not a classical annular flow (still at 50 percent quality), but right at the exit of the bend, it appears as though there is some evidence of an annular flow. But that quickly dies down. At the exit of the straight section (downstream of the bend), you have a little periodic buildup of the liquid thickness at the bottom, but really no evidence of a wave or a surge that is being blown along. There does seem to be a very thin liquid film at the top of the tube, however. Really, though, it's not enough of a thickness to think in terms of an annular film, but there is some liquid activity -- a very thin film at the top of the tube.

We're now at 60 percent quality. There's not much difference between 60 percent and 50 percent from what I can see (entering the bend). After the bend you notice what appears to be a wetting of the top of the tube. It almost looks as though it is covered by a spray at the top of the tube. About 12 inches downstream of the tube, you don't see much evidence of that same spraying or wetting of the top of the tube. It appears as though the stratified liquid at the bottom of the tube, exiting from the bend, is flatter than at lower qualities. You see some evidence of waviness from the

other side as it enters the bend, but it appears as though there's such a high vapor velocity that we have very high frequency, small amplitude waves at the interface. With the naked eye, you really can't tell too much about what's happening at the interface. It definitely needs to be slowed down by some high-speed photography. Something that does seem to be clearly evident now is that there is a thin-liquid film at the top of the tube. This is evident even beyond the region where the top of the tube appears to be wetted by a spray. I can look 3 to 5 feet down from the exit of the bend and still see evidence of that thin film at the top of the tube, which indicates an annular type flow. Yet, one must say that it is a very thin film at the top of the tube (especially compared with the liquid layer at the bottom of the tube).

Some high-speed films were just taken at this condition (60 percent quality). It looked as though the camera was at an angle of about 15 degrees to the tube's horizontal midplane, with the lens located about 2 feet away, so the result is that the view is slightly downward upon the liquid at the bottom of the tube. One possible advantage of that is that one might see a good bit more of the wavy action on that interface. The disadvantage of that view is that one can't get a very accurate indication of the thickness of the liquid film flowing along the tube bottom.

The quality has now been changed to 80 percent, and I must say that there is not a great change from that at 60 percent. Actually, it appears as though it's a stratified flow, but there is wetting at the top of the tube right after the bend, and also continued wetting downstream of the bend. But again, the amount of liquid that's in the top portion is really very little; It's just enough of a film to wet the top of the tube. There might be a little bit of rippling of that film at the top, but not much. It is just enough rippling to allow me to see that it is an annular type flow. There's not much difference in the flow before the bend and after

the bend. There does seem to be a little more intermittently of the wave pattern about 6 feet downstream of the bend, that is about where the photographs are taken. I'll now take a look right at the exit of the straight section (following the bend) to see whether there is evidence of an annular film there. Well, there's no doubt about it, there is evidence of an annular type film at the top of the tube even at the test section exit. In fact, it's more evident here than it was at the - oh say, about a foot downstream of the bend. Again, the film is still thin, but there seems to be more evidence of such a film at this quality. Possibly, it's because the a shearing action of the vapor which may be depositing droplets about the periphery of the tube.

It's April 16. We're beginning our KC135 tests. We're just on our way up now, and we'll be conducting our tests at a number of different qualities, and I'll announce a quality and a parabola number before each of our photographic runs, and will also be talking into this recorder concerning general observations for all of the different parabolas. Anything that is of interest, I'll try and put on the recorder.

One thing we notice in going up to the 33,000 ft. level (the apparatus has been operating at 20 percent and 5 percent quality) is that just because of the angle of inclination in the climb, the flow in the upstream side preceding the bend is definitely wavy slug, but after the bend (that is going downhill), it's very clearly a stratified type flow. There is some small, very slight evidence of a liquid film moving up toward the top of the tube, but pretty much it's a stratified flow. (Excitement mounting in background) In the slug type flow (upstream of the bend) it looks as though the portions of the pure liquid (slugs) are about 6 to 8 inches in length, separated by vapor (segments, plugs) that are of variable length, maybe as short as 6 inches but up to about 18 inches.

Now, we seem to be in level flight, but on the upstream side of the flow, we have more of a stratified flow, and, after the bend, we have a kind of slug flow. One possibility is that we are slowing down, or perhaps the aircraft may be nosed slightly downward. At this point, however, I see essentially the reverse of what the flow has been like during the climb in the straight sections preceding and following the bend.

We're going into the 2-g portion now of our zero g, and there is zero g. Oh, it looks as though there's a bubble type flow and small slugs. Oh, there is quite a change in the flow pattern! There are elongated bubbles - it looks as though the bubbles - oh yes! - they are Taylor bubbles moving right through the center of the flow channel. Well, there is similar type behavior after the bend -- very long vapor bubbles, Taylor bubbles. Preceding the bend, it seems to be more turbulent. (Here loud peals of laughter and excitement almost drown out the dictating voice.)

We're going into the 3rd parabola. We're now in zero-gravity. There are small Taylor bubbles initially (much laughter), small Taylor bubbles on the downstream side; much longer ones on the other side of the flow channel. Now they're much more elongated into the - - A H H ! ! It seems as though there's a development (a developing flow) during the zero-gravity period. We start out with small Taylor bubbles, and coalescences processes lead to the (development of) larger, much longer Taylor bubbles.

We're going to be running at 10 percent quality now in these (3) parabolas coming up. It looks like we're going into the high-g portion for this second set of parabolas. I notice stratified flow after the bend, still a wavy, somewhat slug type flow on the other side.

We're now in zero-gravity. Well, again a similar type behavior on this side (downstream of the bend) - much - oh, many more small bubbles this time, yes, a bubble type flow; not too many Taylor bubbles at all, again centering toward the middle of the channel.

Going into the second parabola now - (lots of static and voices calling back and forth - (a very loud "STAND BY") - stratified, wavy flow more on the upstream side than the downstream side. Starting to pull the g's - slug flow on the other side (much noise and loud voices make it difficult to hear), more of a stratified flow on this side. Quite a difference - QUITE A DIFFERENCE! between the two sides. Now in zero-gravity. There is a bubble type flow along the center of the channel, both on this side and the upstream side. (But there is) Pretty much an annular type flow - a thick annular type flow at the exit, and, it appears (as more time elapses in the zero-gravity state) as though there is a developing flow - bubble coalescences along the way (along the tube axis).

Zero-g again - there almost seems to be a frothy annular flow entering the bend. Regarding the influence of the bend, it seems though it's less frothy on this side (downstream of the bend). There's a change to distributed bubbles once you get about 6 feet from the bend, and then a redevelopment into an annular elongated bubble flow. I guess it's more of an annular type flow (after continuing to focus upon it).

In the level flight condition now, it seems as though there's a slug type flow on both sides. Almost a case of stratified flow on one side and a slug flow on the other. Ahhhh - right now, the slug type flow is on this side, and the stratified type flow on the other side (upstream of the bend).

We're going to be running at 15 percent quality for this next set of three parabolas. Before we go to the new operating condition, there is an observation I'd like to make at this point regarding the flow patterns I just observed at 10% quality. It seemed as though there were annular flows (not merely Taylor bubbles) separated by liquid segments that were filled with smaller bubbles, which were, in turn, followed by annular flows. In other words, there is an alternating sequence of a classical annular flow pattern followed by a liquid region mixed with some bubbles, followed in turn by another annular flow pattern. This would appear to be analogous to a slug type flow condition where one has liquid slugs alternating with vapor slugs (or plugs), except that under one-gravity conditions, the vapor slug is near the top of the tube.

We're going to be running three more parabolas at 15 percent quality shortly. We're going into the high-g portion of this first parabola, slug type flow of very long vapor lengths on the other side - pretty much stratified flow on this side though. Its not really a slug type flow - it's more like the development of waves that are bridging across the tube diameter.

Now we're in zero-gravity. On this side, we're getting quite a bubble type flow. By the end of the test section, it's developed into an annular flow. Not too much a case of vapor-liquid-vapor (as I described for the 10 percent quality zero-gravity flow patterns). We're going into the high-g portion again, a wavy type flow on the other side, stratified on this side. Long pause - Up into zero-gravity. (Loud voice - STAND BY FOR PICTURES!). Still developing, still developing - still developing! On the other side, a bubble flow but (developing into) annular flow, since the bubbles are going toward the center of the tube (and have coalesced). Not so much liquid-vapor-liquid-vapor as with the 10 percent quality cases. There is a rapid transition to a stratified type flow once we get down (i.e. leave the zero-gravity condition).

(1) We're now going into the high-g portion of the 3rd parabola - still the same conditions, 15 percent quality. A wavy type flow on the other side, stratified on this side. (REN's voice clear in background). Now in zero-gravity -- stratified flow developing into a wavy flow, and then, the vapor is centered toward the middle of the channel. Vapor is along the center, (now a) bubble flow, still a bubble flow, and then an annular type flow -- a similar type flow pattern (to that seen in the previous parabola). Maybe the most interesting part at this quality was to see the fairly rapid development from a stratified flow (high-g condition) to a wavy flow, and then under zero-gravity conditions for the vapor gets distributed along the center of the channel, changing into a classical annular flow pattern (though the thickness of the annular liquid film may be larger than that typically observed in vertical annular flows, since annular flow under zero-gravity conditions existed here at only 15 percent quality).

(We're at 20 percent on these parabolas coming up. For the first one - we'll just make observations, and then the second one, we'll take the films.

We're going into the high-g portion of it now. We started out with less wave development in the flow. We're evidently going down now. And just in going down, you can see the difference in the flow patterns between one side (of the flow loop) and the other -- stratified in the tube going "downhill" (upstream of the bend) and a wavy type flow tube going "uphill" (downstream of the bend). Now we're going into the climb - stratified on both sides, it looks as though there is some wave development on the other side. Yes, there is still some wave development on the other side -- little surges going along the tube and developing like a surfer's wave,

though the flow on this side is pretty much stratified as we're approaching zero-gravity! Now, we're going into zero-gravity, the flow is stratified, stratified. Now we're in zero-gravity. Now there are bubble streams near the center, and then the development of annular flow! It looks as though it's annular flow, and there is no separation of the annular like flow by an all-liquid region, that is, no liquid-annular flow-liquid alternating pattern, but pretty much a continuous annular flow.

Now we're into the high-g portion. There is flow on the other side (Interchange of voices - Ya! - this one.) It's wavy on the other side, but there is not so much waviness on this side.

OK, we're into zero-gravity again and waiting for the flow to develop (before taking high speed photos). (Voice from background - THERE IT GOES!) Wow, that was a nice annular flow, fully developed annular flow, basically!

In the next parabola, I'm going to concentrate on what's happening thru the bend, to see if there's any difference before and after the bend. (Lot's of voice interchange in background) It's wavy on the other side, with surfing type waves moving downstream about 18 inches apart. Now it's zero-gravity. It's taking awhile for the changes to occur - look's as though it annular before the bend; annular after the bend. There may be a little bit thinning out (of the liquid annulus), and a slowing down of the vapor core as it moves along, but not too much, really. It looks as though it is a pretty nice annular flow.

We're going up in quality now. It looks as though there's beginning to develop just the slightest trace of a film up at the top of the tube. We're going to be going up to 30 percent quality now. We'll see what the difference is. One thing I should mention before going on is that in annular flow, it seems as though the

spacing between the small waves or the ripples is larger than under one-gravity conditions. Also, the amplitude is a little bit larger. There are not real fine, closely spaced ripples, but they are spread out more (or spaced farther apart) over the length of the tube.

Alright! We're going into the 2-g portion of the 30 percent quality condition now. Looks like we have still the wavy type flow on the other side and very little waviness (pretty much a stratified flow) on this side. We're now in zero-gravity. There is channeling of the vapor through the center and a more clearly evident annular type coring pretty much all the way (through the entire transparent portion of the flow loop). The only difference between flow from the bend exit and that further downstream is that there might be some small differences in the nature of the annular flow (e.g. small differences in the wavy structure or patterns at the liquid-vapor core interface). (R. Niggemann yells something about holding the camera on this side, OK - someone yells out - OK!) On the next parabola coming up we'll take some high speed photographs.

There is wavy flow on this side and stratified flow on the other. As we go into the 2-g period, it's more like a stratified flow. On the other side, it's stratified, with a little bit of waviness. On this side, it's stratified. We're coming into the zero-gravity period. We'll wait a little while (before taking the high speed photos) - OK - HERE WE GO!!! OK - go!

It seems as though, from my vantage point, that there's perhaps a little bit more irregularity to the annular film at the exit of the bend. One then appears to have a smoothing out of the annular film along the length of the flow channel, so that by the time the camera is reached, it's really a well developed, nicely developed annular flow. That time, I tried to notice the change that took

place from the 2-g period to the zero-gravity period, and I could see the liquid climbing up to the top of the tube, climbing up the wall, in other words (during that transition period).

We're now in zero-gravity again. (Laughter & voice interchanges) Actually, there's not too much difference (from the observations in the two previous parabolas). There is just a pure annular type flow. That does it for 30 percent quality. From my observations with the naked eye, there's not a great deal of difference between the zero-gravity flows at 20 percent and 30 percent quality. Basically, it's only a matter of the liquid film being a little thinner (at the higher quality).

Now we're going into 40 percent quality operating condition. There's a noticeably different (smaller) liquid level. There is some waviness, but there is not enough depth of liquid to allow the waves that are formed to bridge the tube. There is stratified flow on this side, though! It has a wavy interface. It seems as though the vapor is moving fast enough to perhaps shear away those waves - and possibly generate some droplets close to the interface. We're into the zero-gravity period now. WOW! - There's a very quick change to annular flow. It looks very much the same -- Once more, it's a very definite, pronounced annular flow. Not a great difference -- (from the previous annular flows at 20 and 30 percent quality) pure annular flow!

This is now the high-g portion - same type of behavior (as observed in the first 2-g period). An occasional, frothy being blown through, but it's essentially a wavy, stratified flow.

We're now entering the second zero-gravity period. Zero-g - switching - GO!! Annular flow --- all the way!! Now the third zero-gravity period. Another zero-gravity. (Long pause) Annular flow all the way!

We're at 60 percent quality now. There is stratified flow on this side (Background talking and exchanges - HOW ABOUT NOW?? --- says he wants to turn this one on into the parabola a little ways. "OK" is the response.) "They coming on now, Ed." (Southern accent statement translates to "The new zero-gravity condition is about to begin.") Oh, yeah. "NOW!" (Counting - 16, 17 'rest lost with background noise.'")

It's an annular type flow. There are small ripples on the inner surface, but then there are also some larger, more widely spaced, regularly spaced, waves on that annular.

There's evidence of the annular film up at the top of the tube (now in one-gravity to 1.8g conditions), so you'd have to say it's a semiannular type flow. But the thickness of that film at the top is not significant compared to what it is in zero-gravity. (Long pause - onset of zero-gravity conditions -- much static, noise) - Annular flow - all the way!! It almost seems as though there are waves or bands spaced on the order of inches apart (or as close as an inch apart), along with all the smaller amplitude, more closely spaced ripples along the interface.

On into the high-g portion, and even at the highest-g condition, I can still observe that semiannular flow pattern (that is a stratified liquid flow along the tube bottom, but with a thin annular liquid film along the top portion of the tube wall).

We're again into zero-gravity. There's a very rapid transition to a different (zero-gravity) type of flow. It's annular right away. It looks as though those bands are about two inches apart. It's a very well developed annular flow at the exit section of the transparent length.

We're going to be going up to 80 percent quality. Under normal conditions, it's fairly easy to see the thin film at the top portion of the tube. It has to be classified as a semiannular flow, but it's easier to see that film up at the top (than at 60 percent quality). Alright! Ready to go with an 80 percent run. It's semiannular. (We going to do this on the first one, or second? First? - OK.) (Pause - voices in background re camera positioning).

Well, even at the exit section, it's easy to see a semiannular film a thin film up at the top. We're now into the high-g! I don't see much of a film up at the top now. I guess I do see a slight trace of it. Yes, I do. It's still semiannular. Now going into the zero-gravity period! (Loud voice - GET READY ON THE CAMERA!! - - - GO!!!)

It still seems to be an annular type flow. It's difficult to see whether there might be dispersed flow in the center. It sure seems to be an (conventional, classical) annular type flow. There are much smaller ripples along the interface now -- Much smaller than at the lower qualities. Well, I don't know exactly what the implications of that are, but it seems as though whatever ripples occur on the surface are of small amplitude, and they're spaced closer together!

We're going into the zero-gravity portion again. There's a pretty very rapid change! I don't notice those (larger amplitude) bands that existed at 60 percent. Well (after closer observation), I guess there is some evidence of the bands yet, but in general, the interface has smaller ripples than at lower quality levels. One thing I have to say is that the system seems to be pretty steady. There are no instabilities associated with this system operation. The two-phase flow seems to be a continuous type flow. There isn't a flow reduction and then a speeding up of the flow, or anything like that. It just seems to be a quite steady flow, I (must) say.

Into the zero-gravity period again! Annular flow all the way! I don't, again, see evidence of a dispersed type flow! Very Interesting!

Alright, we're essentially finished. We've gone up to the highest quality (80 percent), and now we're going back down to 5 percent because some digital data was not taken. Also, we're going to go back to 5 percent, because we think that fluid-mechanics wise the change in the flow that occurs from the gravity condition to zero-gravity is most dramatic.

Now we're getting ready for the 5 percent run. It's well, almost a slug type flow -- Call it a semi-slug flow. There are some waves bridging the gap, and there are some liquid slugs that eventually form. Now we're going into the zero-gravity portion and there are bubbles - bubbles developing into these slugs - Yes, Taylor bubbles - and long Taylor bubbles near the tube exit. Very interesting! I think it is the most dramatic flow pattern change!

Now, we're in between the zero-gravity periods - One goes from a wavy flow (upstream of the bend) to a stratified flow (downstream of the bend) -- although looking at the other side, again, I see a slug type flow! On this side - a stratified flow! Very Interesting!! Definitely a slug flow on the other side (upstream of the bend) and on this side, a stratified flow! I don't know whether that is the influence of the bend or not. Now, we're into zero-gravity. We have some small bubbles flowing through liquid type slugs, - also distinct, larger Taylor bubbles. I see the long Taylor bubbles catching up to the smaller bubbles! Yes, there are a lot of small bubbles in the wake of, that is the wakes of the Taylor bubbles. The Taylor bubbles (some of them) seem to accelerate and catch up to the more slowly moving, smaller spherical bubbles.

We're into the next zero-gravity portion. Oh, definitely the Taylor bubbles just move along faster and gobble up the smaller ones. Oh, yes! So there's definitely a developing flow - developing flow. Well, I think that concludes the running that's going to be done today, and I'd have to say, the results, the observations have been very, very interesting. And much as I had preconceived the flow patterns to be and the transitions of the flow patterns to be, especially in the (predominant) tendency toward an annular type flow. Also, another interesting aspect was the development (and growth) of core centered Taylor bubbles. A developing flow pattern was observed that essentially involves the coalescence of bubbles, not so much the coalescence of many small, individual bubbles, but the accumulation (or "absorption") of the smaller bubbles by the larger (faster moving) Taylor bubbles which are centered in the channel core.

Well, that's it, I'll just sign off for now. This ends the first series of the KC135 tests. We're scheduled to run again tomorrow (Friday).

Alright! It's now Friday, April 17. We're on our way up to conduct the second series of tests. Today, we'll start at the high qualities and work downward. We'll start at 80 percent and work down to 10 percent, omitting the 5 percent runs.

Alright! We're at 80 percent quality in level flight now at semiannular flow. Now, we're going into the high-g portion for the first parabola. We're still in high-g. (Pause) Now, we're into low-g. Annular flow all the way, just like yesterday! Just a nice, regular, annular flow all the way from the beginning of the bend to afterwards, and it's the same on the other side. (Pause)

I think we're about to go into the second parabola now! This is the high-g portion. And into the low-g! (Stand by on the camera -

HERE WE GO0000!! It's good!! Ahhhh - It's still a similar type flow - I think I noticed bands, periodic bands, spaced a couple of inches apart or so (maybe a little bit more) traveling down the tube as we have the same annular type flow as in other high quality zero-gravity periods.

Ready for the third zero-gravity period now! No photographs taken of this third one - we did take some of the second. (Pause - Pause) "Hey, Bob"? "Yeahhh"? "Why do we need the light"? Now, we're in the zero-gravity portion. If one tries to follow the flow, one can see those bands, kind of like a couple of inches apart. Annular flow on both sides just as before - (WHOOOPS!! - in background) That should do it for the 80 percent runs.

We're down at 60 percent quality now, in level flight. It looks as though it's still a semiannular type flow, except that there does seem to be a noticeably thicker layer of liquid at the bottom and a little bit of waviness evident, especially on the side preceding the bend.

Alright! We're going to go into the high-g portion of this now. Alright, we're about into zero-gravity now! (Much noise) Annular flow all the way! The bands seems to be about 2 to 4 inches apart. There's a nice steady annular flow all throughout the test section!

Alright! We're into the second parabola now! (OK! NOW! from background with much noise!) GO!

No drastically different behavior (from the first zero-gravity period) Alright, we're getting ready to go into the third!

(WHOOPEE!!!) Now I don't know whether it's my imagination or not that the bands I've have been referring to seem to be spread out a little bit more in the zero-gravity flow. Well - I don't know

whether I can say that exactly, because under zero-gravity, one has an annular flow, but under a one-gravity condition (for the same flow), one would have a semiannular flow, with just a very thin film of liquid near the top, so there is no such thing as being spaced further apart in the zero-gravity condition. The zero-gravity condition is the zero-gravity condition! But again, in comparing the zero-gravity flow pattern to that at one-gravity, it does seem as though the liquid, being more uniformly distributed about the periphery of the tube, has more apparent waviness at the interface. The waves seem to be of larger height compared to the very fine ripply type structure in the one-gravity condition when the film is up near the top of the tube. But superimposed up on all that waviness at the interface are these, Oh, I refer to them as wavy bands, that seem to be moving downstream, spaced about 2 to 4 inches apart. With the naked eye, one can see them just by moving one's head at the same velocity as the bands are moving down the tube. It should be interesting to observe them on the high-speed photos to get a closer look at exactly how they appear in a slowed down state. Now, we'll be going into the 50 percent quality flows. It looks as though under normal-g conditions, we have the liquid near the bottom - still of a trace of an annular film up at the top and some waviness in the bottom flow. It looks as though we're going into the first zero-gravity parabola - well - I guess I was wrong. High-g, right now! I think we're about ready for the zero-gravity. We're now in zero-gravity.

The bands on the other side appear to be about 4 inches apart, on this side pretty much the same. It's actually a complicated structure, but again, an annular type flow throughout. Alright - going into the second zero-gravity period, but we'll take some films this time. Go! - Go Ahead!

Those bands seem to be the same as before. They're more obvious on the other side -- I think maybe it's just the perspective.

We're coming up on the third zero-gravity parabola. There we are. I'll try to take a look at the flow on this side. It's an annular flow throughout -- not much difference (with the previous two parabolas). I see the bands better now. They do seem to be about the same as on the other side. It's interesting whenever you have the transition back to the high-g, those bands do seem to disappear! One has a thinner film and the more closely spaced waves of smaller magnitude as we go to the higher g condition.

Alright, those were all for 50 percent quality. Now, we will be going down to, I believe, 40 percent. I'll check on that. Evidently, we're going down to 30 percent quality -- 30 percent next. Alright! At this new condition of 30 percent quality, there's still a trace of liquid up at the top, but it's more obvious that the liquid at the bottom is thicker, wavier, and, in fact, waves begin to roll up -- surfing type waves is the way I would describe them -- and they reach ultimately -- well, it looks as though they just about reach the top of the tube, by the time we enter the bend. On this downstream side, I do not notice those waves rolling up. The difference might be due to a slight inclination in the plane's path, but, definitely, there's no rolling of waves and wave buildup on the downstream side of the bend. On the upstream side, there definitely is. The waves, as they build up, as they roll and build up, might be viewed as surges of liquid, and you can see such surges coming out of the bend. The overall effect seems to be that the bend destroys that wave or surge and the waviness has to begin again. Upon closer observation though, such waves do not begin to roll up again in this downstream portion of the tube.

Alright, we're going into the high-g portion of the first trajectory for this 30 percent quality. We're now in the zero-gravity portion. Annular, annular. Doesn't seem as though we have the same bands, it almost seems as though the annular flow is a collection of bubbles. There is not a series of bands coming down the tube now, or I should say, a series of bands rolling along the tube length. Alright, we're getting ready to go into the second parabola now!

That's good! That's very good!! Well, the bands are less pronounced as I reported earlier. Still an annular flow, and I don't think that there's any doubt that it is an annular flow. It does give a different appearance though from the annular flow at 50 percent.

Alright - into the third parabola! Well, the entire interface is ripply, yes, some evidence of what I call "those bands," but it's just not as pronounced. That finishes the 30 percent quality. Next stop will be 20 percent.

Now, this next set is going to be a 20 percent quality. Alright, we're about to go into zero-gravity for this first parabola. An annular type flow exists. You can see some traces of bubbles. At least on the other side, I did -- not much. It's basically an annular flow with a noticeably thicker film around the periphery of the tube.

Alright, we're coming up onto the, the second parabola now. Alright, we're into this second parabola. Alright, same general observations. I'm trying to detect any evidence of bubbles in the middle of the flow. I don't see too much evidence of that. There does seem to be intermittent type of flow through the central core, which may be what progresses into these bands, or the band movement, that I reported at the higher qualities.

We are taking photographs at this quality, this range of quality, at 2,000 frames per second, anticipating that since it is an annular type flow, we'll be able to use that higher speed to look at the details of the flow. We weren't anticipating that we would have so much annular flow, and I think for that flow condition these higher camera speeds are an advantage.

Alright, we're in the third zero-gravity portion. One can see small bubbles, traces of small bubbles, in the liquid layer around the periphery. It's an annular flow all the way through the test section). Alright, the next run is going to be at 15 percent.

In level flight, the waves are rolling up and building. It seems as though the high waves are now spaced about 2 to 3 feet apart, whereas whenever we first had these waves building up, we wouldn't have one building up until the entrance of the curved section. But now, we have quite a bit of build up. Again, I notice, there's not the same (extent of) build up on the downstream side of the bend. Some waviness and rippling effect is occurring in the fluid at the bottom, but no build up of waves.

Well, we're about ready to go into the zero-gravity portion of this 15 percent quality - flow now. Alright here it is! Still, an annular type flow for the most part! We seem to have a rolling effect within that annular flow - definitely annular though. This next one coming up will be the one we take the photographs on - I'll try to observe the differences between the upstream side of the bend and the downstream side.

Alright, we're about ready to go into the second parabola. It's an annular flow all the way -- on both sides. I don't see much evidence of bubbles in the flow.

Alright, here we come into the third parabola. There's a quick transition into an annular type flow. There is some evidence of bubbles within the noticeably thicker liquid annulus now. Not much of a change, well, there's not too much of a change between the flow on the other side and this side. At least I didn't seem to

see a great deal of change. What I thought was a change (from the flow upstream of the bend and downstream of the bend), apparently was the result of coming out of the zero-gravity portion. Just about the time I thought I was able to discern some difference, it turned out we definitely came back to the high-g condition.

We've had a power failure now, and the system's shut down, so it'll be awhile before we get started up again.

We're at this 10 percent flow condition right now (level flight, one-gravity conditions) after this power shutdown. On the other side, it seems as though there's a definite slug type flow -- slugs of liquid separated by mostly vapor with a little bit of liquid at the bottom of the (predominantly) vapor portion. However, on the other side of the bend, that is coming out of the bend, we have a stratified type flow, no evidence of the slugs at all! So, I don't know exactly how to explain that. My explanation would be that the all-liquid portion in the other side is "smoothed out" in a sense, so that once the flow gets past the bend we have a continuous layer of liquid at the bottom -- no slugs.

Now, we're running the zero g portion. And now we have small bubbles, Taylor type bubbles, moving down the center of the tube with relative motion (among them). It looks as though the larger ones are catching up with the smaller ones, definitely! By the time we get down to the exit of the straight test section following the bend, we have quite long Taylor bubbles. Additionally, it should be mentioned that at the beginning of the zero-gravity portion, the vapor slugs are relatively small. So it does seem as though there is a coalescence process - a development (or increase in length) of the vapor slugs along the length of the flow channel. This also implies a flow that changes and develops in time from the initiation of the zero-gravity period.

Alright, we're into the second parabola now. There is fairly rapid transition from that slug type flow into the Taylor bubble type flow. It almost seems - well, we have some very, very long bubbles coming out of the bend. It's an annular type flow. Very strange; from an annular type flow exiting the bend into very irregular Taylor type bubbles. They're not smooth - their interfaces are not smooth. And this seems to be consistent with the observations yesterday in which we seemed to have annular flow with a vapor core diameter varying with length; that is, we had a large vapor core tapering down to a smaller vapor core and then going back upward again to the larger size.

We're coming into the third (parabola) now. We'll see what happens in this case. We seem to have an annular flow on the other side, an annular flow exiting - well we don't have evidence of those Taylor bubbles (now). Well, some evidence, some evidence. Yes - well, it looks as though we're right in that transition region (away) from that quality range in which we know we will have a definite annular type flow. We've finished the filming portions of the trajectories, and now we're going into the 40 percent quality regime with the idea being to make system operational changes, so I may not be reporting much during these trajectories.

Well, that concludes the test series. We've gone through the system changes. So now, the next step is to relisten to all that's on this recorder and piece it all together with all the photographic information and other data that we have. So, that's it for April, the 17th.

APPENDIX C

The B-type method for the pressure drop through the 101° bend [1]

$$\Delta P = \Delta P_{LO} \left[1 + \left(\frac{v_g}{v_l} - 1 \right) (Y (B_{101} - B_{101} Y) + Y^2) \right]$$

Where

ΔP = Pressure drop across the bend

ΔP_{DO} = Pressure drop for liquid phase flowing with the total mass flux (liquid and vapor) across the bend

$$= -f_B \frac{L}{D} \frac{G^2}{2 \rho_l}$$

v = Specific volume

G = Mass Velocity

Y = Quality

ρ_l = Liquid density

$$B_{101} = 1 + [B_{90} - 1] \cdot \frac{K_{90}}{K_{101}}$$

$$= 1 + [B_{90} - 1] \cdot \frac{90}{101}$$

$$B_{90} = 1 + 2.2 / \left[\left(f_B \cdot \frac{L}{D} \right) \left(2 + \frac{F}{d} \right) \right]$$

$$K = f_B \frac{L}{D}$$

f_B = Blasius' friction factor $0.3164 / (Rel)^{0.25}$

Rel = Reynold number for liquid phase flowing with the total mass flux

L/D = See Figure 2

r = See Figure 2

d = See Figure 2

L/D vs. r/d map [2]:

Resistance of Bends

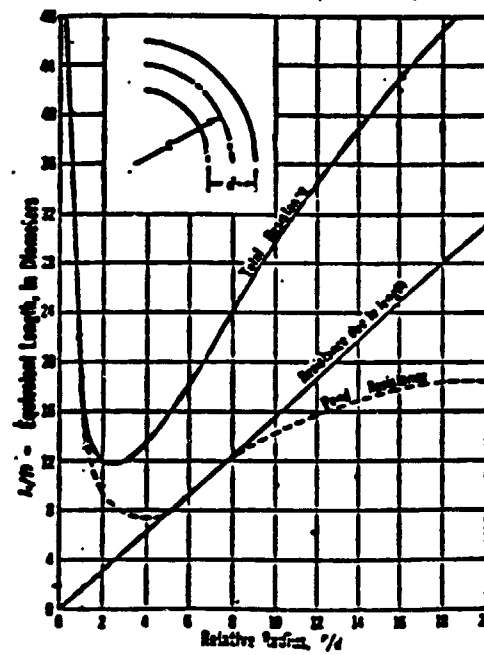


Figure 2

The C-type method for the 45° miter bends:

$$\Delta P_F = (1 - \gamma)^2 \Delta P_{LO} \left(1 + \frac{C}{X} + \frac{1}{X^2}\right)$$

Where

ΔP_{LO} = Pressure drop for the liquid flowing alone with the total mass flux through the bend.

$$\Delta P_{LO} = -K_{LO} \frac{G^2}{2\rho_L} = -f_B \frac{L}{D} \frac{G^2}{2\rho_L}$$

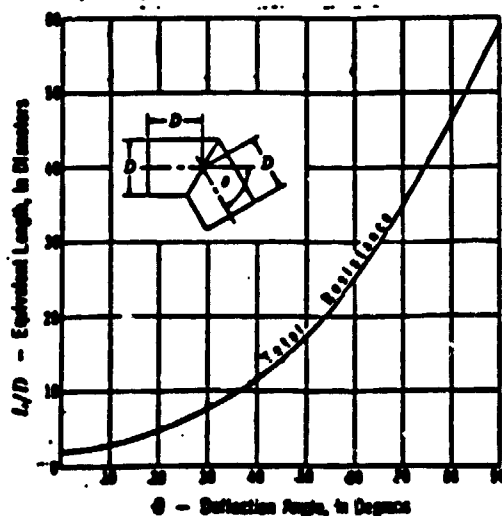
$$X = \frac{1 - \gamma}{\gamma} \left(\frac{\rho_V}{\rho_L}\right)^{\frac{1}{2}} \quad \text{Martinelli parameter}$$

$$C = \left[1 + (C_3 - 1) \left(\frac{\rho_1 - \rho_V}{\rho_1}\right)^{0.5}\right] \left[\left(\frac{\rho_1}{\rho_V}\right)^{0.5} \left(\frac{\rho_V}{\rho_L}\right)^{0.5}\right]$$

$$C_3 = 1 + 20/(L/D)$$

Resistance of Miter Bends⁴

The chart at the lower right shows the resistance of miter bends to the flow of fluids. The chart is based on data published by the American Society of Mechanical Engineers (ASME).



APPENDIX D

$$Re_{vo} = D_i G_t / \mu_v$$

$$Re_{lo} = D_i G_t / \mu_l$$

$$f_{vo} = \text{function}(Re_{vo})$$

$$f_{lo} = \text{function}(Re_{lo})$$

$$\frac{dp}{dL_{lo}} = \frac{2f_{lo} G_t^2}{g_c \rho_l D_i}$$

$$H = \left(\frac{\rho_l}{\rho_v} \right)^{0.91} \left(\frac{\mu_v}{\mu_l} \right)^{0.19} \left(1 - \frac{\mu_v}{\mu_l} \right)^{0.7}$$

$$\rho_H = \frac{1}{\frac{y}{\rho_v} + \frac{1-y}{\rho_l}}$$

$$Fr = \frac{G_t^2}{g D_i \rho_H^3}$$

$$We = \frac{G_t^2}{\rho_H \sigma_l g_c}$$

$$F = y^{0.78} (1-y)^{2.24}$$

$$E = (1-y)^2 + y^2 \left(\frac{\rho_l f_{vo}}{\rho_v f_{lo}} \right)$$

$$\phi_{lo}^2 = E + 3.24 F H / (Fr^{0.64} We^{0.015})$$

$$dP/dL_{TF} = \phi_{lo}^2 \cdot dP/dL_{lo}$$

$$Re_{vo} = Di G_t / \mu_v$$

$$Re_{lo} = Di G_t / \mu_l$$

$$f_{vo} = \text{function}(Re_{vo})$$

$$f_{lo} = \text{function}(Re_{lo})$$

$$\frac{dP}{dL_{lo}} = \frac{2f_{lo} G_t^2}{g_c \rho_l D_i}$$

$$\frac{dP}{dL_{vo}} = \frac{2f_{vo} G_t^2}{g_c \rho_v D_i}$$

$$A^2 = (dP/dL_{vo}) / (dP/dL_{lo})$$

$$\begin{aligned} 0 < A < 9.5, & \quad B = 1494 / G_t^{1/2} \\ 9.5 < A < 28, & \quad B = 14125 / (A G_t^{1/2}) \\ 28 < A, & \quad B = 4.06882 / (A^2 G_t^{1/2}) \end{aligned}$$

where G_t is the mass flux in (lbm/ft²-hr)

$$\phi_{lo}^2 = 1 + (A^2 - 1) \left[B y^{(2-n)/2} (1-y)^{(2-n)/2} + y^{2-n} \right]_{n=0.25}$$

$$dP/dL_{TP} = \phi_{lo}^2 \cdot (dP/dL_{lo})$$

Chisholm, D., "Two-Phase Flow in Pipelines and Heat Exchangers,"
George Godwin, London, 1983.

ETRI METHOD

$$C_g = \text{function } (y, g, D_i, \rho_v, \rho_l, G_t)$$

$$X_{tt} = \left(\frac{1-y}{y} \right)^{0.9} \left(\frac{\rho_v}{\rho_l} \right)^{0.5} \left(\frac{\mu_l}{\mu_v} \right)^{0.1}$$

$$\frac{dP}{dL_l} = \frac{2f_l(1-y)^2 G_t^2}{g_c \rho_l D_i}$$

$$\frac{dP}{dL_v} = \frac{2f_v y^2 G_t^2}{g_c \rho_v D_i}$$

$$\phi_v, \phi_l \text{ and } C = f(\text{Flow Regime}, X, Re_v, Re_l, Fr, We)$$

$$\phi_v^2 = 1 + CX_{tt} + X_{tt}^2$$

$$\frac{dP}{dL_{TF}} = \phi_v^2 \frac{dP}{dL_v}$$

$$\phi_l^2 = 1 + \frac{C}{X_{tt}} + \frac{dP}{X_{tt}^2}$$

$$\frac{dP}{dL_{TF}} = \phi_l^2 \frac{dP}{dL_l}$$

HOMOGENEOUS METHOD

β : Homogeneous Void Fraction

$$= \rho_l y / (\rho_l y + (1-y)\rho_v)$$

ρ_m : Homogeneous Density

$$= (y/\rho_v + (1-y)/\rho_l)^{-1}$$

μ_m : Homogeneous Viscosity

$$= \mu_l (1-\beta)(1 + 2.5\beta) + \mu_v \beta$$

$$Re_m = G_t D / \mu_m$$

$$f_m = f(Re_m)$$

$$\left(\frac{dP}{dL} \right)_m = \frac{2f_m G_t^2}{g_c \rho_m D_i}$$

Lockhart-Martinelli METHOD

$$Re_L = D_i G_t (1-Y)/\mu_L$$

$$Re_V = D_i G_t Y/\mu_V$$

IF $Re_L > 1500$ and $Re_V > 1500$

$$C=20, X = \left(\frac{1-y}{y} \right)^{0.9} \left(\frac{\rho_V}{\rho_L} \right)^{0.5} \left(\frac{\mu_L}{\mu_V} \right)^{0.1}$$

IF $Re_L < 1500$ and $Re_V > 1500$

$$C=12, X = \left(\frac{16}{0.046} \frac{1-y}{y} \frac{\mu_L}{\mu_V} \frac{\rho_V}{\rho_L} \frac{1}{Re_V^{0.8}} \right)$$

IF $Re_L > 1500$ and $Re_V < 1500$

$$C=10, X = \left(\frac{0.046}{16} \frac{1-y}{y} \frac{\mu_L}{\mu_V} \frac{\rho_V}{\rho_L} Re_L^{0.8} \right)$$

IF $Re_L < 1500$ and $Re_V < 1500$

$$C=5, X = \left(\frac{\mu_L}{\mu_V} \frac{\rho_V}{\rho_L} \frac{1-y}{y} \right)^{0.5}$$

$$\frac{dp}{dL_L} = \frac{2f_L(1-y)^2 G_t^2}{8_c \rho_L D_i}$$

$Re_L < 4000$

$$\phi_V^2 = 1 + CX + X^2$$

$$\frac{dP}{dL_{TF}} = \phi_V^2 \frac{dP}{dL_V}$$

$$\frac{dP}{dL_V} = \frac{2f_V y^2 G_t^2}{8_c \rho_V D_i}$$

$Re_L \geq 4000$

$$\phi_L^2 = 1 + \frac{C}{X} + \frac{1}{X^2}$$

$$\frac{dP}{dL_{TF}} = \phi_L^2 \frac{dP}{dL_L}$$

Chisholm Stratified Method

CHISHOLM, D.
Two-phase Flow in
Pipelines and Heat
Exchangers. Book
George Godwin, London
1983

$$Re_l = D_i G_t (1-y) / \mu_l$$

$$Re_v = D_i G_t y / \mu_v$$

IF $Re_l > 2000$ and $Re_v > 2000$

$$X = \left(\frac{1-y}{y} \right)^{0.9} \left(\frac{\mu_v}{\mu_l} \right)^{0.5} \left(\frac{\mu_l}{\mu_v} \right)^{0.1}$$

IF $Re_l > 2000$ and $Re_v < 2000$

$$X = \left(\frac{0.046}{16} \frac{1-y}{y} \frac{\mu_l}{\mu_v} \frac{\mu_v}{\mu_l} \frac{f_v}{f_l} Re_l^{0.8} \right)$$

IF $Re_l < 2000$ and $Re_v > 2000$

$$X = \left(\frac{16}{0.046} \frac{1-y}{y} \frac{\mu_l}{\mu_v} \frac{f_v}{f_l} \frac{1}{Re_v^{0.8}} \right)$$

IF $Re_l < 2000$ and $Re_v < 2000$

$$X = \left(\frac{1-y}{y} \frac{\mu_l}{\mu_v} \frac{f_v}{f_l} \right)^{0.5}$$

$$C = 1.5 \quad \frac{dP}{dL_v} = \frac{2 f_v y^2 G_t^2}{g_c f_v D_i}$$

$$\phi_v^2 = 1 + CX + X^2$$

$$\frac{dP}{dL_{TF}} = \phi_v^2 \frac{dP}{dL_v}$$

①

Taitel & Dukler Stratified Method

(Int. J. Multi-
phase Flow
Vol. 2, pp 591-595
1976)

Given: D_i , G_t , y , μ_e , μ_v , f_e , f_v

1. Calculate Re_e , Re_v and X
(Equations for Re_e , Re_v and X are the same
as described in the Chisholm method)

2. Guess stratified angle ϕ



3. Calculate

$$A = (\pi - \sin 2\phi) / 2\pi$$

$$u_e = 1 / (1 - A)$$

$$u_v = 1 / A$$

$$D_e = \pi(1 - A) / (\pi - \phi)$$

$$D_v = \pi A / (\phi + \sin \phi)$$

$$S_e = \pi - \phi$$

$$S_v = \phi$$

$$S_i = \sin \phi$$

$$A_e = \pi(1 - A) / 4$$

$$A_v = \pi A / 4$$

4. Assume $\tau_e / \tau_v = 3$ (Kawaji, M et al.
Int. J. Multiphase Flow
Vol. 13, No. 2, pp. 145-159, 1987)

5.

$n = 0.2$	if $Re_e > 2000$
$n = 1.0$	if $Re_e \leq 2000$
$m = 0.2$	if $Re_v > 2000$
$m = 1.0$	if $Re_v \leq 2000$

6 Calculate

$$F = -X^2 \frac{(u_e D_e)^{-n}}{(u_v D_v)^{-m}} \frac{S_e}{S_v} u_e^2 + \left[\frac{S_v}{A_v} + \frac{f_i}{f_v} \left(\frac{S_i}{A_i} + \frac{S_i}{A_v} \right) \right] u_v^2$$

7. if $F \neq 0$, go back to step 2 and regress ϕ

8. if $F = 0$, Calculate

$$\phi_v^2 = \frac{1}{4} \frac{u_v^2}{A_v} (u_v D_v)^{-m} \left(S_v + \frac{f_i}{f_v} S_i \right)$$

9. $C_v = 0.046$ if $Re_v > 2000$
 $C_v = 16$ if $Re_v \leq 2000$

10. Calculate $f_v = C_v Re_v^{-m}$

11. Calculate $\frac{dp}{dL_v} = \frac{2 f_v y^2 G_c^2}{g_c \rho_v D_i}$

12. Obtain $\frac{dP}{dL_{TF}} = \phi_v^2 \frac{dp}{dL_v}$

Modified Lockhart-Martinelli Method

(R. Ulbrich, Chemical Engineering Science Vol. 39,
No. 4, pp. 751-765, 1984)

$$\lambda = \left(\frac{1-y}{y}\right)^{0.7} \left(\frac{\mu_v}{\mu_l}\right)^{0.5} \left(\frac{\mu_l}{\mu_v}\right)^{0.1} \quad \text{for } Re_L > 2100 \text{ and } Re_v > 2100$$

$$X = \left(\frac{16}{0.046} \frac{1-y}{y} \frac{\mu_l}{\mu_v} \frac{\mu_v}{\mu_l} \frac{1}{Re_v^{0.8}}\right) \quad \text{for } Re_L < 2100 \text{ and } Re_v > 2100$$

$$X = \left(\frac{0.046}{16} \frac{1-y}{y} \frac{\mu_l}{\mu_v} \frac{\mu_v}{\mu_l} Re_L^{0.8}\right) \quad \text{for } Re_L > 2100 \text{ and } Re_v < 2100$$

$$X = \left(\frac{\mu_l}{\mu_v} \frac{\mu_v}{\mu_l} \frac{1-y}{y}\right)^{0.5} \quad \text{for } Re_L < 2100 \text{ and } Re_v < 2100$$

$$\left(\frac{\Delta P}{\Delta L}\right)_{f,r} = \begin{cases} \left(\frac{\Delta P}{\Delta L}\right)_L \phi_L^2 & \text{for } X \geq 100 \\ \left(\frac{\Delta P}{\Delta L}\right)_c \phi_c^2 & \text{for } X < 100 \end{cases} \quad (4)$$

$$\phi_c = \begin{cases} \exp\left\{\sum_{n=0}^3 [a_n (\ln X)^n]\right\} & \text{for } 0.01 < X < 100 \\ \exp[a_0 \exp(a_1 \ln X)] & \text{for } X \leq 0.01 \end{cases} \quad (5)$$

$$\phi_L = \exp[a_0 \exp(a_1 \ln X)] \quad \text{for } X \geq 100.$$

Table 1. Value of factors in relation (5), according to [15]

	kind of flow			
	$\tau = \tau$ $Re_c > 2100 \quad Re_L > 2100$	$\tau = 1$ $Re_c \leq 2100 \quad Re_L > 2100$	$1 = 1$ $Re_c > 2100 \quad Re_L \leq 2100$	$1 = 1$ $Re_c \leq 2100 \quad Re_L \leq 2100$
a_0	1.442234405141	1.250764152382	1.242340822498	$9.794209405283 \cdot 10^{-1}$
a_1	$4.987124154600 \cdot 10^{-1}$	$5.597574859964 \cdot 10^1$	$5.351838346275 \cdot 10^{-1}$	$5.656477220093 \cdot 10^{-1}$
a_2	$5.843703063595 \cdot 10^{-2}$	$6.699986422058 \cdot 10^{-2}$	$6.968848631602 \cdot 10^{-2}$	$9.627530204125 \cdot 10^{-2}$
a_3	$-1.336126166103 \cdot 10^{-3}$	$-5.573698621418 \cdot 10^{-3}$	$-4.807704507644 \cdot 10^{-3}$	$-4.506708210734 \cdot 10^{-3}$
a_4	$-4.755690575268 \cdot 10^{-4}$	$-6.002645641090 \cdot 10^{-4}$	$-5.805807194990 \cdot 10^{-4}$	$-1.475254575799 \cdot 10^{-3}$
a_5	$3.146521209930 \cdot 10^{-5}$	$1.291950426404 \cdot 10^{-4}$	$1.381135151769 \cdot 10^{-4}$	$7.773050936810 \cdot 10^{-5}$
a_6	1.596	1.0192	1.751	2.682
a_7	0.4148	0.5025	0.4760	0.9960
a_8	118.48	121.75	39.518	302.27
a_9	-1.554	-1.554	-1.263	-1.781

APPENDIX E

FILM LOG

<u>NASA-JSC</u> <u>Roll Number</u>	<u>Date</u>	<u>Shot</u>	<u>Subject</u>	<u>Approximate</u> <u>Time</u>	<u>Film Speed (fps)*</u>
Ground Test					
S87-012	5/7	1	15%	10:49:00	1000
		2	20%	10:55:00	1000
		3	30%	11:01:00	2000
		4	50%	11:23:00	3000
		5	60%	11:28:00	3000
		6	80%	11:35:00	5000
Reduced Gravity Flight Test					
S87-002	4/16	1	5%	12:40:40	400
	4/16	2	Condenser	13:46:09	400
	4/16	3	30%	13:29:02	1000
S87-003	4/16	1	15%	13:08:38	1000
		2	60%	13:46:33	3000
		3	80%	13:56:25	5000
S87-004	4/16	1	20%	13:19:18	1000
		2	40%	13:38:10	2000
S87-005	4/17	1	Condenser		48
	4/16	2	Condenser	13:55:00	400
S87-006	4/17	1	10%	12:07:01	1000
	4/16	2	10%	12:52:09	400
S87-007	4/17	1	80%	11:01:48	5000
	4/17	2	60%	11:11:03	3000
	4/17	3	50%	11:19:46	3000
	4/17	4	30%	11:28:44	2000
	4/17	5	20%	11:37:56	1000
	4/17	6	15%	11:46:52	1000

% Evaporator Exit Quality in Percent

* Frames Per Second

To obtain a copy of the films, see Reference 2.